12-2022

Green Synthesis of Spiro Compounds and the Phytochemical Investigation of Diethyl Ether Fraction of Camu-Camu (*Myrciaria dubia*) Leaves

Judith Anane
The University of Texas Rio Grande Valley

GREEN SYNTHESIS OF SPIRO COMPOUNDS AND THE PHYTOCHEMICAL INVESTIGATION OF DIETHYL ETHER FRACTION OF CAMU-CAMU (*Myrciaria dubia*) LEAVES

A Thesis

by

JUDITH ANANE

Submitted in Partial Fulfillment of the

Requirements for the Degree of

MASTER OF SCIENCE

Major Subject: Chemistry

The University of Texas Rio Grande Valley

December 2022

GREEN SYNTHESIS OF SPIRO COMPOUNDS AND THE PHYTOCHEMICAL CHARACTERIZATION OF DIETHYL ETHER EXTRACT OF CAMU-CAMU (*Myrciaria dubia*) LEAVES

A Thesis
by
JUDITH ANANE

COMMITTEE MEMBERS

Debasish Bandyopadhyay
Chair of Committee

Javier Macossay-Torres
Committee Member

Narayan Bhat
Committee Member

December 2022

ABSTRACT

Anane, Judith, Green Synthesis of Spiro Compounds and the Phytochemical Characterization of Diethyl Ether Extract of Camu-Camu (*Myrciaria Dubia*) Leaves. Master of Science (MS), December, 2022, 154 pp., 16 tables, 80 figures, references, 76 titles.

There are a lot of lucrative plant species found in the Amazon and camu-camu (*Myrciaria dubia* (H.B.K.) Mc Vaugh) is distinct among them. This is due to its exceptional Vitamin C content which varies from 1600 to 6112 mg/100g of pulp. Besides the fruits which is popularly used, different parts of camu-camu plants including the stems, leaves, seeds, barks, and roots are also traditionally used in folklore practices for treating various ailments and diseases and research has showed the presence of antioxidant, antimicrobial, anticancer, anti-inflammatory agents present in these parts. In this study, the characterization of a bioactive compound, isolated from the diethyl ether extract of camu-camu (*Myrciaria dubia*) leaves was conducted using Fourier Transform Infrared spectroscopy (FT-IR), mass spectroscopy (MS), and nuclear magnetic resonance spectroscopy (NMR). A more environmentally benign green synthetic method was used to synthesize spiro compounds and their derivatives in a five-component reaction involving 1,3-diketo, hydroxyl amine, activated methylene, isatin, ammonium acetate, sulfamerazine, and sulfathiazole. Microwave irradiation was used in a short time range (5 – 30 min) and moderate temperature (80°C), with water as a solvent, and *N*, *N*-Diisopropylethylamine (DIPEA) as a catalyst to give high yield of products. This presents a sustainable and faster alternative to the classical synthesis approach.

DEDICATION

I dedicate the successful completion of my thesis to my mom, Mrs. Veronica Anane, her unconditional love, and support was the fuel to accomplishing my dreams. I also want to dedicate this to my family for always loving and standing with me.

ACKNOWLEDGMENTS

I want to express my sincere gratitude to my advisor Dr. Debasish Bandyopadhyay for his support, guidance, and patience throughout this research. I want to also thank my thesis committee members Dr. Narayan Bhat and Dr. Macossay-Torres for their willingness to help and assist whenever necessary with my thesis. A big thanks goes to Mr. Thomas Eubanks for always helping me with any instrumental need, I am grateful. I want to also appreciate all my lab mates for their support throughout my studies.

I am also grateful to Ms. Marianella Franklin and the whole Sustainability office for the Graduate Sustainability Fellowship awarded me and the guidance given me during my fellowship year, it was helpful. Many thanks also go to the chemistry department and university of Texas Rio Grande Valley for all the financial assistance and facilities made accessible to me.

Finally, I want to thank my family and loved ones for their immense support that has seen me through both high and low times during my studies.

TABLE OF CONTENTS

Page

ABSTRACT iii

DEDICATION iv

ACKNOWLEDGMENTS v

TABLE OF CONTENTS vi

LIST OF TABLES viii

LIST OF FIGURES ix

CHAPTER I. INTRODUCTION 1

Phytochemical investigation of diethyl ether fraction of camu-camu (*Myrciaria dubia*) leaves (Part A) 1

Medicinal application of camu-camu 1

Green synthesis of spiro compounds (Part B) 3

Introduction to Green synthesis of spiro compounds 3

CHAPTER II. LITERATURE REVIEW 9

Phytochemical investigation of diethyl ether fraction of camu-camu (*Myrciaria dubia*) leaves (Part A) 9

Bioactive compounds present in different parts of camu-camu (Myrciaria dubia) 9

Proximate composition 17

Biological activity of parts of camu-camu 22

Antioxidant activity 22

Antimicrobial activity 33

Anticancer activity 37

Pharmacological properties of β-sitosterol 44

Green synthesis of spiro compounds (Part b) 45

Spirocyclic compounds 45

Biological activities of different derivations of spiro cyclic heterocyclic compounds 48

CHAPTER III. METHODOLOGY 52

Camu-camu (*Myrciaria dubia)* (Part A) 52

Experiment 52
Characterization of isolated compound 53
Green synthesis (Part b) Experimental 53
Chemicals and apparatus 53
Optimization of reaction for solvent selection 54
General procedure for preparation of spiro indoline pyrazolo-pyridine compounds 55
Isolation of pure product 56
CHAPTER IV. RESULTS AND DISCUSSION....57
Camu-camu (*Myrciaria dubia*) (Part A) 57
Characterization of steroid 1 57
Green synthesis of spiro compound (Part B) 69
Optimization of solvent for reaction....69
Results for the synthesis of spiro[oxindole pyrano pyridine]....70
Characterization....71
Characterization of DBJA-1 71
Characterization of DBJA-2 84
Characterization of DBJA-3 95
Characterization of DBJA-4 107
Characterization of DBJA-9 119
Characterization of DBJA-11 131
CHAPTER V. CONCLUSION....144
REFERENCES 145
BIOGRAPHICAL SKETCH 154

LIST OF TABLES

Page

Table 1: Structure and biological activities of isolated compounds from the leaves, peels, seed and fruit of camu-camu (Myrciaria dubia)..... 12

Table 2: Proximate composition of different parts of camu-camu (Myrciaria dubia) 19

Table 3: Antioxidant activity of different parts of camu-camu using DPPH, TP, AA, and DHA assays. 28

Table 4: Antimicrobial activity of different parts of camu-camu (Myrciaria dubia) 33

Table 5: Anticancer activity of different parts of camu-camu (Myrciaria dubia) 39

Table 6: Other Biological activities of different parts of camu-camu (Myrciaria dubia).....42

Table 7: Reaction components and time for the synthesis of DBJA-1, 2,3,4,9 and 11.....55

Table 8: Different carbon positions in steroid 1 and their chemical shifts 66

Table 9: Solvents used for reaction and masses of products obtained.....69

Table 10: Mass of product, percentage yield, melting point, and color of reaction products.....71

Table 11: Different carbon positions in DBJA-1 and their chemical shifts.....82

Table 12: Different carbon positions in DBJA-2 and their chemical shifts.....93

Table 13: Different carbon positions in DBJA-3 and their chemical shifts.....105

Table 14: Different carbon positions in DBJA-4 and their chemical shifts.....117

Table 15: Different carbon positions in DBJA-9 and their chemical shifts.....129

Table 16: Different carbon positions in DBJA-11 and their chemical shifts.....141

LIST OF FIGURES

Page

Figure 1: Marketed drugs with spiro scaffold in its structure 48
Figure 2: Structures of synthesized spirocyclic derivatives 51
Figure 3: General synthetic reaction scheme for DBJA 1, 2, 3, 4, 9, and 11 58
Figure 4: Structure of steroid 1 58
Figure 5: FT-IR spectrum of steroid 1 58
Figure 6: ^{1}H NMR of steroid 1 59
Figure 7: ^{13}C NMR of steroid 1 60
Figure 8: C^{13}APT NMR of steroid 1 60
Figure 9: C^{13}DEPT90° NMR of steroid 61
Figure 10: C^{13}DEPT135° NMR of steroid 1 62
Figure 11: COSY of steroid 1 63
Figure 12: HMBCGP of steroid 1 64
Figure 13: Mass Spectroscopy of steroid 1 65
Figure 14: X-ray structure of steroid 1 65
Figure 15: Optimization with different solvent to determine solvent with highest product yield 70
Figure 16: Structure of DBJA-1 72
Figure 17: FT-IR spectrum of DBJA-1 73
Figure 18: ^{1}H NMR spectrum of DBJA-1 74
Figure 19: C^{13} NMR spectrum of DBJA-1 75
Figure 20: C^{13}APT NMR spectrum of DBJA-1 76
Figure 21: C^{13}DEPT90° NMR spectrum of DBJA-1 77
Figure 22: C^{13}DEPT135° NMR spectrum of DBJA-1 78
Figure 23: COSY spectrum of DBJA-1 79
Figure 24: HMBCGP spectrum of DBJA-1 80

Figure 25: HMQCGP 2D NMR spectrum of DBJA-1 81
Figure 26: Mass spectroscopy spectrum of DBJA-1 82
Figure 27: Structure of DBJA-2.....85
Figure 28: FT-IR spectrum of DBJA-2.....85
Figure 29: ^{1}H NMR spectrum of DBJA-2 86
Figure 30: C^{13} NMR spectrum of DBJA-2 87
Figure 31: C^{13}APT NMR spectrum of DBJA-2.....88
Figure 32: C^{13}DEPT90° NMR spectrum of DBJA-2.....88
Figure 33: C^{13}DEPT135° NMR spectrum of DBJA-2.....89
Figure 34: COSY spectrum of DBJA-2 90
Figure 35: HMBCGP spectrum of DBJA-2 91
Figure 36: HMQCGP spectrum of DBJA-2 92
Figure 37: Mass spectroscopy spectrum of DBJA-2 92
Figure 38: Structure of DBJA-3.....95
Figure 39: FT-IR spectrum of DBJA-3.....96
Figure 40: ^{1}H NMR spectrum of DBJA-3 97
Figure 41: C^{13} NMR spectrum of DBJA-3 98
Figure 42: C^{13}APT NMR spectrum of DBJA-3.....99
Figure 43: C^{13}DEPT90° NMR spectrum of DBJA-3.....100
Figure 44: C^{13}DEPT135° NMR spectrum of DBJA-3.....101
Figure 45: COSYGPDFPHSM 2D NMR spectrum of DBJA-3 102
Figure 46: HMBCGP 2D NMR spectrum of DBJA-3 103
Figure 47: HMQCGP 2D NMR spectrum of DBJA-3 104
Figure 48: Mass spectroscopy spectrum of DBJA-3 105
Figure 49: Structure of DBJA-4.....107

Figure 50: FT-IR spectrum of DBJA-4 108
Figure 51: ^{1}H NMR spectrum of DBJA-4 109
Figure 52: C^{13} NMR spectrum of DBJA-4 110
Figure 53: C^{13}APT NMR spectrum of DBJA-4.....111
Figure 54: C^{13}DEPT90° NMR spectrum of DBJA-4.....112
Figure 55: C^{13}DEPT135° NMR spectrum of DBJA-4.....113
Figure 56: COSYGPDFPHSM 2D NMR spectrum of DBJA-4.....114
Figure 57: HMBCPG 2D NMR spectrum of DBJA-4.....115
Figure 58: HMQCPG 2D NMR spectrum of DBJA-4.....116
Figure 59: Mass spectroscopy spectrum of DBJA-4 116
Figure 60: Structure of DBJA-9.....119
Figure 61: FT-IR spectrum of DBJA-9.....120
Figure 62: ^{1}H NMR spectrum of DBJA-9 121
Figure 63: C^{13} NMR spectrum of DBJA-9 122
Figure 64: C^{13}APT NMR spectrum of DBJA-9.....123
Figure 65: C^{13}DEPT90° NMR spectrum of DBJA-9.....124
Figure 66: C13DEPT135° NMR spectrum of DBJA-9 125
Figure 67: COSYGPDFPHSM 2D NMR spectrum of DBJA-9.....126
Figure 68: HMBCGP 2D NMR spectrum of DBJA-9.....127
Figure 69: HMQCGP 2D NMR spectrum of DBJA-9 128
Figure 70: Mass spectroscopy spectrum of DBJA-9 128
Figure 71: Structure of DBJA-11.....131
Figure 72: FT-IR spectrum of DBJA-11.....132
Figure 73: ^{1}H NMR spectrum of DBJA-11 133
Figure 74: C^{13} NMR spectrum of DBJA-11 134

Figure 75: C^{13}APT NMR spectrum of DBJA-11 135
Figure 76: C^{13}DEPT90° NMR spectrum of DBJA-11 136
Figure 77: C13DEPT135° NMR spectrum of DBJA-11 137
Figure 78: COSYGPDFPHSM 2D NMR spectrum of DBJA-11 138
Figure 79: HMBCGP 2D NMR spectrum of DBJA-11 139
Figure 80: HMQCGP 2D NMR spectrum of DBJA-11 140
Figure 81: Mass spectroscopy spectrum of DBJA-11 140

CHAPTER I

INTRODUCTION

Phytochemical investigation of diethyl ether fraction of camu-camu (*Myrciaria dubia*) leaves (Part A)

Medicinal application of camu-camu

The most skilled chemist is Mother Nature, and she can generate a wide range of chemicals in a highly selective way. Natural resources contain a great diversity of chemical molecules produced as a response to several biotic and abiotic factors affecting the organisms' biosynthetic pathways and are the products of enzyme-catalyzed reactions that occur naturally within cells (Leskovar et al., 2008). They have various functions, including fuel, structure, signaling, stimulatory and inhibitory effects on enzymes, the catalytic activity of their own (usually as a cofactor to an enzyme), defense, and interactions with other organisms (e.g., pigments, odorants, and pheromones) (Demain, 1980). Plants are able to compete and survive in their environment by using natural products. The antifungal, antimicrobial, poisonous, or toxic qualities that plants have to fend off diseases or consumption are provided by compounds (Flores, 2020).

Natural products are valuable sources of bioactive compounds useful in many areas from pharmacology, to cosmetics, food, etc. In the pharmaceutical sector, natural products from plants, marine organisms, or microorganisms have been valuable sources of important drugs/leads approved for the treatment of human diseases. Dating the time when humans started

resorting to nature for medicine is almost impossible since nature has existed way before civilization began (Flores, 2020). The evidence of our ties with naturally derived medicine can be traced as far back as 60,000 years (Flores, 2020). Currently, up to four billion people making up 80% of the world's population, are thought to rely on herbal medicines as their main source of healthcare, and in those communities, traditional medicine, which includes the use of herbs, is regarded as an essential aspect of culture (Ekor, 2014). In the pharmaceutical industry, 25% of commercial drugs are extracted from nature. Drugs like aspirin (from willow tree bark), digoxin (from flower of *Digitalis ianata*) and morphine (from opium) were all derived from plant sources (Mathur and Hoskin, 2017).

There are a lot of lucrative plant species found in the Amazon and camu-camu ((*Myrciaria dubia* (H.B.K.) Mc Vaugh) is distinct among them (Aguiar and Souza, 2015). This is due to its exceptional Vitamin C content which varies from 1600 to 6112 mg/100g of pulp (Aguiar and Souza, 2015; Yuyama et al., 2002). Camu-camu is a low-growing shrub found throughout the Amazon rainforest of Colombia, Venezuela, Brazil, and mainly in Peru (Chirinos et al., 2010). Its fruit is round with a diameter of 2-4 centimeters, and it has a smooth, shiny skin with an average weight of 8.4 grams. Its color varies from dark red to purplish-black when ripe and each fruit has one to four (commonly two to three) kidney shaped, ellipsoid seeds covered with fibril filament (Aguiar and Souza, 2015). The Amazonian natives who are aware of the plant's sustenance make use of its berry-like fruits by eating them or, more frequently, by incorporating them into purees, drinks, and cocktails. Besides its high level of Vitamin C content, the fruit has a variety of antioxidants, flavonoids, and other important nutraceuticals

making it very popular in international trade and can be found as powder or tablet solid in supplement and grocery stores worldwide (Leskovar et al., 2008).

Besides the fruits which is popularly used, different parts of camu-camu plants including the stems, leaves, seeds, barks, and roots are also traditionally used in folklore practices for treating various ailments and diseases (Leskovar et al., 2008).

There is a need to investigate the bioactive compounds responsible for the observed biological activities seen in the different parts of camu-camu plant. In this study, the characterization of a bioactive compound, isolated from the diethyl ether extract of camu-camu (*Myrciaria dubia*) leaves was conducted using Fourier Transform Infrared spectroscopy (FT-IR), mass spectroscopy (MS), and nuclear magnetic resonance spectroscopy (NMR).

Green synthesis of spiro compounds (Part B)

Introduction to Green synthesis of spiro compounds

Heterocycles make up the largest and most diverse classical division of organic chemistry (Majumder et al., 2013). They are cyclic compounds with at least one ring structure that possesses one or more heteroatom (atoms besides carbon) in their ring structure (Bandyopadhyay et al., 2021). Every homocyclic molecule can be converted into a series of heterocyclic counterpart simply by replacing one or more of the carbon ring atoms with heteroatoms. This can be done irrespective of the structure and functionality of the homocyclic molecule. The three most common heteroatoms are oxygen, nitrogen, and sulfur (Bandyopadhyay and Banik, 2021).

Heterocycles have wide applicability in different industries including as cosmetics, reprography, information storage, polymers, solvents, antioxidants, and accelerators for vulcanization (Majumder et al., 2013). They are also extensively used in the pharmaceutical fields. They are considered as privileged structures (Jampilek, 2019) and are typically found in biologically active natural products and synthetic compounds (Nishanth et al., 2021). They play a central role in modern drug design due to their diverse and fascinating medicinal properties and are present in more than 85% of all biologically active chemical entities (Bandyopadhyay et al., 2021; Jampilek, 2019).

Many bioactive natural products such as vitamins, hormones, glycosides, alkaloids, and antibiotics have heterocyclic compounds as part of their structure. Some natural drugs like morphine, quinine, codeine, papaverine, emetine and so on possess N-containing heterocycles (Majumder et al., 2013). Many heterocyclic compounds have also been found to possess high potency as anticancer, antimicrobial, antioxidant, anti-inflammatory agents. For instance, among the 50 bestselling anticancer drugs on the market, 10 are heterocyclic compounds containing nitrogen, oxygen, and sulfur as heteroatoms in their structural motif namely (Nishanth et al., 2021). In 2018, revenue worldwide ranked the small molecule heterocyclic drugs Eliquis (Apixaban), Revlimid (racemic mixture of Lenalidomide), and Xarelto (Rivaroxaban) as the second, third, and tenth, respectively, in the list of top-selling prescription medicines. Also, the bestselling drug in pharmaceutical history, Lipitor (Atorvastatin), is a heterocyclic small molecule. Diabetes, AIDS, cancer, cardiovascular diseases (CVDs), and central nervous system (CNS) diseases are part of the dreadful health problems facing the healthcare system globally. It

is interesting to note that heterocyclic small molecules are part of the frontline drugs being used against these deadly diseases (Bandyopadhyay et al., 2021). This buttresses the importance of heterocyclic compounds and the need to synthesize new one for treatment of diseases.

Spiro compounds are cyclic structures joined at a central carbon forming a quaternary carbon. Due to the steric strain of the quaternary carbon, spirocyclic compounds are regarded as significant building blocks for the straightforward availability of various cyclic products by a sequential process (Ghasemzadeh and Abdollahi-Basir, 2019). Numerous natural materials include spiro rings, such as spiroketals, which are known as insect pheromones (Zheng et al, 2014). Recent interest in spiro compounds is increasing due to their intriguing conformational characteristics and structural implications on biological systems (Pradhan et al., 2006). The spiro functionality can be found in either alkaloid, lactone, or terpenoid phytochemicals and they exhibit very good biological activities (Pradhan et al., 2006). Another interesting compound is pyrazolopyridines which are nitrogen-containing fused heterocycles and demonstrate remarkable pharmacological activity like anxiolytic activity, antimicrobial activity, xanthine oxidase inhibitors and so on (Naglaa et al., 2022), anti-inflammatory, anti-tumor, antidepressants, and infertility (Das and Banik, 2020). Oxindoles are a group of endogenous hetero-aromatic chemical compounds that are found in the tissues and bodily fluids of mammals as well as in the natural products of many plants. History shows its usefulness in conventional medicine, as seen by treatments from bygone eras for infections, cancer, gastric ulcers, arthritis, and other mild physical inflammations (Mahadu et al., 2021).

The importance of heterocyclic compounds and their wide applicability has resulted in the high demand on synthetic organic chemist to develop novel methodologies for the preparation of these compounds (Majumber et al., 2013). Classical methodologies used to prepare heterocyclic small molecules compromised the safety of the environment. For instance, these methods involved prolonged heating, longer reaction time, exposure of hazardous chemicals to the environment, tedious equipment setups, and high boiling solvents (Nishanth et al, 2021; Bandyopadhyay and Banik, 2021). The need to replace these archaic classical methods has brought an emphasis on green chemistry. Early in the 1990s, the idea of green chemistry originated, and it has since gained widespread acceptance as a means of addressing the core scientific problems of environmental and human health protection while also achieving commercial viability (Majumber et al., 2013). New methods in line with green chemistry have emerged which involve solvent-free synthesis, replacement of hazardous solvent with environmentally safe and cheaper ones (Bandyopadhyay and Banik, 2021), reduction or elimination of generation of hazardous substances (Majumber et al., 2013), energy efficient techniques (Nishanth et al, 2021) and so on.

The 12 fundamental principles of green synthesis for the production of chemicals were published by Paul Anastas and his team (Anastas and Eghbali, 2010; Ananstas and Warner, 1998). Several eco-friendly techniques like microwave-assisted organic synthesis, organic synthesis on water, solvent-free synthesis, nanoparticle-catalyzed organic synthesis, sonochemical synthesis and so on have been invented based on these principles (Nishanth et al., 2021).

Microwave radiation has a span of radiation between 30 GHz and 300 MHz. It consists of both electric and magnetic fields and hence it is considered an electromagnetic energy (Majumder et al., 2013). Gedye et al. were the first to report the use of microwave ovens in the synthesis of some organic compounds in the year 1986 (Bandyopadhyay and Banik, 2021). The time saved by applying microwave irradiation in safe reaction media, together with improved yields in conventional medicinal chemistry and the assembling of heterocyclic systems, are the main benefits of these methods (Nishanth et al., 2021). The fast rate of reaction rate is due to material–wave interactions leading to dielectric heating. The electromagnetic energy of microwave does not affect the structure of molecules but acts as nonionizing radiation that causes molecular motions of ions and rotation of the dipoles. The molecules briefly spend slightly more time, on average, orienting themselves in the direction of the electric field than in other directions because of the applied MW field. When the field is withdrawn, thermal agitation causes the molecules to return to an unorganized form in the relaxation time and thermal energy is then released. Therefore, for this phenomenon to occur, a substance (solvent or reactant) must be able to absorb MWs and transform them into heat. Compared to traditional heating, this internal heating is significantly more uniform (Majumder et al., 2013).

Another eco-friendly technique involves organic synthesis on water. The advantage of using water as a solvent in place of conventional organic solvent is that water is cheap and nontoxic, its smooth conditions lead to improvements in yield and selectivity, and in some situations, the time-consuming protection-deprotection procedures can be avoided, in reactions involving transition metal catalysts, water can help with ligand exchange (Lubineau and Augé,

1999) and product purification can be achieved by simple filtration (Govindaraju and Tabassum, 2021).

Due to its "green" character, the efficient building of molecular complexity via multi-component, domino, or cascade reactions has recently attracted a lot of interest in the organic chemistry community. By enabling reactive products to go through additional chemical transformations before workup, it is possible to use relatively simple starting materials to substantially enhance the levels of molecular complexity in a single-pot process. A successful process of this nature will result in significant savings in terms of solvent, waste disposal, and the time needed for workups and purifications. Often, this can be accomplished by carefully designing the substrate and cascade sequences and carefully controlling the reaction conditions (Wu et al., 2012).

In this study, a more environmentally benign green synthetic method was used to synthesize spiro indoline pyrazolo-pyridine compounds and their derivatives in a five-component reaction involving 1,3-diketo, hydroxyl amine, activated methylene, isatin, ammonium acetate, sulfamerazine, and sulfathiazole. Microwave irradiation was used in a short time range (5 – 30 min) and moderate temperature (80°C), with water as solvent, and *N, N*-Diisopropylethylamine (DIPEA) as a catalyst to give a high yield of products. This presents a sustainable and faster alternative to the classical synthesis approach.

CHAPTER II

LITERATURE REVIEW

Phytochemical investigation of diethyl ether fraction of camu-camu (*Myrciaria dubia*) leaves (Part A)

Bioactive compounds present in different parts of camu-camu (Myrciaria dubia)

Diabetes mellitus is a condition that prevents the secretion or response of insulin. Under normal circumstances, aldose reductase (AR) has little catalytic activity for the conversion of glucose to sorbitol because it has a poor affinity for glucose. But in diabetes mellitus, the polyol pathway speeds up the production of sorbitol in tissues that are resistant to insulin. Due to these factors, AR inhibitors can prevent the conversion of glucose to sorbitol and lower the risk of complications from diabetes. H. Ueda et al. evaluated camu-camu leaves for the possible presence of aldose reductase (AR) inhibitors and isolated and identified three compounds that showed significant inhibition against human recombinant AR (HRAR) and rat lens AR (RLAR). The inhibitors isolated from camu-camu leaves were identified as ellagic acid (**1**), 4-O-methylellagic acid (**2**), and 4-(α -rhamnopyranosyl)ellagic acid (**3**). Compound **2** was isolated for the first time in nature from this study (Table 1) (Ueda et al., 2004).

T. Kaneshima et al. isolated and characterized some C-glycosidic ellagitannins from camu-camu seed and peels and studied the relationship between their antioxidant activities and structures. Pure tannin compounds grandinin (**4**), vescalagin (**5**), castalagin (**6**), methylvescalagin (**7**), stachyurin (**8**), and casuarinin (**9**) were isolated from crude camu-camu seeds and peel.

Vescalagin (**5**) and castalagin (**6**) made up approximately 5% and 10% of the total polyphenols respectively, making them the main C-glycosidic ellagitannins. The C-glycosidic ellagitannins have been usually isolated from the wood, branches, leaves, and bark of plants of different genus but its isolation from the seeds and peel of camu-camu is the first instance of plants belonging to Myrtaceae (Kaneshima et al., 2016). Fidelis et al. also identified vescalagin and castalagin in camu-camu flour (Table 1) (Fidelis et al., 2020). Research on C-glycosidic ellagitannins has shown their inhibition of adipocyte differentiation and inhibition of human breast cancer cell line growth (MCF-7), decrease of insulin resistance, and antiherpes virus activity (Fidelis et al., 2020). Camu-camu (Myrciaria dubia) seeds and peel are industrial waste products from the production of camu-camu juice, thus using the seeds and peel as functional food additives could be profitable for the camu-camu industry (Fidelis et al., 2020).

Four antimicrobial acylphloroglucinols constituents of camu-camu seeds and peel were isolated and characterized by T. Kaneshima et al. Compounds **10** and **11** were isolated from the 90% acetonitrile layer of peel and **12** and **13** were isolated from the seeds. Compound **10** was a new compound and was name myrciarone A. Compound **11** was identified as an acylphloroglucinol isolated from Rhodomyrtus tomentosa (Kaneshima et al, 2013). Compound **12** was an acylphloroglucinol, isomyrtucommulone B and this is the first report of isomyrtucommulone B being isolated from a natural source. Compound **13** was also new and was appropriately named myrciarone B. These compounds were known through this study to be responsible for the antimicrobial activity camu-camu exerted on some microbes (Table 1)

(Kaneshima et al., 2017). Acylphloroglucinols besides being antimicrobial agents are also known to inhibit CNS neurotransmitters (Verotta, 2002).

Yazawa et al. evaluated camu-camu seed for its anti-inflammatory activity and found it to have a high potency as an anti-inflammatory agent. The active compound responsible for releasing inflammatory mediators was observed and isolated to be betulinic acid (3β-hydroxy-lup-20(29)-en-28-oic acid) (**14**), a compound known to be an anti-inflammatory triterpenoid. Betulinic acid is also known in literature to show antitumor activity by inhibiting the phosphorylation effect of IκB thereby inhibiting NF- κB activation (Pisha et al., 1995; Takada and Aggarwal, 2003). The first report of betulinic acid as a natural constituent of the Myrciaria (including camu-camu) was seen in this study (Table 1) (Yazawa et al, 2011).

Several kinds of lyophilized fruits have been found to have hepatotoxicity effects by suppressing D-galactosamine (GalN)-induced liver injury in rats when added to the diets of rats (Camere-Colarossi et al., 2016). T. Akachi et al., therefore, analyzed lyophilized camu-camu fruit juice for its protective effects against D-galactosamine (GalN)-induced liver injury in rats. The study showed that camu-camu juice suppresses GalN-induced increases in plasma ALT, AST, and LDH activities and bilirubin concentration (liver injury markers). The active compound responsible for the observed activity was isolated as 1-methylmalate (**15**) (Akachi et al., 2010). 1-methylmalate has also been shown to exhibit a monoamine oxidase-inhibitory activity (Han et al., 2001) and inhibits the lipopolysaccharide-induced production of IL-10 and

increases the lipopolysaccharide-induced production of IL-12 and tumor necrosis factor-α in human peripheral blood polynuclear cells (Suga et al., 2005).

Roumy et al. conducted an inventory of the plants used against infections in the Loreto, an Amazonian region of Peru by interviewing the inhabitants of the regions and selected 81 plants that were evaluated for their antimicrobial activities against 36 sensitive and multi-resistant bacteria or yeast. Camu-camu seed, peel, and leaf methanolic extracts produced triterpenic apolar active chemicals that were detected using the Liebermann-Burchard reaction. The two compounds betulinic acid (**14**) and β-sitosterol (**16**) were isolated from the plant. Betulinic acid (**14**) was previously recovered from *M. dubia* seed (Yazawa et al., 2011) but not from a leaf or peel, and β-sitosterol (**16**) was discovered for the first time in this plant species (Roumy et al., 2019).

Table 1: Structure and biological activities of isolated compounds from the leaves, peels, seed and fruit of camu-camu (Myrciaria dubia)

Entry	**Part of plant isolated**	**Compound isolated**	**Structure of compound**	**Biological activity**	**Ref.**

Table 1, cont.

1.	Leaves	ellagic acid (**1**), 4-O-methylellagic acid (**2**), 4-(a-rhamnopyranosyl)ellagic acid (**3**)	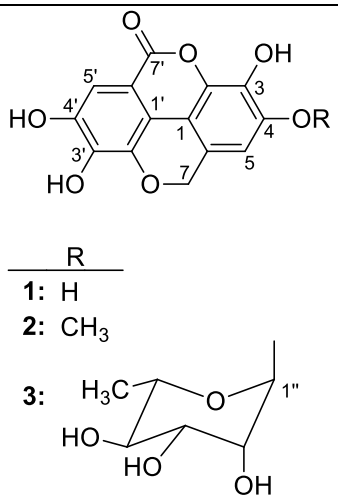	aldose reductase (AR) inhibition	Ueda et al., 2004
2.	Peel and seed	grandinin (**4**)	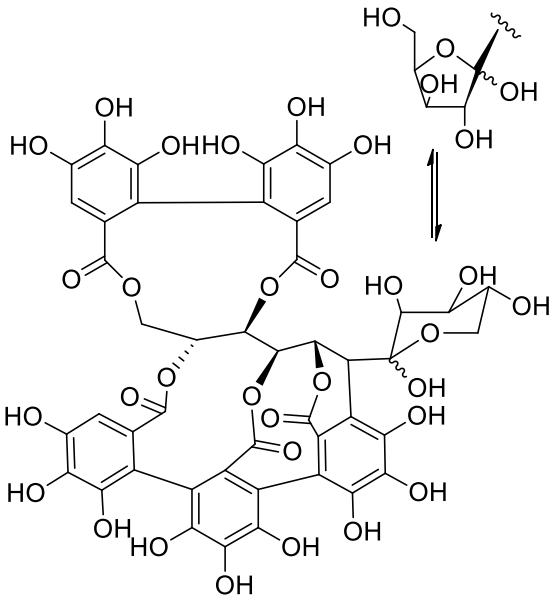	Antioxidant	Kaneshima et al, 2016

Table 1, cont.

		vescalagin (**5**), castalagin (**6**), methylvescalagin (**7**)	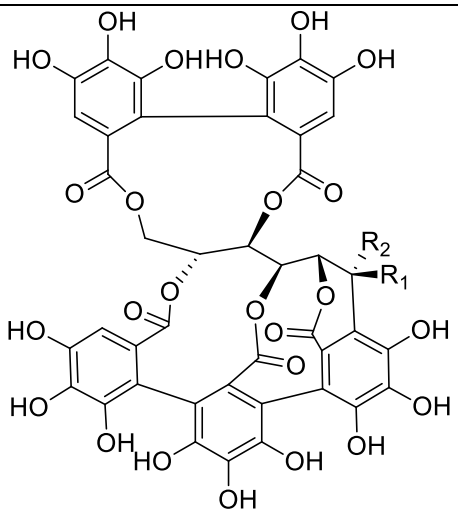 **2** R_1 = OH, R_2 = H **3** R_1 = H, R_2 = OH **4** R_1 = OMe, R_2 = H		
		stachyurin (**8**), casuarinin (**9**)	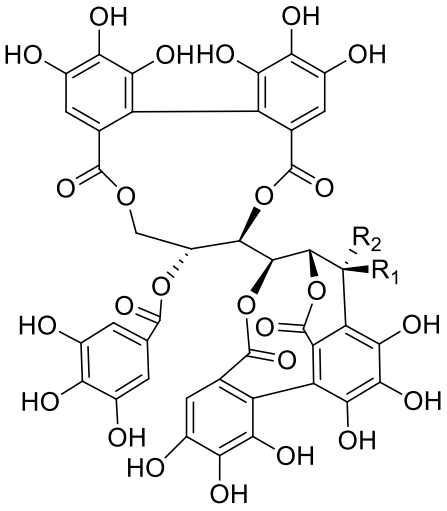 **5** R_1 = OH, R_2 = H **6** R_1 = H, R_2 = OH		

Table 1, cont.

3.	Seeds and peel	Myrciarone A (**10**), Rhodomyrtus (**11**), Isomyrtucommulone B (**12**), Myrciarone B (**13**)	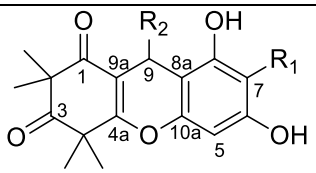 Comp. No. R_1 R_2 **10** 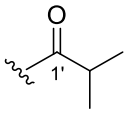 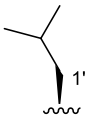 **11** 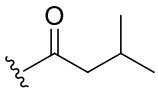  **12** 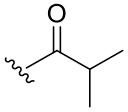  **13** 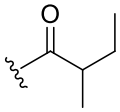 	Antimicrobial	Kaneshima et al, 2013
4.	Seed	Betulinic acid (**14**)	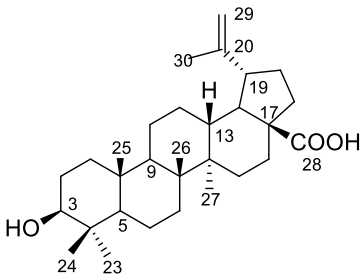	Anti-inflammatory	Yazawa et al., 2011

Table 1, cont.

5.	Fruit	1-methylmalate (**15**)	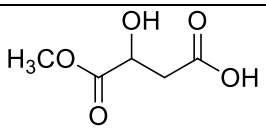	Liver injury suppression	Akachi et al., 2010
6.	seed, peel, and leaf	Betulinic acid (**14**) β-sitosterol (**16**)	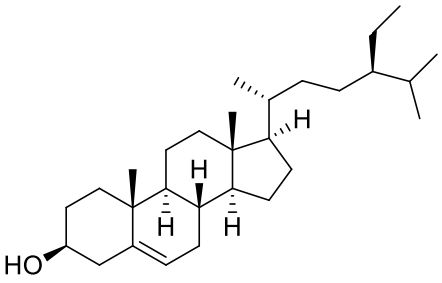	-	Roumy et al. 2019

Structures drawn as presented in original journal.

Proximate composition

Camu-camu is widely known for its high ascorbic acid content but it's *in natura* consumption is low due to the extreme acidity of the pulp and bitterness of the peels. There is therefore the need to develop camu-camu to a more consumptive form without negatively affecting its nutritional quality and extend its shelf life. Aguiar et al. based on this, produced freeze-dried camu-camu pulp and evaluated the antioxidant capacity, chemical composition and mineral contents of it. The study revealed that freeze-dried camu-camu contains high concentrations of vitamin C (approximately 20.31 g/100g), dietary fiber (19.23 g/100 g), and potassium (796.99 mg/100g). Carbohydrate, magnesium, and calcium were significantly present

in concentrations of 47.00 ± 0.00g/100g, 33.47 ± 1.30, and 22.12 ± 2.54 respectively. It was also high in phenolic compounds such as anthocyanins (0.739 mg/g) and flavonoids (16.93 mg/100g). Upon the analysis of some essential amino acids present in camu-camu, arginine (0.692 g/100g) and glutamic acid (0.619 g/100g) were found to be most abundant (Aguiar and Souza, 2015).

Fresh and dried (hot air dried and freeze dried) camu-camu depulping residue was investigated for its physicochemical characteristics, bioactive content, in vitro antidiabetic potential and antimicrobial activities by Azevêdo et al.. For the phytochemical characterization, it was found that both drying methods (hot air-dried and freeze-dried) led to a 10-fold decrease in fruit moisture content meaning an increase in shelf life and a decrease susceptibility to spoilage due to microbial activities on fruit. The pH of all the fresh and dried fruit residues was acidic (<4.5) but in comparison to the fresh residue both dried fruits had lower pH value ($p < 0.05$). This low pH of camu-camu fruit makes it undesirable for natural consumption. In comparison to the fresh residue, the solubility of the freeze-dried and hot air-dried camu-camu samples was four times higher. Freeze dried samples possessed ascorbic acid two times more than hot air-dried samples. The bioactive compounds anthocyanins, carotenoids, total phenolics, and proanthocyanidins were significantly reduced in both dried samples. The main polyphenolic compounds present were ellagic acid, syringic acid, quercetin, myricetin, and catechin (Silva de Azevêdo et al., 2014). Similar polyphenolics were observed by Fujita et al. in spray-dried and freeze-dried camu-camu pulp (Fujita et al., 2015).

Grigio et al. evaluated qualitative attributes, antioxidant capacity and functional potential, of different parts of camu-camu fruit. The amounts of ascorbic acid, phenolic compounds, anthocyanins, and flavonoids as well as the pH, soluble solids, and titratable acidity of the seed, peel, pulp, pulp and peel together, and whole fruit were assessed. The seed showed the highest pH value (3.93) hence it was the least acidic of all the parts analyzed. The seed also showed the highest number of soluble solids with a mean value of 13.86 Brix and the whole fruit had the lowest (5.53). This value incinerate that the seed has the highest sugar content as well. The pulp and whole fruit possessed the highest titratable acidity of 4.86 and 4.69 mg citric acid 100 g-1 sample respectively inferring many acids present in those parts. The peels on the other hand had the least acidity with a value of 2.96 mg citric acid 100 g-1 sample. The peel showed highest content of both anthocyanins and flavonoids with values of 407 and 550 μg g-1 samples respectively and this could be due to its higher intensity of purple color. The pulp possessed lower content of anthocyanins (13.6 μg g-1 sample) but none was detected in the seeds. Phenolic content was highest in the pulp (141 mg g-1 sample) but was also undetected in the seeds in this study. The peel+pulp had the highest ascorbic acid content 4,426 mg 100 g-1 sample and the seeds had the lowest (551 mg 100 g-1 sample) (Grigio et al., 2017).

Table 2: Proximate composition of different parts of camu-camu (*Myrciaria dubia*)

Entry	**Plant part**	**Proximate test**	**Proximate composition**	**Ref.**

Table 2, cont.

1.	Pulp	Potassium (mg/100g)	796.99 ± 43.94				Aguiar and Souza, 2015
		Carbohydrate (g/100g)	47.00 ± 0.00				
		Magnesium (mg/100g)	33.47 ± 1.30				
		Calcium (mg/100g)	22.12 ± 2.54				
		Arginine (g/100g)	0.692				
		Glutamic acid (g/100g)	0.619				
		Vitamin C (g/100g)	20.31 ± 0.04				
		Crude fiber (g/100g)	19.23 ± 0.00				
2.	Pulp		**FR**	**HAD50**	**HAD80**	**FD**	Silva de Azevêdo
		Moisture (%)	86.0 ± 1.2	5.9 ± 1.2	5.9 ± 0.9	5.9 ± 0.1	

Table 2, cont.

		pH	3.3 ± 0.1	3.3 ± 0.1	3.8 ± 0.1	3.3 ± 0.1	et al. 2014
		Solubility (%)	12.0 ± 0.1	14.2 ± 0.1	14.2 ± 0.1	13.3 ± 0.1	
3.	Pulp, Seed, whole fruit, peel, peel+pulp		**Peel+pulp**	**Pulp**	**Peel**	**Whole fruit**	**Seed**	Grigio et al., 2017
		pH	3.12 ± 0	3.09±0.1	3.16 ±0	3.09 ±0	3.93±0	
		Soluble solids (°Brix)	6.93 ± 0.2	5.53 ± 0	7.00±0.2	7.26±0	13.86±1.3	
		Titratable acidity(mg citric acid 100 g-1 sample)	4.05±0	4.86±0	2.96±0.1	4.69±0.1	4.33±0.1	
		Anthocyanin (µg g-1 sample)	50.7±1.5	13.6±1.3	107.2±2.6	29.9±0.6	ND	
		Flavonoids (µg g-1 sample)	440.9±4.9	91.5±6.5	550.8±12.3	517.6±21.0	49.6±2.8E	

Table 2, cont.

		Phenolic (mg g-1 sample)	130.6±2.9	141.2±3.9	98.1±0.6	117.7±5.9	ND	
		Ascorbic acid (mg 100 g-1 sample)	4,426±90	2,916±55	3,068±135	3,204±61	551±31	

Results expressed as mean ± standard deviation; FR – Fresh, HAD50 – hot air dried at 50°C and 4m/s, HAD80 – hot air dried at 80°C and 6m/s, FD – Freeze dried; ND – Not detected

Biological activity of parts of camu-camu

Antioxidant activity

Aguiar et al. evaluated the antioxidant activity of freeze-dried camu-camu pulp using the 2,2-dyphenyl-picrylhydrazil (DPPH) assay. The freeze-dried camu-camu pulp showed very high antioxidant activity of 52,000 µmol TE/g, a value six times more than freeze-dried acai, a fruit known for its high antioxidant capacity. The remarkable antioxidant capacity of camu-camu may be due to the presence of phenolic constituents and the nutritional components of the fruit. Also, the ripening process largely contributes to the extent of bioactive properties exhibited by camu-camu including its reduction potential. This study was conducted during ripening and could also be a major contributor to the high antioxidant activity recorded (Aguiar and Souza, 2015).

The total phenolics (TP), ascorbic acid (AA), dehydroascorbic acid (DHA) and antioxidant capacity (DPPH) of camu camu fruit at three maturity stages was analyzed by Chirinos et al. The fruit is green when it is immature, but as it ripens, anthocyanins present in the fruit cause it to turn red and purple (Zanatta et al., 2005). Apart from color, there are also noticeable changes in the profiles and contents of other phytochemicals, such as vitamin C, phenolic compounds, and carotenoids. The results obtained in this study confirmed this knowledge as the fruit's total phenolic content increased from the fully green to the green-reddish stage before falling off at the red stage. At the full maturity stage (red stage) it showed a TP of 1320 mg GAE/100 g FW which was still very high when compared to other popular fruits and berries like cherries, plums, strawberry (Wu et al. 2004) blueberry, cranberry, lingonberry (Zheng and Wang, 2003). The amount of AA in the fruit reduced as it matured, reaching a value of 2010 mg AA/100 g FW at full maturity but was higher than DHA content with 12 to 19-fold difference. During ripening, the DPPH antioxidant capacity followed the same pattern as the TP content, reaching a value of 167 µmol TE/g FW at full maturity. The antioxidant activity displayed by camu-camu are therefore affected as the fruit matures (Chirinos et al., 2010).

Upon evaluating the antioxidant activity of camu-camu seeds, Carmo et al. observed statistically significant differences in the activity of the various seed extracts. Of the different extracts, 50% H2O + 50% EtOH extract exhibited the highest antioxidant activity when the FRAP, DPPH, and the Folin-Ciocalteau reducing capacity assays were employed while the 100% EtOH extract showed the lowest antioxidant capacity in all the assays (Table 3). According to Pearson's correlation, there is a connection between specific phenolic components of camu-camu

seed extracts and their in vitro antioxidant activity. The extracts' antioxidant ability decreases with decreasing phenolic components. Methylvescalagin showed a significant and positive correlation with the antioxidant assays employed and was responsible for the high antioxidant capacity observed in the 50% H2O + 50% EtOH extract (Vieira Do Carmo et al., 2019).

Like Carmo et al., Fidelis et al. also observed statistically significant differences in the activity of the various seed extracts. The aqueous extract exhibited the highest antioxidant activity by the FRAP, DPPH, and the Folin-Ciocalteau reducing capacity when compared to the other extracts (Table 3). The high antioxidant activity observed in the aqueous extract was attributed to the higher total phenolic content in the aqueous extract in comparison to the others (Fidelis et al., 2018).

Grigio et al. employed both the FRAP and DPPH assay to evaluate the antioxidant activity of the peel + pulp, pulp, peel, whole fruit, and seed of camu-camu. The peel + pulp, pulp, peel, and whole fruit showed very good antioxidant activity in both methods employed but the value recorded for the seeds was very low (Table 3) (Grigio et al., 2017).

Myoda et al. understudied the residual by-products (seeds and peel) of camu-camu fruit juice production as a potential functional resource for the food industry. The free radical scavenging activities were tested using the DPPH radical scavenging assay and reducing power of the camu-camu seed and peel extracts. The results obtained showed the seed extract possessing significantly higher antioxidant activity in comparison to the peel extract in both DPPH and reducing power assays (Table 3). Of the various extraction fractions (crude, water,

25%, 50%, 75%, and 100% MeOH), 25% and 50% MeOH showed the highest antioxidant activity for both the seed and peel in both antioxidant assays (Table 3). The IC_{50} values recorded for both the 25% and 50% MeOH fraction of the seed extract 12.8 µg/g and 15.6 µg/g respectively was lower than that of the standard antioxidant agent, ascorbic acid, of values 21.4 µg/g and hence demonstrates higher antioxidant activity. This infers the presence of compounds of good hydrogen donating capacity present in the seed. The reducing power which is a significant indicator of antioxidant potential demonstrated a similar trend as the DPPH radical scavenging activity. The 25% to 75% MeOH fraction of both seed and peel extracts showed significantly higher reducing power in relation to the other fractions (Table 3). Total phenolic contents of both seeds and peels of camu-camu were also evaluated in this study and the results obtained showed 369.4 ± 9.6 mg/g of total phenols in seed and 203.8 ± 7.7 mg/g in peel. The total phenol content of the seed was appreciably higher than that of the peels ($p < 0.01$) as was consistent with the antioxidant activity seen in both antioxidant activity assays. A significant correlation was seen between the total phenolic content and the DPPH radical scavenging activity ($r = 0.99$), or the reducing power ($r= 0.97$) of both seed and peels hence it is inferred to be responsible for the observed antioxidant activity [46]. Further work by Kaneshima et al. in relation to this study investigated and isolated the compounds in camu-camu seeds responsible for its high antioxidant activity to be vescalagin and castalagin (Kaneshima, et al. 2013).

The *in vivo* antioxidant and anti-inflammatory potential of camu-camu fruit in humans was evaluated by Inoue et al. This was done by giving 20 male smoking volunteers who are considered to have an accelerated oxidative stress state 70ml of 100% camu-camu juice (this

amount corresponds to 1050mg of vitamin C tablets) for 7 days. Urine and peripheral blood from all participants were taken before the intake of dietary supplements (that is, 100% camu-camu, vitamin C). Levels of oxidative stress markers like urine 8-hydroxy-deoxyguanosine (8- OHdG) and serum total reactive oxygen species (ROS) and levels of inflammatory markers like high sensitivity C-reactive protein (hsCRP) and multiple-cytokine were measured. The findings showed that 7 days after daily ingesting 70 ml of 100% camu-camu juice that had 1050 mg of vitamin C, oxidative stress markers (urinary 8-OHdG and serum total ROS levels), and inflammatory markers (hsCRP, IL-6 and IL-8) decreased. At the washout stage, one month after stopping camu-camu consumption, all these markers' levels except IL-6 were returned. However, similar subjects who took daily vitamin C supplements of 1050 mg did not see these alterations. These findings imply that, despite vitamin C tablets possessing comparable vitamin C content as camu-camu juice, camu-camu has stronger anti-oxidative and anti-inflammatory properties. Two possible reasons for this occurrence were stipulated by the authors. First one being that camu-camu likely possesses antioxidative compounds besides vitamin C, carotenoids, anthocyanines and so on which make it more active as an antioxidant agent. Secondly, it’s possible that camu-camu contains substances that boost the *in vivo* bioavailability to absorb or excrete vitamin C hence making it more effective (Inoue et al. 2010).

Ju et al. manufactured a biodegradable film using teff starch (TFS) films containing camu-camu extract (CCE) and determined its applicability as an antioxidant packaging by examining the radical scavenging activities of the camu-camu added to film. ABTS and DPPH radical scavenging assays were employed in the determination of antioxidant properties of the

TFS films with CCE. The CCE-containing TFS films' ABTS radical scavenging activities revealed that the films with 1.0% or 2.0% CCE eliminated 100% of the radicals. The DPPH radical scavenging activities of the TFS films, on the other hand, ranged from 42.64% to 89.19%, and the addition of 2.0% CCE resulted in the highest radical scavenging activity (Table 3). The presence of phenolic and other antioxidant compounds in camu-camu extracts boosted the antioxidant activity of the TFS film. CCE-containing TFS films act as better antioxidant packaging because they cause a rapid migration of polyphenols (compounds responsible for antioxidant activity) into the aqueous system of foods containing high water content (zju and Song, 2019).

Silva de Azevêdo et al. investigated fresh and dried (hot air dried and freeze dried) camu-camu depulping residue for its antioxidant activity using the DPPH radical scavenging assay. The antioxidant activity of both the air-dried (HAD50 and HAD80) freeze dried (FD) samples were significantly lower than that of the fresh residue (FR) with values 34.5, 28.3, 32.4, and 166.6 μmol TE/g DW respectively (Table 3). This observation was attributed to the loss of ascorbic acid due to its instability in the presence of oxygen and at high temperatures, which are seen when drying. The loss of ascorbic acid due to drying will significantly affect antioxidant activity since it is the major contributor to camu-camu fruit antioxidant capacity. (Silva de Azevêdo et al, 2014).

Fidelis et al. optimise the extraction of phenolic compounds from camu-camu seeds and assessed the antioxidant activity of the extracts. Three distinct solvents were investigated during

the extractions: ultrapure water, ethyl alcohol (EtOH), and propanone. The extractions were carried out using a 1:20 (sample:solvent, m/v) ratio. The solitary effects, binary, and ternary solvent mixtures were assessed using an augmented simplex centroid mixture design with 10 combinations of solvents. Three different antioxidant mechanisms—single electron transfer (DPPH and FCRC), transition metal ion chelation (Cu2+ chelating activity), and hydrogen atom transfer extracts (inhibition of lipid peroxidation)—were examined in the current investigation on all camu-camu seed extracts (inhibition of lipid peroxidation). The findings demonstrated that the extracts could eliminate the DPPH radical, and the ternary solvent mixture extract (water/ethyl alcohol/propanone) of ratio 0.666:0.167:0.167 and 0.333:0.333:0.334 had the highest antioxidant activity in all the antioxidant assays as shown in Table 3. The FCRC ranged from 1502 to 6909 mg GAE/100 g of seed, and the ternary mixture (0.333 water:0.333 ethyl alcohol:0.334 propanone, v/v/v) had the best antioxidant activity. The amount of pyrocatechol violet-Cu2+ complex formation that was chelated by Cu2+ ranged from 77 to 95%. The ternary mixture of water, ethyl alcohol, and propanone (0.333:0.333:0.334 and 0.666:0.167:0.167, v/v/v) presented the lowest values, indicating a higher antioxidant activity (p 0.05), as did the binary combinations of water and ethyl alcohol, water and propanone (0.5:0.5, v/v), and water and propanone (Fidelis et al., 2020).

Table 3: Antioxidant activity of different parts of camu-camu using DPPH, TP, AA, and DHA assays.

Entry	**Plant Part**	**Antioxidant test**	**Antioxidant activity**			**Ref**
1.	Fruit		**Initial stage (Full green)**	**Semi-ripe stage (Green-red)**	**Ripe stage (Red)**	Chirinos et al. 2010
		TP (mg GAE/100g FW)	1120 ± 47y	1420±193y	1320±120y	
		AA (mg/100 g FW)	2280±34y	1910±45x	2010±65x	
		DHA (mg/100g FW)	120±12x	152±9y	121±18x	
		DPPH (µmol TE/g FW)	153±8x	185±11y	167±11y	
2.	Seed		80%MeOH	Vescalagin	Castalagin	Gallic acid

Table 3, cont.

		DPPH (IC50; µg/mL)	20.5±0.4	20.9±0.2	19.4±0.4	10.1±0.2	Kaneshima et al., 2013 [28]
3.	Seed		**50% H2O+50% EtOH**		**100% EtOH**		Vieira Do Carmo et al., 2019
		FRAP (mg AAE/100 g)	8070 ± 511		2248 ± 34		
		FCRC (mg GAE/ 100g)	4918 ± 85		1502 ± 64		
		DPPH (mg AAE/100 g)	4340 ± 117		1111 ± 48		
5.	Seed coat		**H_2O**				Fidelis et al., 2018
		FCRC (mg GAE/ 100)	8522 ± 318				
		FRAP (mg AAE/100 g)	7425 ± 247				

Table 3, cont.

		DPPH (mg AAE/100 g)	2838 ± 176					
6.	Peel +pulp, Pulp, Peel, Whole fruit, and Seed		**Pulp + peel**	**Pulp**	**Peel**	**Whole fruit**	**Seed**	Grigio at al., 2017
		FRAP (mg AAE/100g)	11.7±0.2	11.7±0.3	11.7±0	11.5±0.4	8.4±0.2	
		DPPH (mg AAE/100 g)	8.53±0	8.46±0	8.53±0	8.59±0	2.45±0	
7.	Seed and peel		**Seed**			**Peel**		Myoda et al., 2010
			25%	50%	75%	25%	50%	75%
		DPPH (IC_{50} :µg/g)	12.8±0.7	15.6±0.9	20.7±0.9	36.4±2.3	27.8±1.4	37.4±1.0

Table 3, cont.

		Reducing power (abs)	0.85±0.01	0.±0.01	0.65±0.01	0.22±0.01	0.50±0.01	0.44±0.02	
8.	Fruit	**CCE conc. (%)**	**0.3**		**0.6**	**1.0**	**2.0**		Ju and Song, 2019
		ABTS (%) DPPH (%)	49.84 ± 0.59 42.64 ± 2.38		87.25 ± 1.07 72.21 ± 3.16	100.00 ± 0.00 87.28 ± 0.56	100.00 ± 0.00 89.19 ± 0.00		
9.	Fruit	DPPH (µmol TE/g DW)	**FR**		**HAD50**	**HAD80**	**FD**		Silva de Azevêdo et al., 2014
			166.6 ± 1.1		34.5 ± 0.2	28.3 ± 1.1	32.4 ± 1.6		
10.	Seed		**H_2O /EtOH/C_3H_60 0.333:0.333:0.334 (v/v/v)**		**H_2O/EtOH/ C_3H_60 0.666:0.167:0.167 (v/v/v)**	**H_2O/EtOH 0.5:0.5 (v/v)**	**H_2O / C_3H_60 0.5:0.5 (v/v)**		Fidelis et al., 2020

Table 3, cont.

		DPPH (mg AAE/100 g)	4409 ± 60	4455 ± 15	4187 ± 61	4216 ± 36	
		FCRC (mg GAE/100 g)	6909 ± 110	6264 ± 208	4354 ± 115	6579 ± 658	
		Cu^{2+} chelating activity (%)	77 ± 1	77 ± 1	77 ± 1	77 ± 1	
		Lipid peroxidation inhibition(%)	83 ± 0	84 ± 0	86 ± 0	84 ± 2	

CCE: camu-camu extract, HAD50 (hot air dried, 50 °C and 4 m/s), HAD80 (hot air dried, 80 °C and 6 m/s), FD: freeze dried, FR: fresh residue; TP: Total phenolics, AA: ascorbic, DHA: dehydroascorbic acid, DPPH: 1,1-diphenyl-2-picrylhydrazyl, FRAP: ferric-reducing antioxidant power, FCRC: Folin-Ciocalteu reducing capacity, ABTS: 2,2'-azino-bis (3-ethylbenzothiazoline-6-sulfonic acid), GAE :gallic acid equivalence, AAE: ascorbic acid equivalence,

Antimicrobial activity

Azevêdo et al. investigated fresh and dried (hot air-dried and freeze-dried) camu-camu depulping residue for its antimicrobial activities against *Staphylococcus aureus* (ATCC 29213) using the microdilution method with Ampicillin as the positive control. Two polyphenolic-rich fractions (polyphenolic-rich fraction 1 (PP1) and polyphenolic-rich fraction 2 (PP2)) were prepared from the aqueous extracts for antimicrobial activity determination. The results of the analysis revealed that, the raw extracts from samples that were hot air-dried (HAD50 and HAD80) and freeze-dried (FD) had lower MIC values comparable to standard drug ampicillin but that of the fresh residue (FR), PP1 and PP2 were relatively high (Table 4). This may be due the high concentration of bioactive compounds due to drying in the freeze dried and hot air-dried samples. Also, the synergistic interactions between the phytochemicals found on water extracts could contribute to the higher antimicrobial effects of the dried samples. These are not so for the PP1 and PP2 fractions (Silva de Azevêdo et al., 2014).

The antimicrobial activity of the optimized lyophilized extract (OLE) of camu-camu seed coat was evaluated by Willemann et al. against some selected gram-positive and gram-negative bacteria Pseudomonas aeruginosa IAL 1853, Salmonella enteritidis S2887, Salmonella Typhimurium IAL 2431, Escherichia coli IAL 2064, Bacillus cereus ATCC 14579, Staphylococcus aureus ATCC 13565, Listeria monocytogenes ATCC 7644, and Saccharomyces cerevisiae NCYC 1006 the plate-cavity agar diffusion method at a concentration of 2 mg/well. OLE showed significant inhibition (Table 4) against all the selected microbes Pseudomonas

aeruginosa IAL 1853, Salmonella Enteritidis S2887, Salmonella Typhimurium IAL 2431, Escherichia coli IAL 2064, Bacillus cereus ATCC 14579, Staphylococcus aureus ATCC 13565, Listeria monocytogenes ATCC 7644 except Saccharomyces cerevisiae NCYC 1006 (Willemann et al. 2020).

The *in vitro* antibacterial effect of camu-camu seed and pulp methanol extract against high prevalence microorganisms in the oral cavity like Streptococcus mutans (ATCC 25175) and Streptococcus sanguinis (ATCC 10556) was evaluated by Camere-Colarossi et al. using the cup-plate agar diffusion method with chlorhexidine solution as a control. Compared to the pulp extract, the *M. dubia* seeds extract demonstrated a significant antibacterial impact on both *S. mutans* and *S. sanguinis*. For both strains, the Shapiro Wilk test revealed that the extract from the seeds group does not have a normal distribution. The antibacterial activity of both seeds and pulp extracts is like that of the standard (Chlorhexidine) against both strains (Table 4). This proves that methanol was an effective solvent, capable of extracting more phenols and flavonoids to exert biological activity. However, due to antibacterial activity even at low concentrations, the MIC of the *M. dubia* seeds methanol extract could not be measured (Camere-Colarossi et al., 2016).

The antimicrobial activity of the lyophilized optimized camu-camu seed extract (LOCSE) was evaluated against Pseudomonas aeruginosa (IAL 1853), Salmonella Enteritidis (S 2887), Salmonella Typhimurium (IAL 2431), Escherichia coli (IAL 2064), Bacillus cereus (ATCC 14579), Staphylococcus aureus (ATCC 13565), Listeria monocytogenes (ATCC 7644), and

Saccharomyces cerevisiae (NCYC 1006) by Fidelis et al. using the diffusion method on plate-cavity agar. LOCSE demonstrated antimicrobial activity against all the selected microbes (Table 4) (Fidelis et al., 2020).

Table 4: Antimicrobial activity of different parts of camu-camu (*Myrciaria dubia)*

Entry No.	Plant part	Antimicrobial activity		Ref.
1.	Seed coat	Bacteria	Activity/mm	Willemann et al. 2020
		E. coli	10.5 ± 0.3	
		S. enteritidis		
		P. aeruginosa	10.5 ± 1.1	
		S. typhimurium		
		B. cereus	8.9 ± 1.6	
		S. aureus		
		L. monocytogenes	8.9 ± 1.6	
			8.8 ± 0.7	
			11.5 ± 1.1	
			11.9 ± 4.0	

Table 4, cont.

2.	Fruit	*S. aureus*	MIC (mg/ml)			Silva de Azevêdo et al., 2014
				Raw	PP1	PP2
			FR	2.5	2.5	2.5
			FD	0.3125	2.5	2.5
			HAD50	0.625	2.5	2.5
			HAD80	0.3125	2.5	2.5
			Ampicilin	0.25		
3.	Seeds		Median zone of inhibition (mm)			Camere-Colarossi et al., 2016
	Pulp		Seeds	Pulp	Chlorhexidine	
		S. mutans	17.93	16.15	23.41	
		S. sanguinis	16.50	18.61	22.56	
4.	Seed		Zone of inhibition (mm)			Fidelis et al., 2020
		P. aeruginosa	8.72 ± 1.35			
		S. Enteritidis	6.82 ± 1.36			
		S. Typhimurium	6.42 ± 1.00			
		E. coli	6.74 ± 0.80			
		B. cereus	9.04 ± 1.36			
		S. aureus	9.70 ± 1.92			
			8.58 ± 0.82			

Table 4, cont.

		L. monocytogenes S. cerevisiae	5.74 ± 0.68	

Anticancer activity

The MTT assay was used by Willemann et al. to assess the cytotoxicity of OLE towards normal (IMR90) and malignant (Caco-2, HepG2, and A549) cells. In this study, IC_{50} (OLE concentration that inhibits 50% cell growth), GI_{50} (OLE concentration that inhibits 50% cell growth relative to untreated cells), and LC_{50} (OLE concentration that causes 50% cell death) were calculated using different OLE concentrations (0, 400, 800, 1,200, 1,600, and 2,000 µg/mL). The IC_{50} values obtained ranged from 409.6 µg/mL (A549 cells) to 789.7 µg/mL (HepG2). Also, OLE reduced the viability and development of cancerous (GI50 increased from 185.0 to 237.1 g/mL) and normal (IMR90 GI50 = 199.9 g/mL) cell lines. However, when the LC50 for IMR90 was higher than 2,000 g/mL, OLE cytotoxic action against cancer cells became more substantial (LC50 from 531 to 1,404 g/mL). Vescalagin and castalagin were the primary components of OLE. Thus, we assume that the ellagitannins are responsible for the cytotoxicity seen in cells (Willemann et al. 2020).

The *in vitro* cytotoxic effect of the optimized camu-camu seed extract (LOCSE) was evaluated by Fidelis et al. against lung adenocarcinoma epithelial cell (A549), human colon

carcinoma (HCT8) and noncancerous human lung fibroblast (IMR90). The MTT (3- (4,5-dimethylthiazol-2-yl)-2,5-diphenyl tetrazolium bromide) assay was used to evaluate cell viability and the parameters IC50, GI50 and LC50 were calculated. LOCSE demonstrated cytotoxic and antiproliferative effects against A549 and HCT8 cancer cell lines in the cancer cell viability assays (LC50 HCT8 = 802.5 g/mL; LC50 A549 = 1008 g/mL). The LOCSE extract showed a biphasic effect on the behavior of cancer cells; at low concentrations (100 g/mL), it promoted cell proliferation and acted as a pro-carcinogen, but at higher doses (200 - 900 g/mL), it exhibited antiproliferative activity. Here, A549 cells showed greater resistance to the LOCSE once their GI50 values were larger (> 900 g/mL), indicating less antiproliferative activity. However, compared to A549 cells, HCT8 cells displayed increased LOCSE sensitivity since they had lower GI50 values (320.7 g/mL). Normal cell growth was not inhibited by LOCSE - IMR90, indicating the relative specificity of the extract and its safety in *in vitro* experiments (Fidelis et al., 2020).

Table 5: Anticancer activity of different parts of camu-camu (*Myrciaria dubia*)

Entry No.	Plant part	Anticancer activity				Ref.
1.	Seed coat	Cell lines	IC_{50}	GI_{50}	LC_{50}	

Table 5, cont.

		Caco-2 HepG2 A549 IMR90 (normal cell)	414.9 789.7 409.6 684.2	237.1 185.0 196.3 199.9	531.8 1404.0 735.7 >2000	Willemann et al. 2020
2.	Seed	Cell lines	IC_{50}	GI_{50}	LC_{50}	Fidelis et al., 2020
		HCT8 A549 IMR90	830.8 581.1 >900	320.7 >900 >900	802.5 1008 NC	

Willemann evaluated the ability of OLE to inhibit α-amylase and α-glucosidase. Dietary starch and polysaccharides are hydrolyzed into simple sugars by -amylase and -glucosidase. Inhibiting these enzyme activities *in vivo* decreases glucose absorption and postprandial hyperglycemia hence controlling serum glucose. This avoids clinical complications like metabolic syndrome, heart disease, renal function recession, and blindness in diabetes-II individuals. OLE at a concentration of 20 mg/mL was able to significantly inhibit the activity of α-amylase and α-glucosidase (Table 6) (Willemann et al. 2020).

An extract of camu-camu seeds (50% H2O + 50% H2O) was evaluated by Carmo et al. for its ability to inhibit the induced cisplatin chromosomal aberrations in A549 cells. Cisplatin is an anticancer medication that has high mutagenicity causing sister-chromatid exchange and the

enhancement of chromosome abnormalities. In this study, chromosome aberrations were significantly increased in cells treated with cisplatin as expected compared to the negative control group (cells received only culture medium) (Table 6). Treatment of cells with camu-camu seed extract alone did not induce significant aberrations proving its non-clastogenicity/aneugenicity. Apart from demonstrating no toxicity, the extract in comparison to cisplatin was able to protect the cells by decreasing 37% the chromosomal breaks index. This implies that camu-camu seed extract may attenuate cisplatin-induced mutagenic damage (Vieira Do Carmo et al., 2019).

A spectrophotometric test was used by Fidelis et al. to assess the extracts' angiotensin I-converting enzyme inhibitory (ACEI) activity. The seed coat extracts showed an inhibition of 28–40% of ACE I activity with the propanone extract being highest among the extracts (Table W). This study found a significant (p 0.05) and positive correlation between the levels of p-coumaric, rosmarinic, ferulic, caffeic, ellagic acids, quercetin-3-rutinoside, and quercetin with the in vitro inhibition of ACE I activity and docking molecular experiments and the structure-activity relationship show that phenolic acids and flavonoids are responsible for inhibiting ACE I (Fidelis et al., 2018).

Silva De Azevêdo et al. investigated fresh and dried (hot air dried and freeze dried) camu-camu depulping residue for its ability to inhibit alpha-amylase and alpha-glucosidase. Inhibiting alpha-amylase and alpha-glucosidase can modulate carbohydrate digestion and retard postprandial glycemia, thereby efficiently managing the early stages of diabetes type 2. All

extracts showed moderate *in vitro* alpha-amylase inhibition with FD showing highest inhibition (Table 6). The increased amylolytic inhibition seen for FD extracts may be explained by the well-preserved and concentrated active chemicals discovered in this sample. All the extracts had similarly strong alpha-glucosidase inhibitory activity (Table 6). The optimum possible antienzymatic association has been thought to be the combination of moderate alpha-amylase and robust alpha-glucosidase inhibitory activities, as this would eliminate any potential pain brought on by undigested carbohydrates and the resulting stomach distension. This ideal inhibitory combination was evident in all experimental groups, both fresh and dried (FD and HAD), indicating their suitability as dietary sources for natural antidiabetic agents (Silva de Azevêdo et al., 2014).

J. Yunis-Aguinaga et al. evaluated the effect of the oral administration of camu-camu plant on the immune and physiological parameters in Nile tilapia (*Oreochromis niloticus*). The results obtained show a significant increase in the level of white blood cells count in blood and exudate, lysozyme activity, burst respiratory activity, serum bactericidal activity, direct agglutination, and melanomacrophage centers count after 5 weeks of orally administering camu-camu plant at a dose of 500 mg/kg. The plant supplement did not appreciably improve the red blood cells count, hematocrit, hemoglobin, and biochemical profile of fish when compared with the control group. There were no histopathological lesions in the intestine, kidney, spleen, or gills of fish (Yunis-Aguinaga et al., 2016).

Table 6: Other Biological activities of different parts of camu-camu (Myrciaria dubia)

Entry No.	**Plant Part**	**Biological activity Performed**	**Activity**		**Ref.**
1.	Seed coat	Inhibition of α-amylase and α-glucosidase	**Enzyme**	**Percentage of Inhibition (%)**	Willemann et al. 2020
			α-amylase	11.9 ± 0.4	
			α-glucosidase	39.4± 0.1	
2.	Seed	Chromosomal aberration		**Chromosomal break index CBI)**	Vieira Do Carmo et al., 2019
			Cisplatin	1.62 ± 2.2	
			Negative control	0.22 ± 0.55	
			Camu-camu	0.06 ± 0.24	
3.	Seed coat	Antihypertensive activity	Extract	**%Inhibition of ACE-I**	Fidelis et al., 2018
			Propanone	40	
			Water	28	

Table 6, cont.

4.	Fruit	Antienzymatic activity		**Enzymatic inhibition (%)**		Silva de Azevêdo et al., 2014
				Alpha-amylase	**Alpha-glucosidase**	
			FR	24	95	
			HAD50	39	96	
			HAD80	42	94	
			FD	55	96	

Pharmacological potency of β-sitosterol

The equivalents of cholesterol in animal products are phytosterols, often known as plant sterols (PS). The three PS that are most prevalent are stigmasterol, campesterol, and β-sitosterol. Although PS has structures comparable to cholesterol, it is absorbed more slowly than cholesterol. Different societies and populations consume different amounts of PS. Asians and vegetarians ingest 345–400 mg per day as opposed to Western societies' 80 mg per day . Additionally, different communities have different rates of colon, breast, and prostate cancer, with Western societies having the highest rates and Asians and vegetarians having the lowest

rates. This raises the possibility that PS may act as a preventative factor in the growth of cancer (Awad et al., 2000; Gould et al., 1969; Rao and Janezic, 1992; Rose et al., 1986). β-sitosterol which has been isolated in many plants including camu-camu (*Myrciaria dubia*) has been found to possess anti-inflammatory, anticancer, antimicrobial, hypocholesterolemia activity and angiogenic and analgesic effects among many other pharmacological applications (Saeidnia et al. 2014).

Green synthesis of spiro compounds (Part b)

Spirocyclic compounds

Spiro-cyclic compounds have been reported to show better pharmacokinetic properties due to their ability to bind to target protein with reduced conformational entropy and restriction. Spiro-cyclic scaffolds' noncoplanar structure can also help them conform selectively to their targets (Zheng et al., 2014; Zhao and Akritopoulou, 2010; Welsch et al., 2010). Compared to flat aromatic compounds, spiro-containing systems not only have more than three dimensions, but also add novel structural elements for patentability. Although flat aromatic rings and spirocyclic rings can both affect the ligand binding entropy, it has been proposed that compounds with an excessive number of flat rings have poor suboptimal physical characteristics and are less likely to be effectively developed as drugs (Aldeghi et al., 2014; Richie et al., 2009; Lovering et al., 2009; Lovering, 2013). Due to these reasons, interest in incorporating these compounds in drug synthesis have grown in recent times even though it is frequently linked to greater synthetic effort as a result of more synthetic processes, stereocenters, or uncommon reaction techniques

(Hiesinger et al., 2021). A number of marketed drugs that have the spiro scaffold incorporated in them is seen if Figure 1.

The first spirocyclic compound to be discovered was spironolactone (Figure 1**)** in 1957. Its discovery was a breakthrough in the development of mineralocorticoid receptor (MR) antagonists. The combination of antimetallocorticoid activity and the cardio tonic effects of digitoxin, which carries a lactone ring, was what spurred the addition of the spirolactone moiety to the progesterone molecule. Unexpectedly, the spirolactone series demonstrated oral bioavailability and inhibited aldosterone activity, which finally resulted in the drug's approval in 1959. Spirolactone antiandrogens continued to be developed over the years, which eventually led to the making of progestogens. Drospirenone, a progesterone analog having antiandrogenic and antiminer allocorticoid activity, was created in 1976 and received approval as a contraceptive in 2000 (Garthwaite and McMahon, 2004; Cella et al. 1959; Cella and Tweit, 1959; Quintavalla, 2018; Elger et al. 2003). Pyrazolo pyridine derivatives have also shown potential biological activity against diabetes, dementia, depression, bipolar disorder, Alzheimer's disease, schizophrenia, as well as acting as enzyme inhibitors (Dress et al., 2005; Kung and Wager, 2005; Swetha et al., 2018). These compounds have therefore attracted the attention of researchers and have been incorporated into the synthesis of bioactive compounds (Ibrahim et al., 2018).

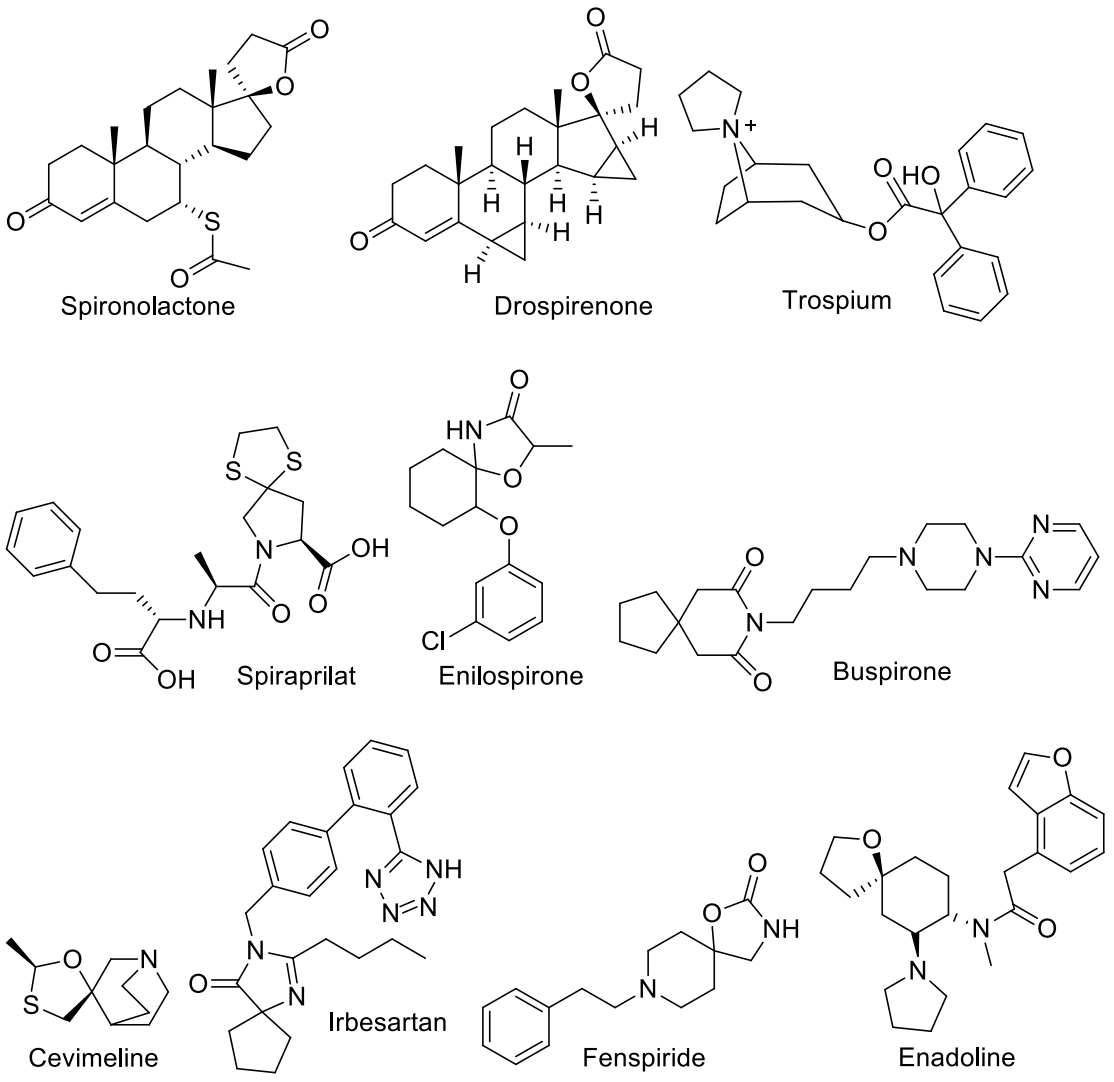

Figure 1: Marketed drugs with spiro scaffold in its structure

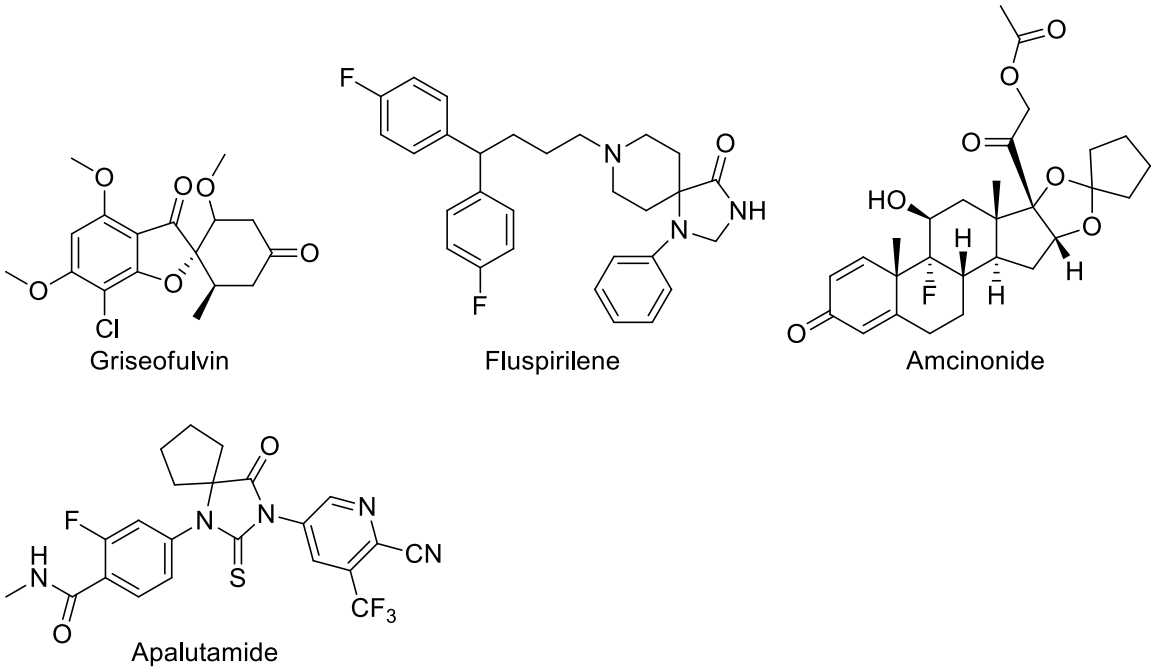

Figure 1, cont.

Biological activities of different derivations of spiro cyclic heterocyclic compounds

A series of novel pyrazolo[3,4-b] dihydropyridine-based spiro-oxindoles were synthesized and their anticancer potential was evaluated by Ibrahim et al. Two compound **17** and **18** were found to show exception potency and broad spectrum of anticancer activity. Both **17** and **18** compounds greatly inhibited p53-MDM2 interaction with IC50 values of 52.1 ± 1.39 and 95.2 ± 2.2 nM respectively. At the cellular level, compound **17** significantly elevated p53 and p21 levels and differentially caused apoptosis in p53 wild-type MCF-7 cells compared to p53 mutant MDA-MB-231 breast cancer cells. Mechanistically, the inhibited p53-MDM2 protein–protein interaction by **17** and **18** resulted in the restoration of p53 activity in cells harboring wild-type

p53 and bring about the release of p53 transcriptional activity and increase in the level of its targeted gene product p21 protein. Once activated, p53 ought to trigger apoptosis to eliminate the cancer cells that are damaged [65].

An efficient and fast microwave-promoted one-pot synthesis of different spiro[indoline-3,4′-pyrazolo[3,4-b] pyridine derivatives was conducted by Naglaa et al. The antioxidant, cytotoxicity, and antimicrobial activities of the novel compounds were analyzed. Using the phosphomolybdenum antioxidant method, the synthesized compound's total antioxidant capacity (TAC) was evaluated. Compounds **19** – **24** were found to show very good antioxidant activity due to the presence or absence of certain functional groups like carbonyl, hydroxyl, methoxy, and carboxylic groups which are able to reduce Mo(VI) to Mo(V) forming a green phosphate/Mo(V) complex at pH acidic. When tested for cytotoxicity compounds **22, 24, 25, 26,** and **27** showed potent cytotoxicity against the three selected human tumor cells HePG2 H, CT-116, and MCF-7. Compounds **19** – **24** showed high antimicrobial activity against gram positive *Staphylococcus aureus* and gram-negative *Pseudomonas aeruginosa* bacterial strains as well as two different fungi *Candida albicans* (yeast) and *Aspergillus niger* (fungus) [16].

One-pot synthesis with recyclable NiO-SiO2 as a catalyst was conducted by Yagnam et al. to produce biologically active new spirooxindole-fused pyrazolo pyridine derivatives. These compounds were analysed for their antimicrobial activity against *Klebsiella pneumoniae, Staphylococcus aureus, Escherichia coli, Bacillus subtilis, Candida albicans, and Aspergillus fumigatus.* Of the synthesized compounds, compounds **28 – 32** showed potent antimicrobial

activity. Compound **28** had both antibacterial and antifungal activity and was able to inhibit all the tested microbes to a good extent. Compounds **30, 31** and **32** showed antifungal activity against *Candida albicans, and Aspergillus fumigatus* and **28**, **29**, and **31** showed good antimicrobial activity against all gram positive and gram-negative bacteria. The substituted functional groups of the isatin ring [5-methyl(**29**) and 4,7-dichloro(**32**)] are thought to have a substantial role in the microbial inhibitory activity, according to analysis of the structure-activity relationship [64].

A four-component one-pot reaction domino reactions was used to synthesize spiro[indoline-3,4'-pyrazolo[3,4-b]pyridine derivatives by Ibrahim et al.. The insecticidal and fungicidal activities of the synthesized novel compound was evaluated against cotton leafworm *Spodoptera littoralis* and soil-borne fungi *Rhizoctonia solani* and *Fusarium solani* respectively. For the insecticidal activity, the standard insecticide, chlorpyrifos-ethyl was used as a positive control to compare the potency of the synthesized compounds. Of the synthesized derivatives, compound **33** showed the highest insecticidal activity in comparison to chlorpyrifos-ethyl. However, even the activity of compound **33** was very low as it showed 1.2% toxicity as compared to chlorpyrifos-ethyl. In other words, chlorpyrifos-ethyl has 89.9-fold activity higher than compound **33** meaning the synthesized derivatives have very low insecticidal activity against the selected pest. The *in vitro* antifungal activity of the synthesized derivatives against *Rhizoctonia solani* and *Fusarium solani* soil-borne fungi showed that compound **34** has high potency against *Rhizoctonia solani* when compared to standard fungicide pencycuron.

Compound **34** had 1.12-fold fungicidal activity as that of the standard drug pencycuron making it very comparable in activity as the standard. Compounds **33** and **35** also showed moderate fungicidal activity against *Rhizoctonia solani* as compared with standard. Compound **36** was found to show comparable fungicidal activity as standard drug pencycuron against *Fusarium solani.* The substituent 2-nicotinoyl at position 50 of the pyrazolopyridine ring system may cause good fungicidal activity of derivatives **34** and **36** against the tested fungi [67].

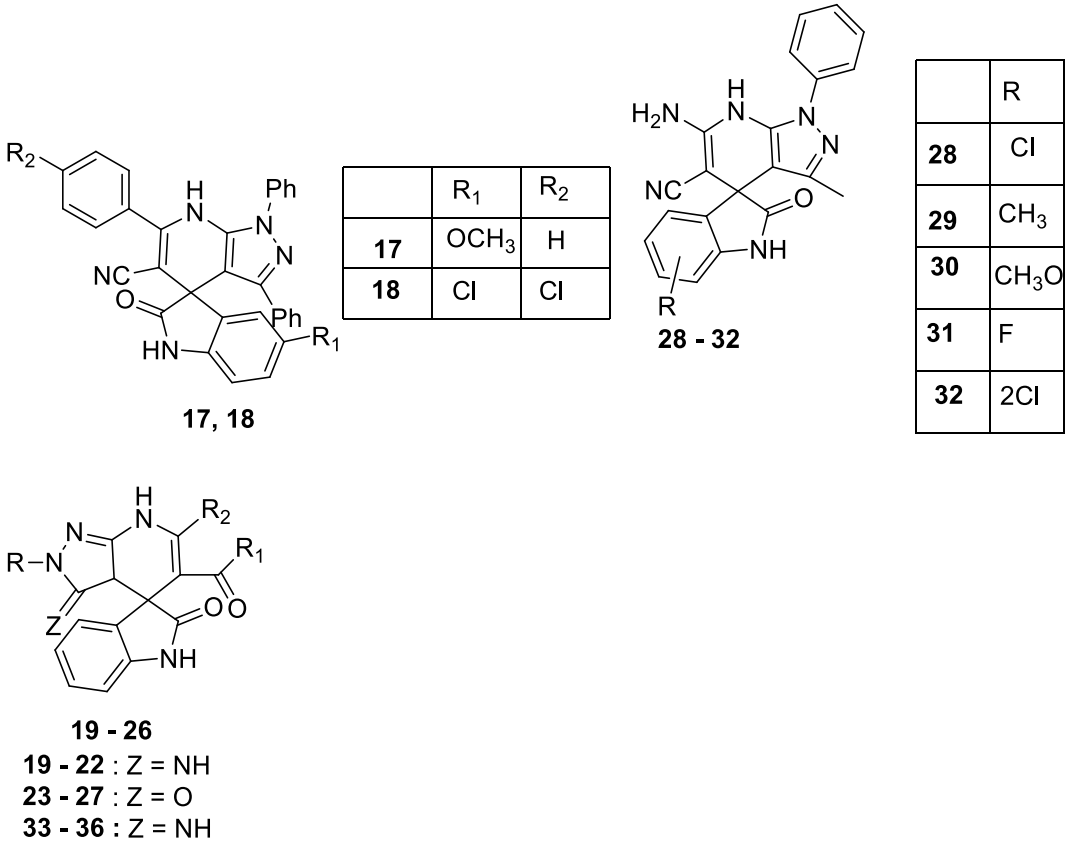

	R_1	R_2
17	OCH_3	H
18	Cl	Cl

Figure 2: Structures of synthesized spirocyclic derivatives

CHAPTER III

METHODOLOGY

Camu-camu (*Myrciaria dubia*) (Part A)

Experimental

A series of experiments have already been conducted by a senior lab mate Mr. Jorge Flores to a certain point from where I took over from. He extracted non-polar components of camu-camu leaves using diethyl ether (DEE) as solvent. He was able to isolate four pure compounds from the DEE leaf using column chromatography. There were compounds present in the DEE leaf extract that were not pure yet and my research was to put these compounds together and separate the compounds.

This section outlines the work I have conducted on camu-camu DEE fraction after taking over from Jorge Flores (Flores, 2020).

Characterization of an isolated compound

Melting point of the synthesized products were determined using Barnstead Thermolyne, Electrothermal Mel-temp. NMR spectra was determined on Bruker Ascend 500 MHz with with DMSO as solvent and TMS as an internal standard. Bruker 600 MHz. Spectra were generated using TopSpin software. Bruker Alpha modular Platinum-ATR FT-IR Spectrometer was used for the FT-IR spectrum. Mass spectrum was determined using Advion expression s compact mass spectrometer.

Green synthesis (Part b) Experimental

Chemicals and apparatus

All materials used in the experiment were commercial reagent grade and were not further purified before use. All solvents for entire experimental procedures were purchased from Fisher-Scientific (Pittsburgh, PA) and all additional chemicals were purchased from Sigma-Aldrich Corporation (St. Louis, MO). The Anton Paar Microwave Synthesis Reactor was used for microwave irradiation. UltraPure Silica Gels (Silicycle) was purchased from 2500, boul. du Parc-Technologique, Québec (Québec) G1P 4S6 CANADA. The melting point of the synthesized products were determined using Barnstead Thermolyne, Electrothermal Mel-temp. NMR spectra were determined on Bruker Ascend 500 MHz with DMSO as solvent and TMS as an internal standard. Bruker 600 MHz. Spectras were generated using TopSpin software. Bruker Alpha modular Platinum-ATR FT-IR Spectrometer was used for the FT-IR spectrum. The mass spectrum was determined using Advion expression s compact mass spectrometer.

Optimization of reaction for solvent selection

To identify the best solvent conducive for the experiment, an optimization was conducted using different solvents namely: Water, toluene, ethyl acetate, ethanol, methanol, and acetonitrile under the same reaction conditions. The products were washed with dichloromethane and dried using vacuum filtration. The resulting masses were measured and compared for best solvent.

General procedure for preparation of spiro indoline pyrazolo-pyridine compounds

To 1 mmol each of ethyl acetoacetate and hydrazine hydrate, 0.5ml of N, N-Diisopropylethylamine (DIPEA) catalyst was added and put in a microwaved synthesizer at 80°C for 5minutes. To the same reaction, 1 mmol each of malononitrile and isatin was added along with deionized water (approximately 0.5 ml) as a solvent and irradiated in a microwave synthesizer for 5 minutes at 80°C. 2 mmol of ammonium acetate was then added as a source of nitrogen along with deionized water (approximately 0.5 ml) and finally irradiated for 5mins at 80°C. TLC was used to monitor the end of the reaction. Several components of the reaction were changed as shown in table 7 to produce different derivatives of the spiro compounds.

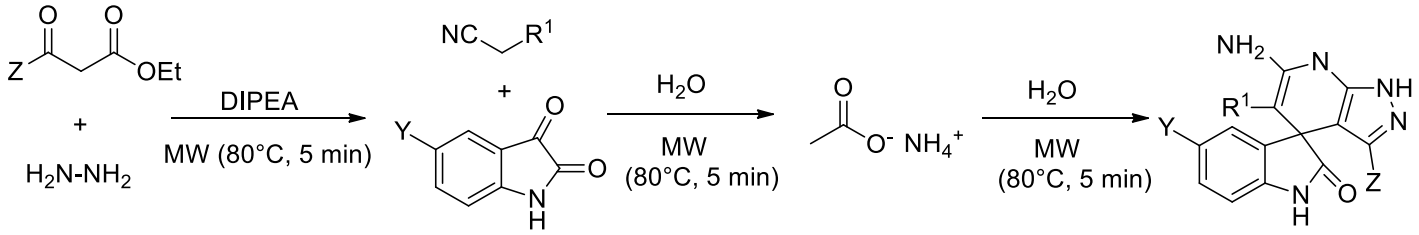

Figure 3: General synthetic reaction scheme for DBJA 1, 2, 3, 4, 9, and 11

Table 7: Reaction components and time for the synthesis of DBJA-1, 2,3,4,9 and 11

Entry	**1,3-diketo (A)**	**Hydroxyl Amine (B)**	**Activated Methylene (C)**	**Isatin (D)**	**Nitrogen source**	**Time/ min**

Table 7, cont.

DBJA 1	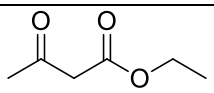	$NH_2—NH_2$	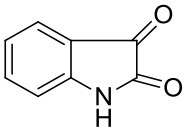	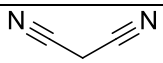	NH_4OAc	15
DBJA 2	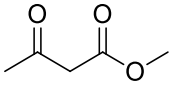	$NH_2—NH_2$	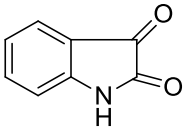	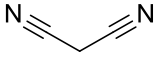	NH_4OAc	15
DBJA 3	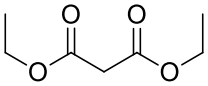	$NH_2—NH_2$	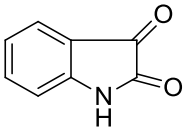	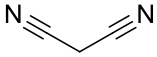	NH_4OAc	25
DBJA 4	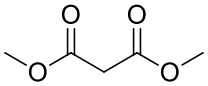	$NH_2—NH_2$	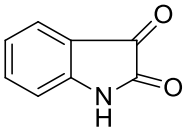	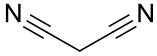	NH_4OAc	15
DBJA 9	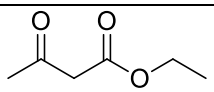	$NH_2—NH_2$	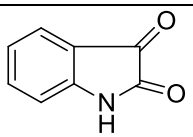	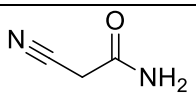	NH_4OAc	15
DBJA 11	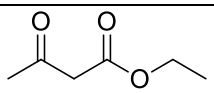	$NH_2—NH_2$	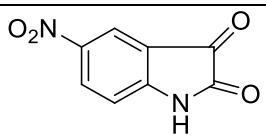	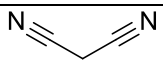	NH_4OAc	15

Isolation of pure product

The impure product from reaction mixture was purified in either of two ways.

1. Reaction 1 - 4 were washed with dichloromethane (DCM) or methanol to obtain pure product using vacuum filtration.

2. Column chromatography of silica gel was used to isolate the pure compound from the reaction mixture of Reaction 5 – 6 using ethyl acetate – hexane and methanol – ethyl acetate as solvent.

Pure isolated compounds were characterized using Fourier Transform Infrared (FTIR) spectroscopy, mass spectroscopy (MS), and nuclear magnetic resonance (NMR) spectroscopy.

CHAPTER IV

RESULTS AND DISCUSSION

Camu-camu (*Myrciaria dubia*) (Part A)

Characterization of steroid 1

Steroid 1: Rf: 0.57 (25% ethyl acetate in 75% hexanes); MP: 132.7 – 133.8 °C; IR (cm^{-1}): 3428 (OH), 2932 (CH_3), 2863 (CH_2), 2850 (CH_2), 1640 (C=C); ^{1}H NMR (600 MHz, DMSO) δ 0.67 – 3.53 (m, 51H), 5.34 (q, J = 1.88 Hz, 1H), 5.35 (d, J = 1.88 Hz, 1H); ^{13}C NMR (150 MHz, DMSO) δ 11.87,11.99, 18.79, 19.05, 19.40, 21.09, 23.04, 24.31, 26.11, 28.25, 29.18, 31.92, 33.97, 36.15, 35.51, 37.27, 39.79, 42.30, 42.33, 45.86, 50.15, 56.08, 56.78, 71.82, 121.72, 140.77 ppm; MS: expected mass = 414.39 m/z, mass found = 411.36 m/z (M - 3).

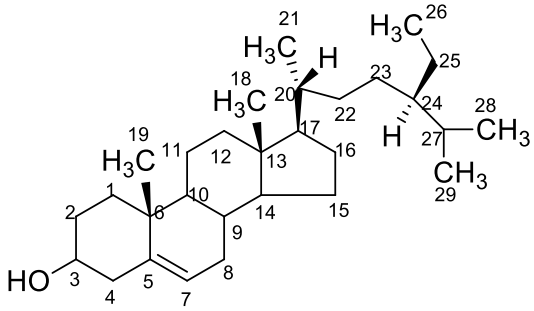

Figure 4: structure of steroid 1

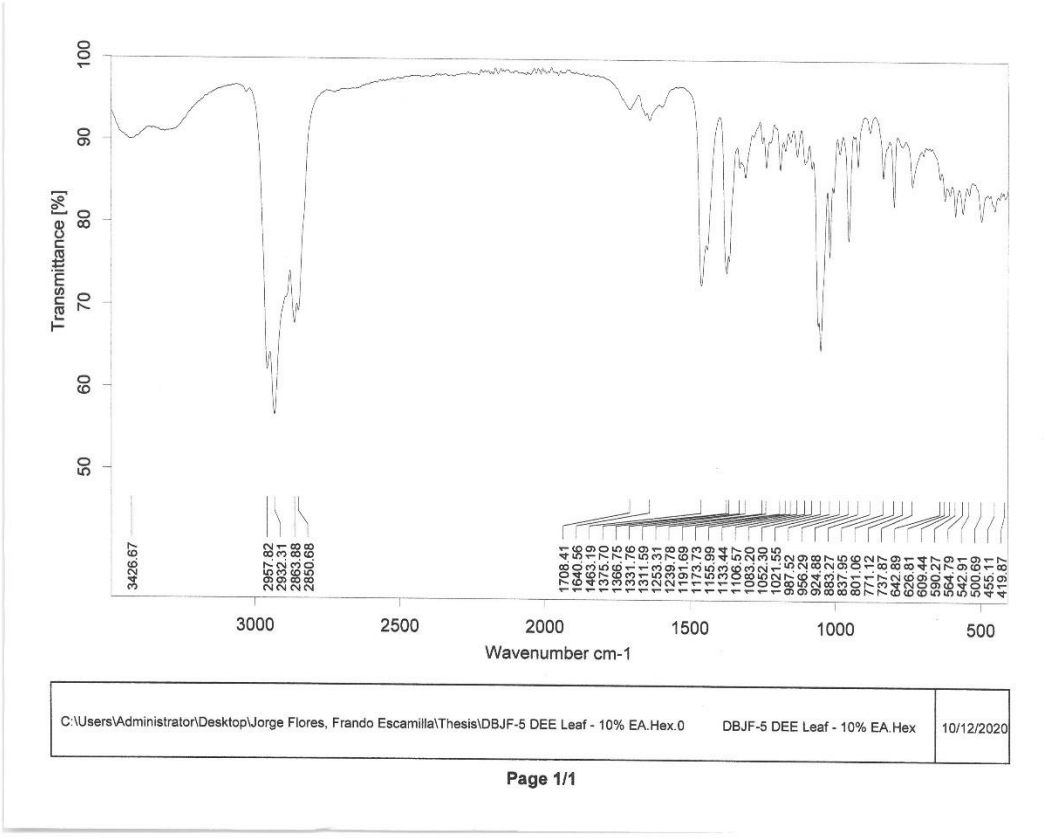

Figure 5: FT-IR spectrum of steroid 1

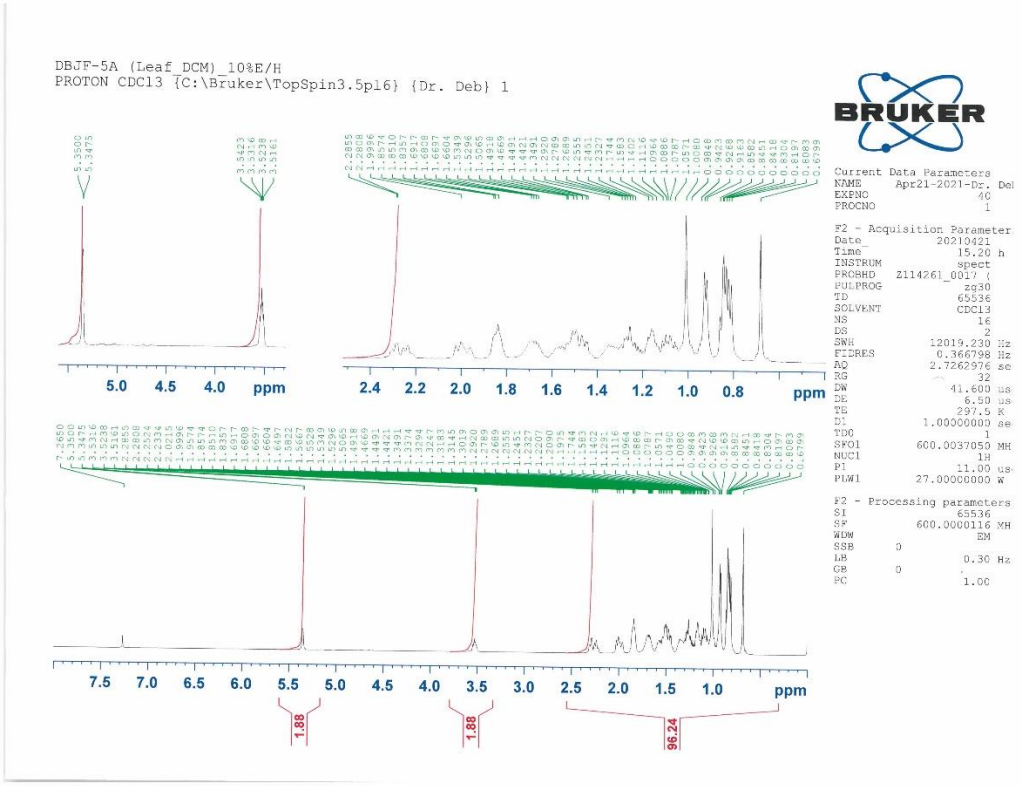

Figure 6: ^{1}H NMR of steroid 1

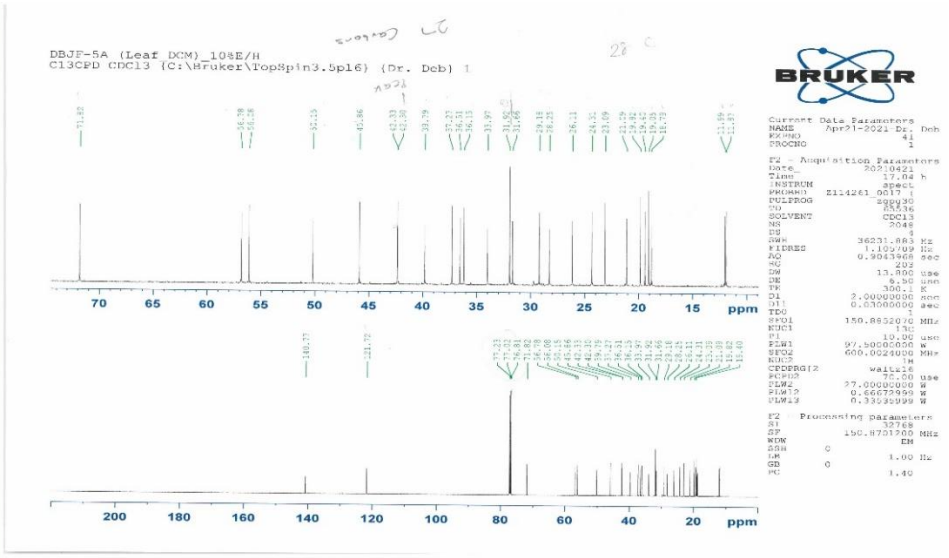

Figure 7: ^{13}C NMR of steroid 1

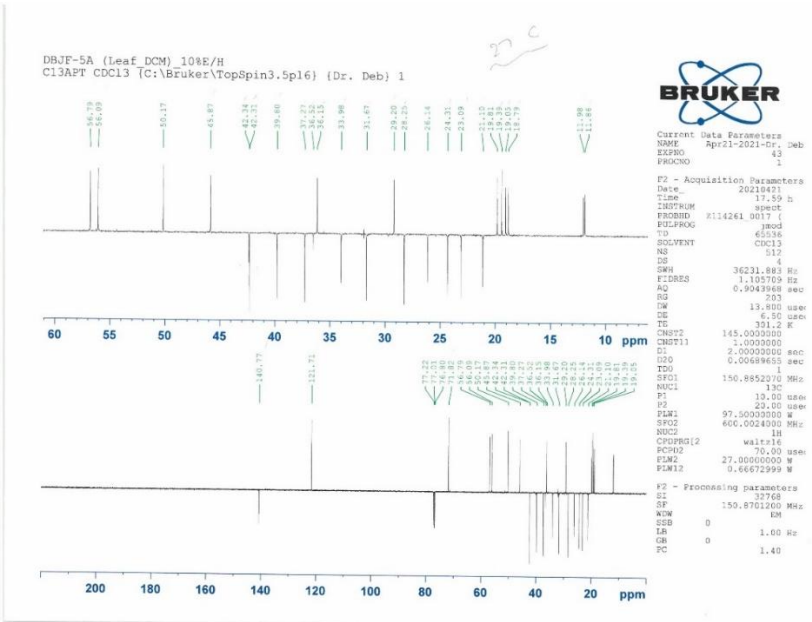

Figure 8: C^{13}APT NMR of steroid 1

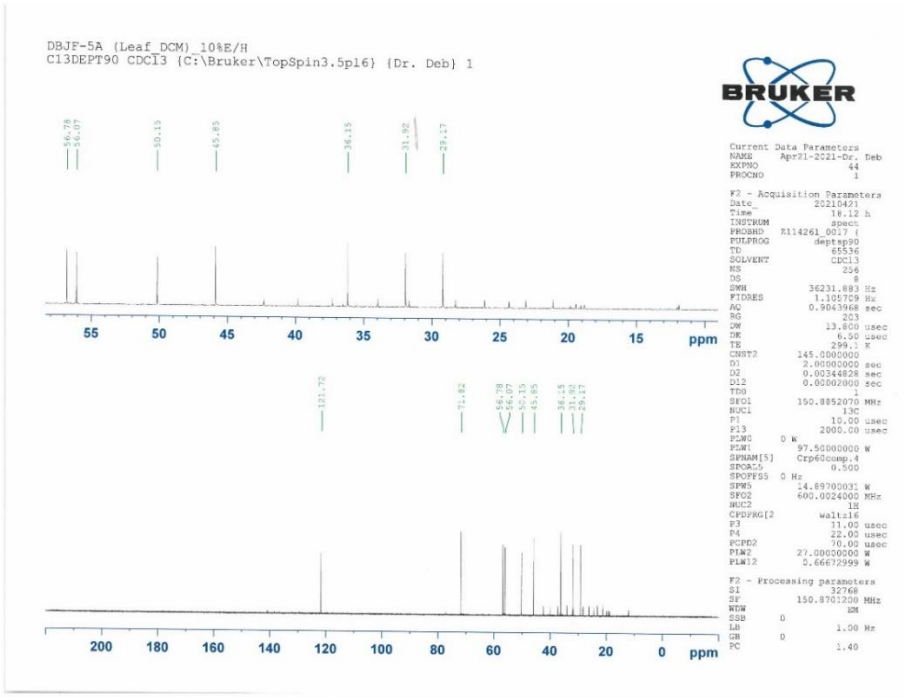

Figure 9: C^{13}DEPT90° NMR of steroid

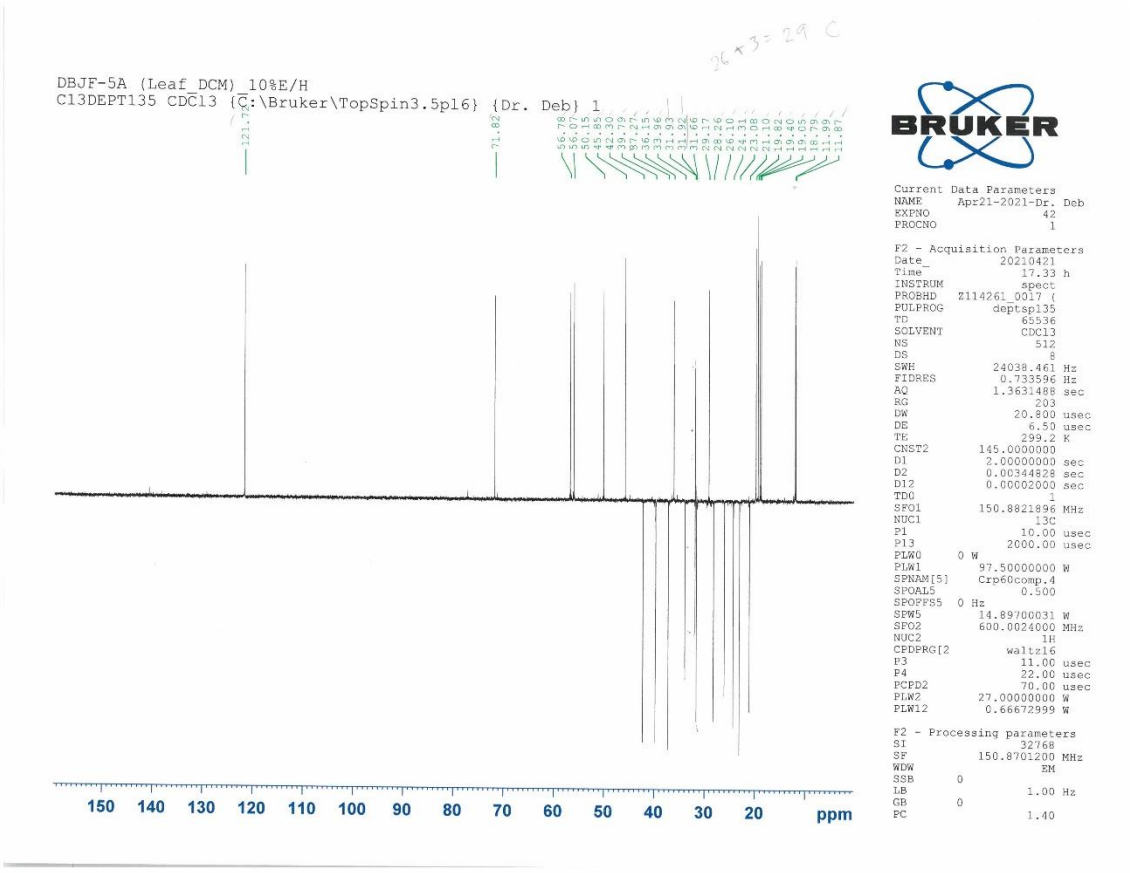

Figure 10: C^{13}DEPT135° NMR of steroid 1

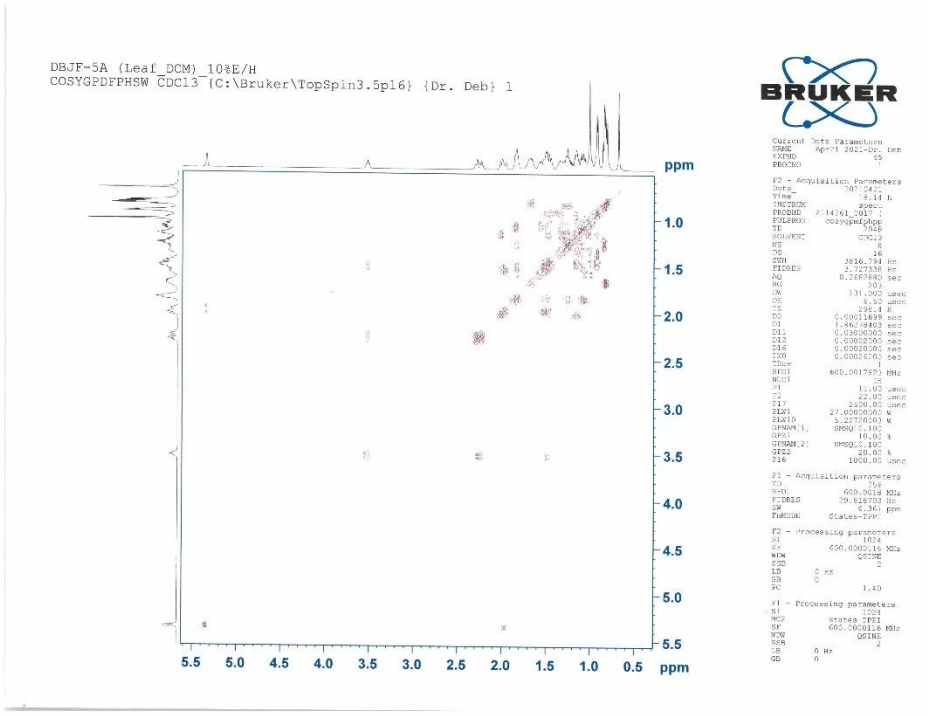

Figure 11: COSY of steroid 1

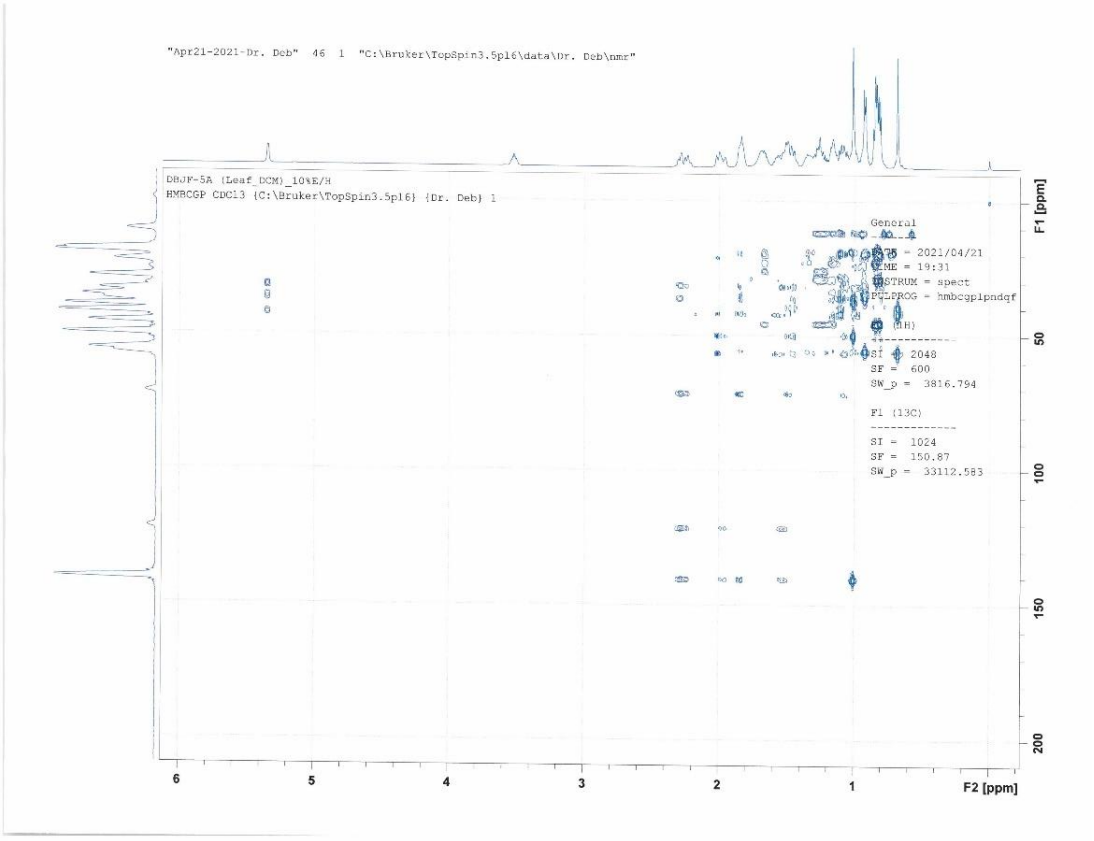

Figure 12: HMBCGP of steroid 1

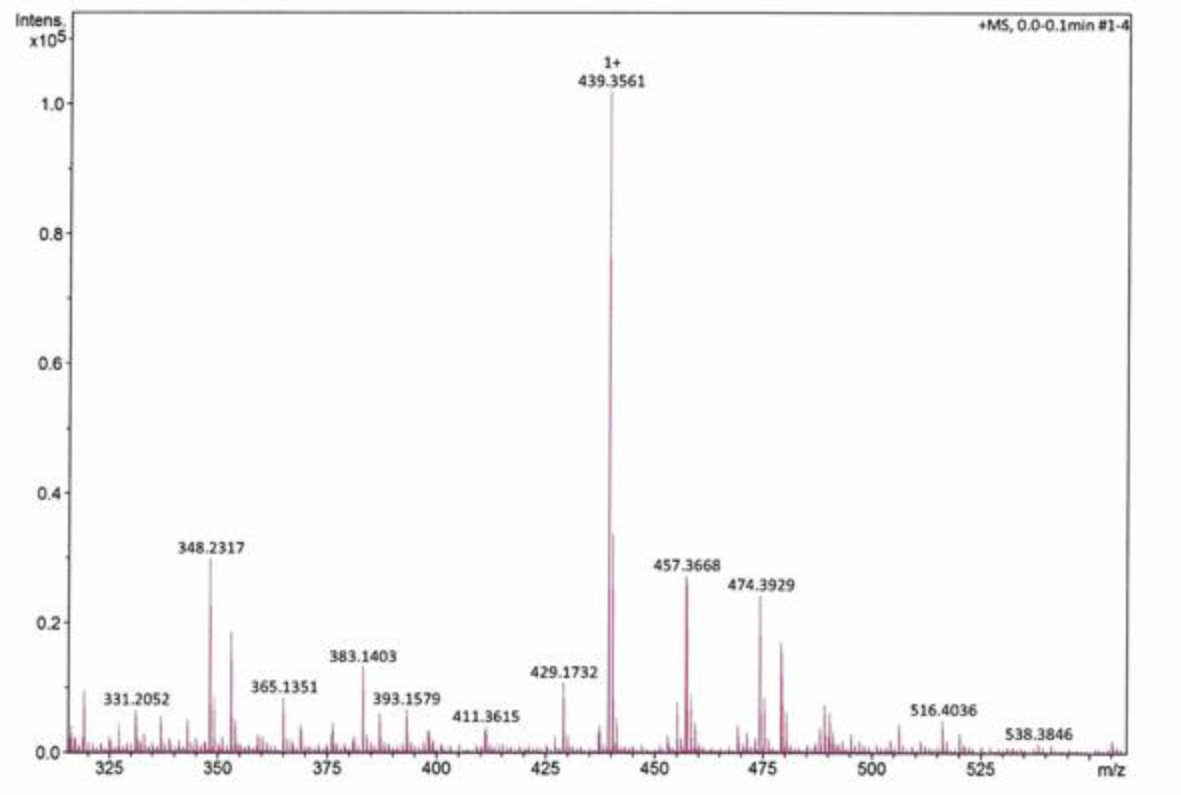

Figure 13: Mass Spectroscopy of steroid 1

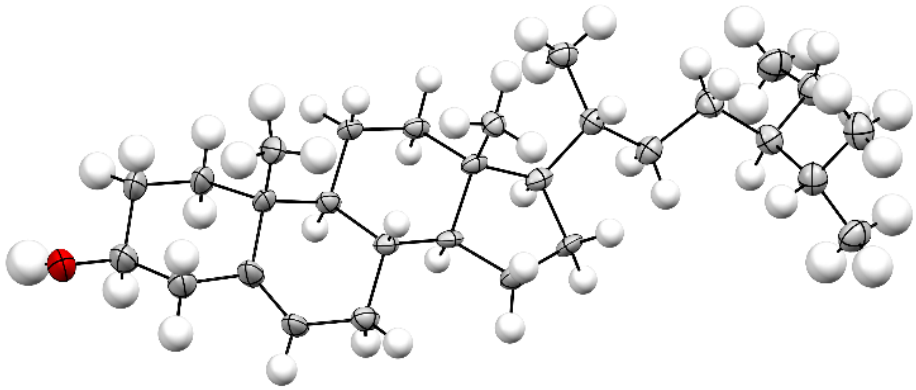

Figure 14: X-ray structure of steroid 1

Table 8: Different carbon positions in steroid 1 and their chemical shifts

Position	**Type**	**Chemical shift, δ (ppm)** ^{13}**C NMR**
1	CH_2	37.27
2	CH_2	31.66
3	CH(OH)	71.82
4	CH_2	42.30
5	C(=)	140.77
6	C	37.27
7	CH(=)	121.72
8	CH_2	33.97
9	CH	31.92
10	CH	50.15
11	CH_2	21.09
12	CH_2	39.79

Table 8, cont.

13	C	42.33
14	CH	56.78
15	CH_2	26.11
16	CH_2	24.31
17	CH	56.08
18	CH_3	11.87
19	CH_3	18.79
20	CH	36.15
21	CH_3	19.05
22	CH_2	33.97
23	CH_2	26.11
24	CH	45.86
25	CH_2	23.09
26	CH_3	11.99
27	CH	29.18

Table 8, cont.

28	CH_3	19.82
29	CH_3	19.40

The FT-IR spectrum of the isolated steroid confirmed the presence of the broad, weak O-H stretch at 3428 cm^{-1}. The presence of alkane functional group was observed at absorbances of 2957 and 2932 cm^{-1} for methyl carbon (CH_3) and 2863 and 2850 cm^{-1} for methylene (CH_2) carbons. A C=C stretch was observed at 1640 cm^{-1} signifying the presence of the unconjugated olefinic carbons. In the proton NMR of steroid, a singlet peak observed at 0.69 and 1.00 ppm represents the chemical shift observed by the methyl carbons attached to the quaternary carbons. The complex multiplex observed at 2.00 and 2.30 ppm is caused by the chemical shift experienced by the two methylene carbons adjacent to the C-OH carbon. The proton attached to C-OH experienced a chemical shift that caused a multiplex at 3.54 ppm. The presence of an olefinic proton was confirmed by the chemical shift it experienced as a multiplex at 5.37 ppm. The ^{13}C NMR spectrum of steroid showed 29 carbon atoms present in steroid structure. ^{13}C APT, DEPT90 and DEPT135 confirmed the presence of 6 methyl carbons, 11 methylene carbons, 9 methine carbons and 3 quaternary carbons as consistent with structure. Some notable signals in the ^{13}C NMR are the two methyl carbons attached to the quaternary carbon of 19 and 11 ppm. The C-OH carbon also gave a signal of 71 ppm and finally the two carbons of the C=C bond showed signals at 140 and 121 ppm. 2D NMR spectra (COSY and HMBCGP) was also used to

confirm the structure of the isolated steroid by showing the proton-proton correlations and proton-carbon correlations. The mass spectrum showed a strong peak at 439 m/z which is 25 higher than the expected mass of 414 m/z which can be due to the addition of a Na atom and two hydrogen atoms. The peak at 411 m/z corresponds to M-3 or the loss of three hydrogen atoms.

Green synthesis of spiro compounds (Part b)

Optimization of solvent for reaction

Table 9: Solvents used for reaction and masses of products obtained

Solvent/ml	Mass of product/g	Yield/%
Water	0.239	82
Toluene	0.189	64
Methanol	0.188	63
Ethyl acetate	0.183	57
Ethanol	0.166	64
Acetonitrile	0.147	50

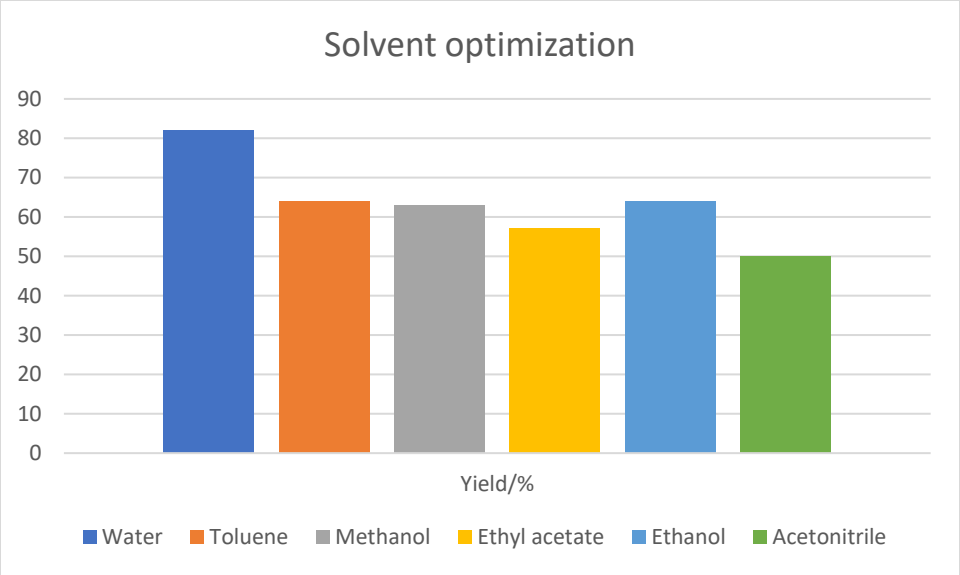

Fig 15: Optimization with different solvent to determine solvent with highest product yield.

From the data obtained, water gave the highest product when compared to all the other solvents with a mass of 0.239g. The use of water in place of the conventional organic solvents provides a smooth condition for the reaction to occur hence the improved yield and selectivity observed (Das and Banik, 2020). One of the reasons for the improved results is because water minimizes the Gibbs energy of solvation by excluding nonpolar species of the reactants causing the hydrophobic surfaces of the reactants to interact strongly to produce the desired product selectively. This phenomenon is known as the hydrophobic effect. However, in organic solvents, these forces appear to be too weak to compete with the steric and electronic effect hence reducing selectivity (Wu et al., 2004). Besides giving a high yield of product, water is also considered to be a very eco-friendly solvent and its use in a reaction is considered a green approach. Water is cheap and has low toxicity and products obtained from its reaction can be

easily purified using filtration (Khetmalis et al., 2021). From this study, water gave the highest yield of 82% and acetonitrile had the lowest yield of 50%.

Results for the synthesis of spiro[oxindole pyrano pyridine]

Table 10: Mass of product, percentage yield, melting point, and color of reaction products

Compound	**Product/g**	**Yield/%**	**Melting point/°C**	**Color**
DBJA 1	0.239	82	269 – 270	Light pink
DBJA 2	0.076	26	269 – 270	Cream
DBJA 3	0.120	41	229 – 230	Orange
DBJA 4	0.174	60	216 – 220	Yellowish green
DBJA 9	0.105	36	202 – 206	Light yellow
DBJA 11	0.275	94	254 – 256	Cream

Characterization

1. **Characterization of DBJA-1**

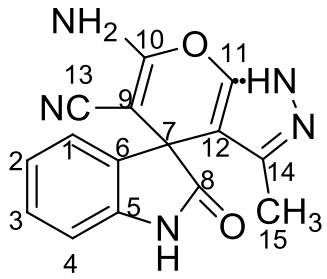

Figure 16: Structure of DBJA-1

DBJA-1: MP 269 – 270°C; IR (cm^{-1}): 3335.92 (NH_2), 3258.98 (CONH), 3129.95 (Ar), 2181 (CN), 1708.72 (CO); ^{1}H NMR (600 MHz, DMSO) δ 1.53 (s, *J* = 21.88 Hz 3H), 6.91 (m, *J* = 21.88 Hz, 3H), 7.3 (q, *J* = 22.17 Hz, 3H) 10.58 (s, *J* = 7.39 Hz, 1H), 12.27 (s, *J* = 7.35 Hz, 1H); ^{13}C NMR (150 MHz, DMSO) δ 9.41, 47.76, 55.67, 95.88, 110.12, 119.17, 122.95, 124.98, 129.35, 133.16, 135.16, 141.99, 155.74, 162.94, 178.47 ppm. MS: 293 m/z (M)

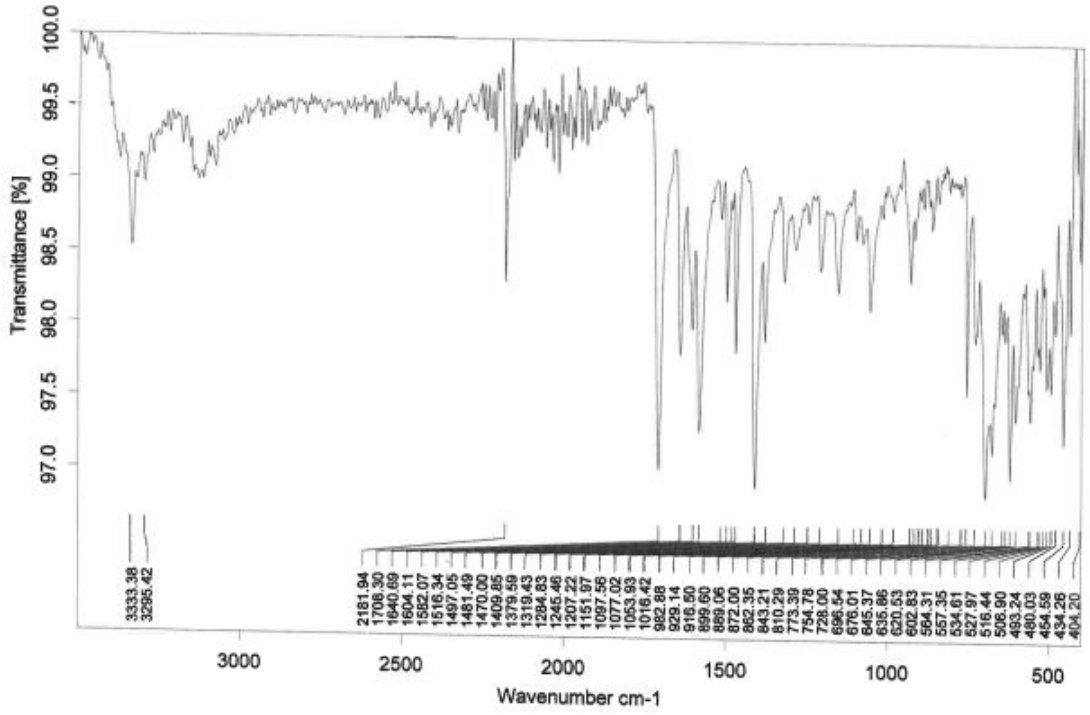

Figure 17: FT-IR spectrum of DBJA-1

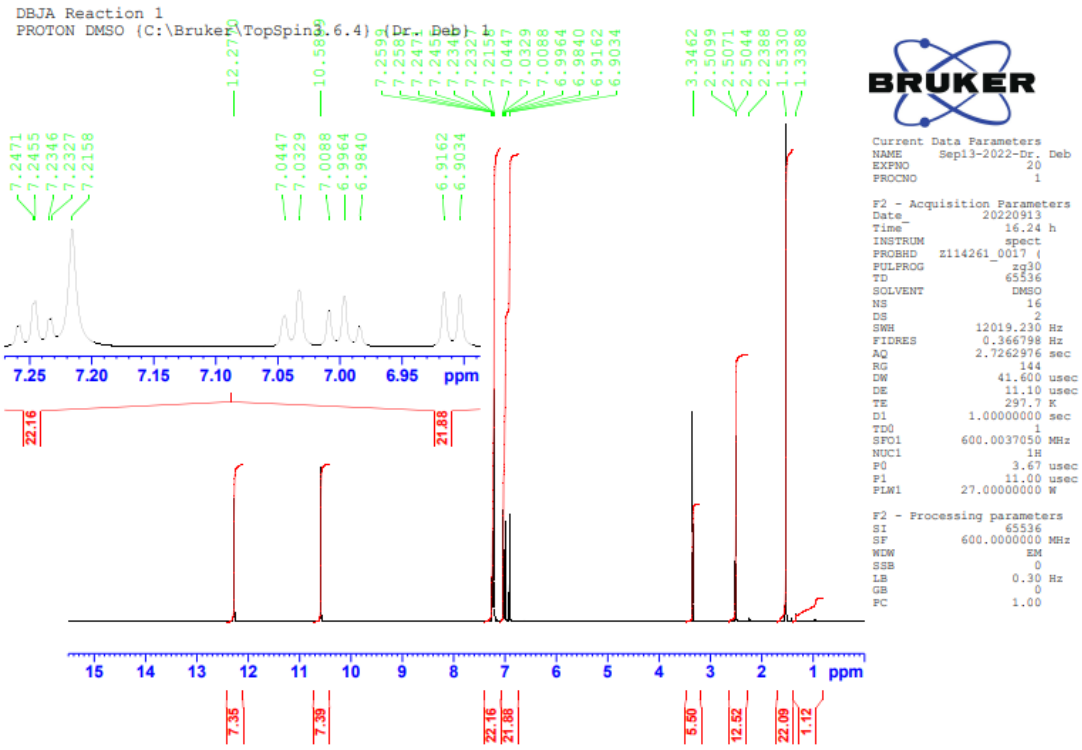

Figure 18: ^{1}H NMR spectrum of DBJA-1

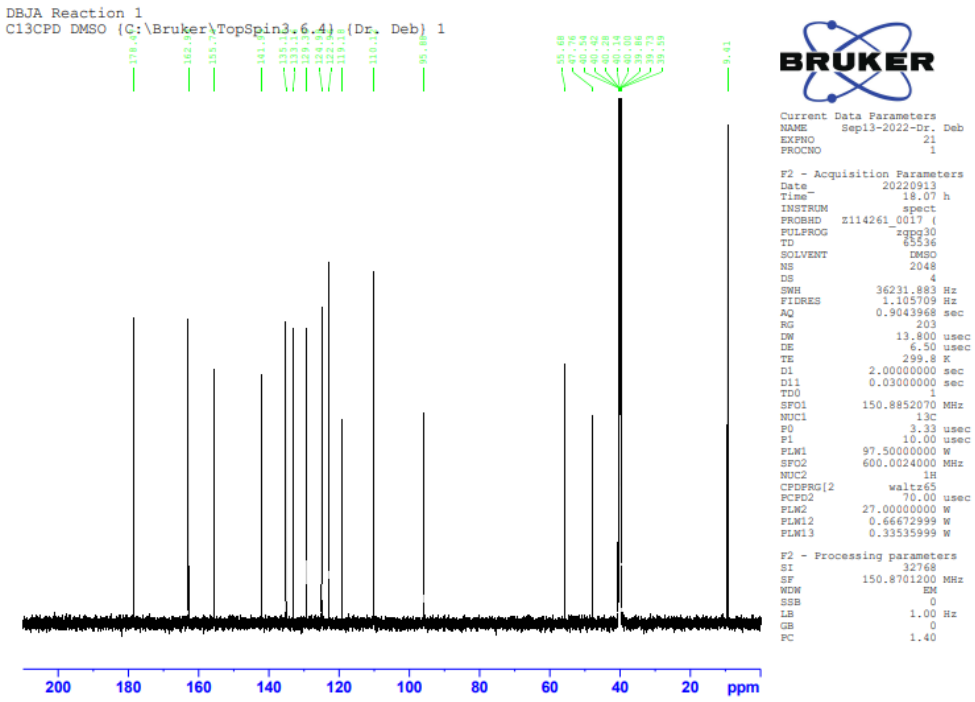

Figure 19: C^{13} NMR spectrum of DBJA-1

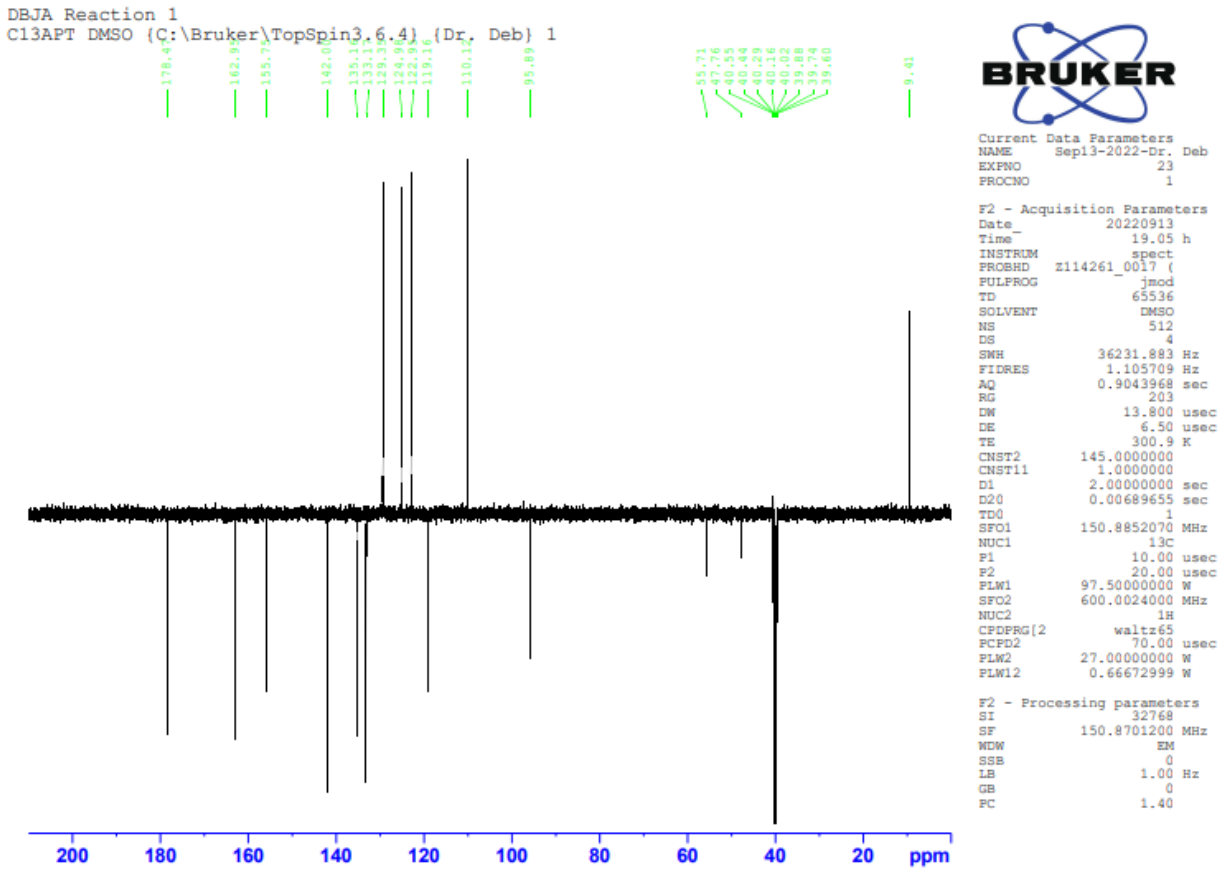

Figure 20: C^{13}APT NMR spectrum of DBJA-1

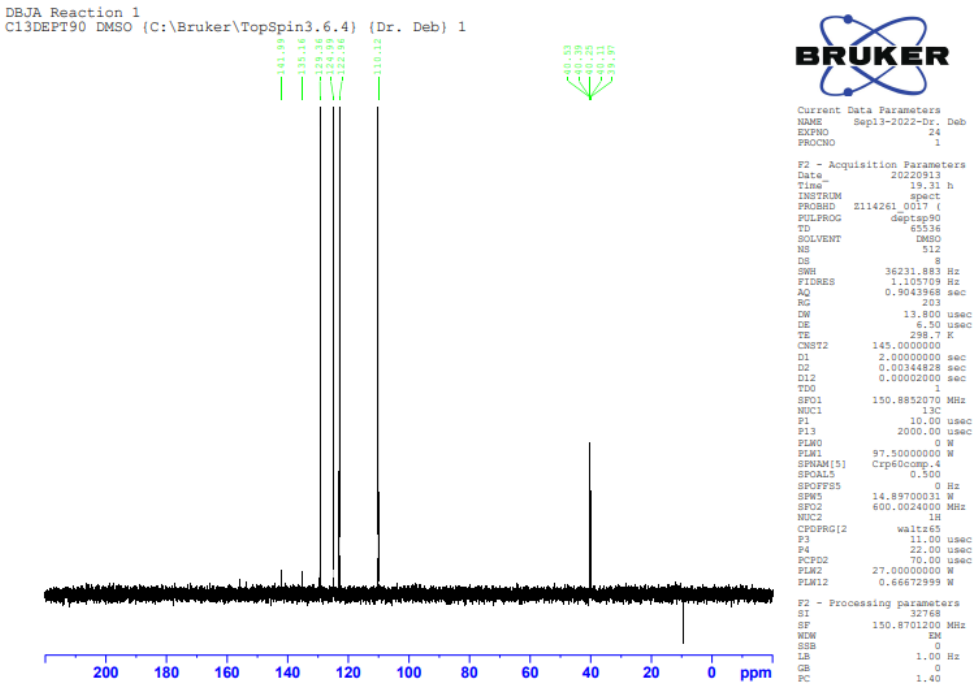

Figure 21: C^{13}DEPT90° NMR spectrum of DBJA-1

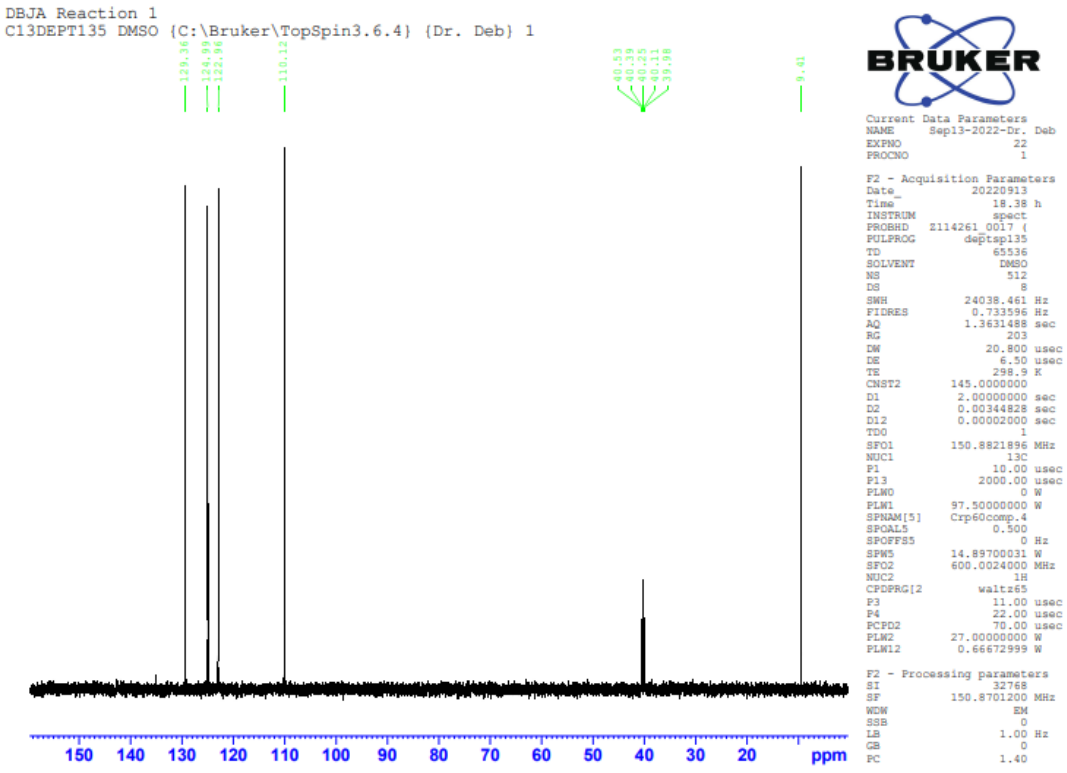

Figure 22: C^{13}DEPT135° NMR spectrum of DBJA-1

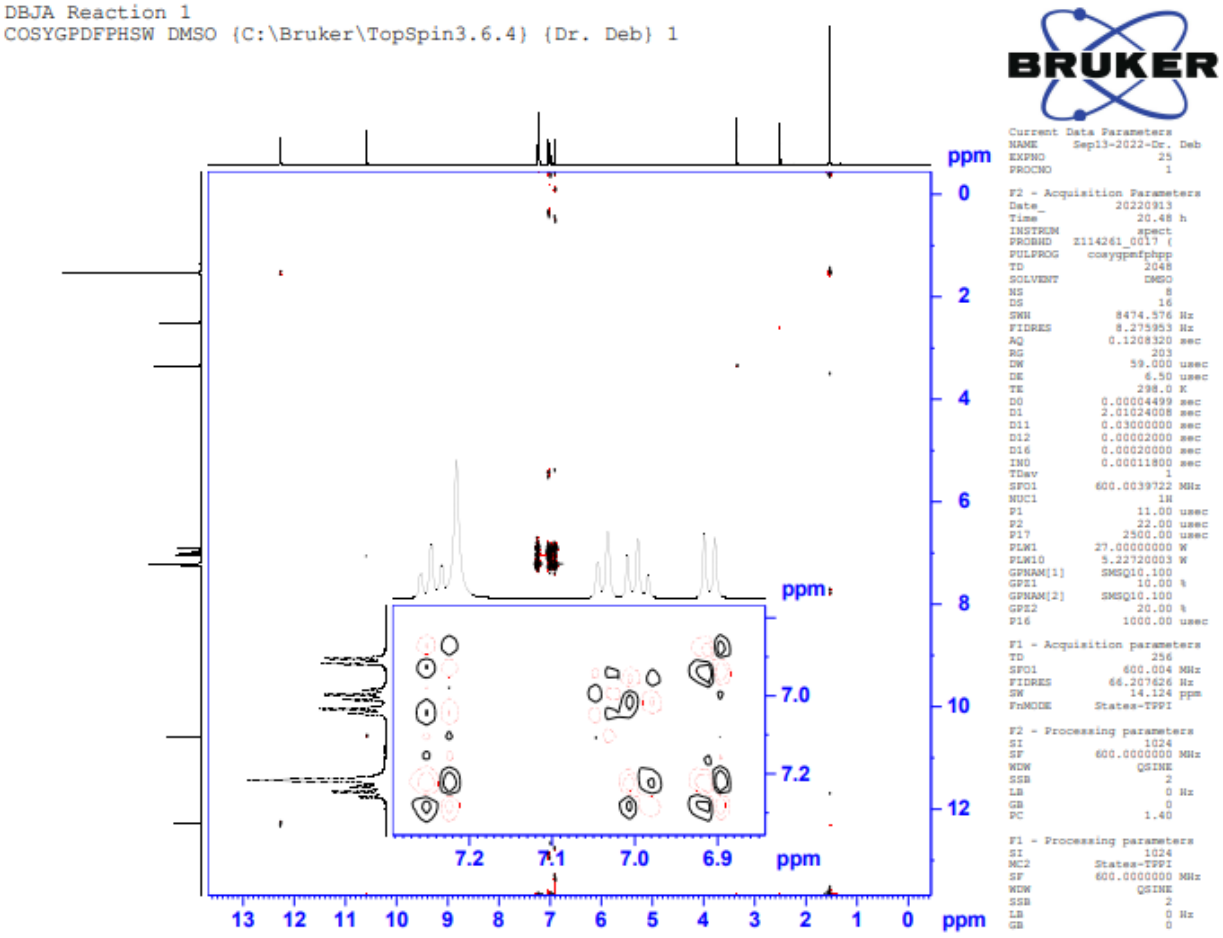

Figure 23: COSY spectrum of DBJA-1

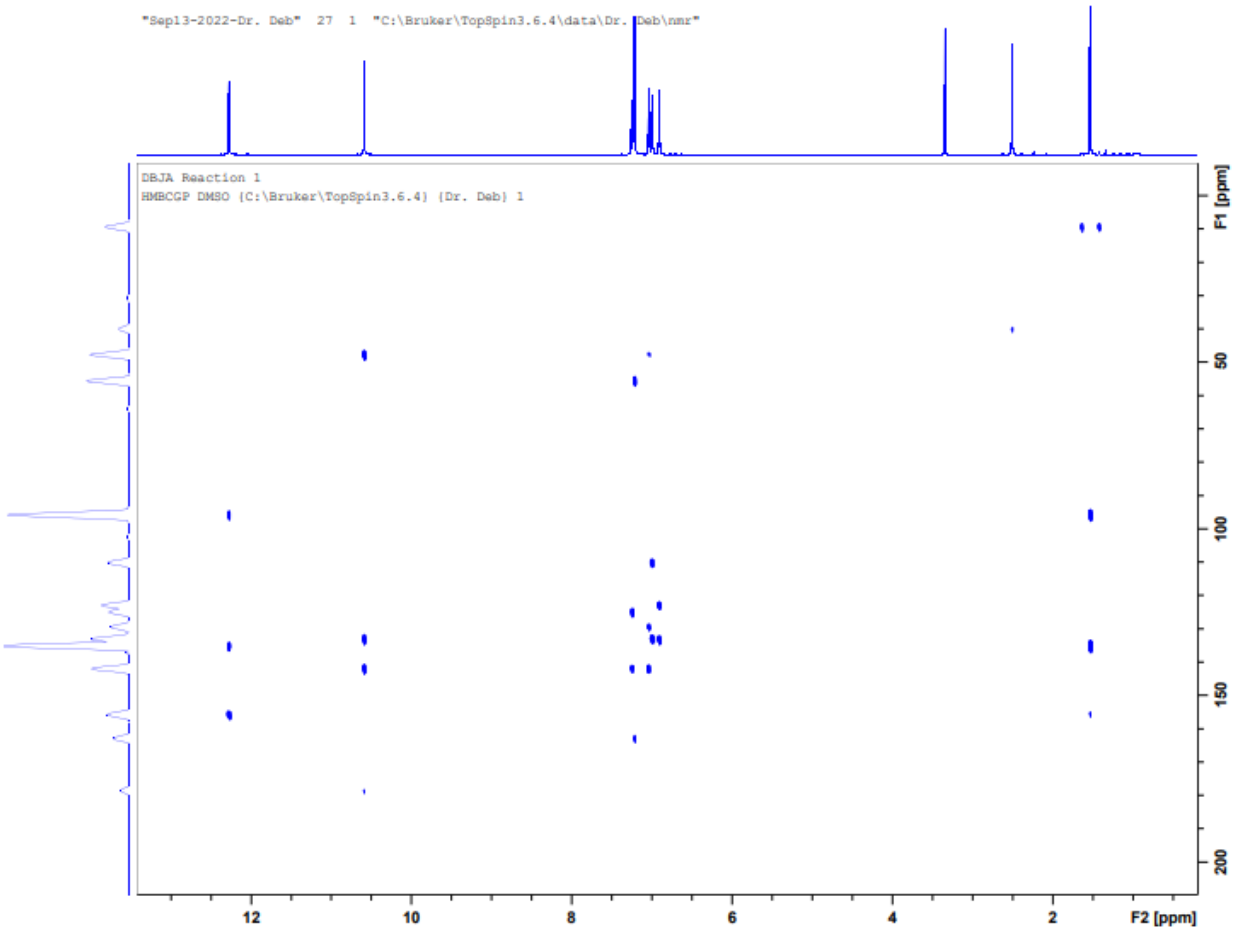

Figure 24: HMBCGP spectrum of DBJA-1

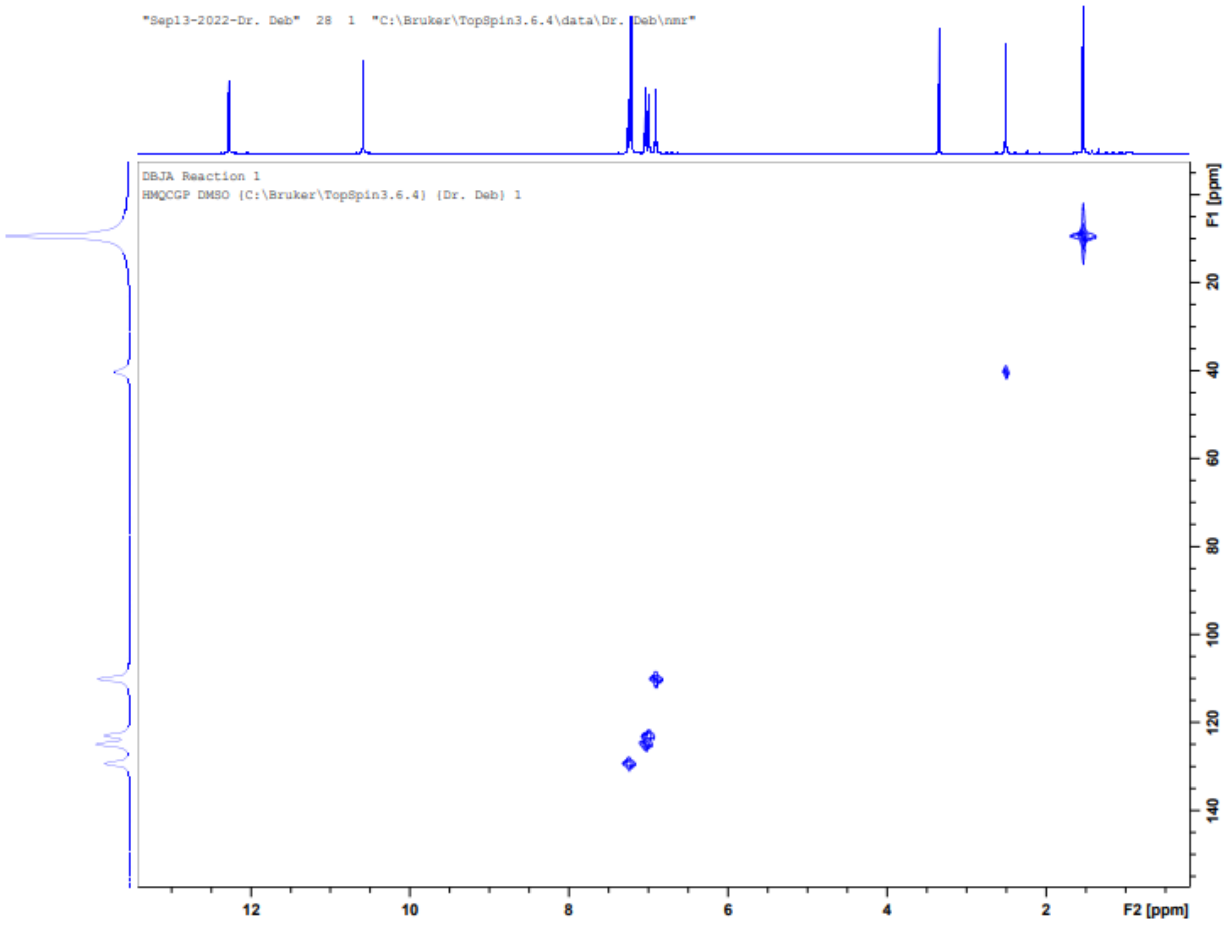

Figure 25: HMQCGP spectrum of DBJA-1

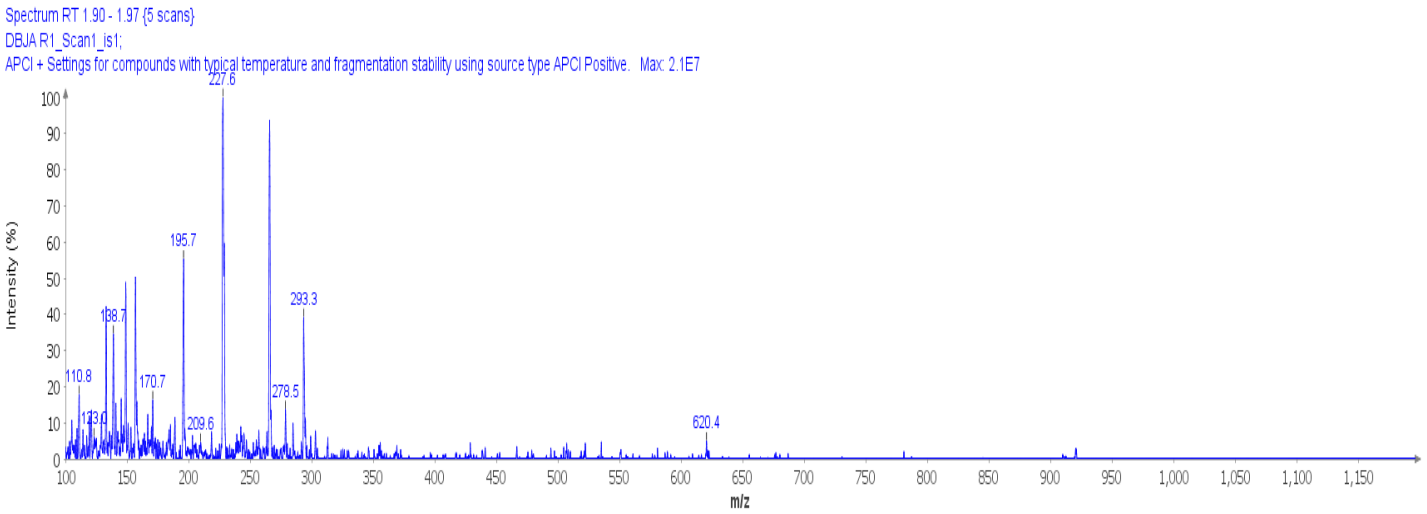

Figure 26: Mass spectroscopy spectrum of DBJA-1

Table 11: Different carbon positions in DBJA-1 and their chemical shifts

Position	**Type**	**Chemical shift, δ (ppm) ^{13}C NMR**
1	CH(=)	124.98
2	CH(=)	122.95
3	CH(=)	129.35
4	CH(=)	110.11
5	C(=)	141.99

Table 11, cont.

6	C(=)	133.16
7	C	47.75
8	CO	162.94
9	C(CN)	55.67
10	$C(NH_2)$	178.46
11	C(N)	155.74
12	C(=)	95.88
13	CN	119.17
14	$C(CH_3)$	135.16
15	CH_3	9.41

From the FT-IR (Fig 1a) spectrum, the presence of a medium peaks at 3335 cm^{-1} and 3258 cm^{-1} inferred the presence of amine and amide stretching vibrations found on the pyridine ring and on oxindole ring respectively. A medium peak at 3129 cm^{-1} representing aromatic C=C stretching vibration was also observed confirming the presence of an aromatic functional group in compound. Peaks at 2181 cm^{-1}, 1708 cm^{-1}, and 1582 cm^{-1} showed the presence of nitrile stretch on pyridine ring, carbonyl carbon of the amide and C-C aromatic stretch respectively.

Characterization with ^{1}H NMR showed chemical shifts representing proton of an aromatic ring (δ H = 6.98 – 7.24 ppm), amide (δ H = 10.58 ppm) and methyl group (δ H = 1.53 ppm). Chemical shift at 2.50ppm and 3.34ppm represent solvent DMSO and residual water in reaction respectively. With the help of ^{13}C CPD APT and DEPT (90 and 135) 1D NMR spectroscopy, the presence of one methyl group (δ 9.41ppm), four methine aromatic carbons (δ 110.11, 122.95, 124.98, and 129.35ppm), and eight quaternary carbons (CO at δ 178.46 ppm and CN at δ 119.17ppm) were confirmed as consistent with structure. 2D NMR spectra (COSY and HMBCGP and HMQCGP) was also used to confirm the structure of the isolated compound by showing the proton-proton correlations and proton-carbon correlations. Further characterization with mass spectroscopy showed a molecular ion peak of 293 m/z confirming the molecular mass of 293 amu of compound.

Characterization of DBJA-2

DBJA-2 : MP 269 – 270°C; FT-IR (cm-1): 3334 (NH2), 3294 (CONH), 3126 (Aromatic C=C), 2179 (CN), 1706 (CO); 1H NMR (600 MHz, DMSO) δ 1.53 (s, 3H), 6.91 (d, J = 2.97 Hz, 1H), 6.98 – 7.04 (m, 2H), 7.23 (m, 3H) 10.58 (s, 1H), 12.27 (s, 1H); 13C NMR (150 MHz, DMSO) δ 9.41,47.76, 55.67, 95.88, 110.12, 119.17, 122.95, 124.98, 129.35, 133.16, 135.16, 141.99, 155.74, 162.94, 178.47. MS: 293m/z (M).

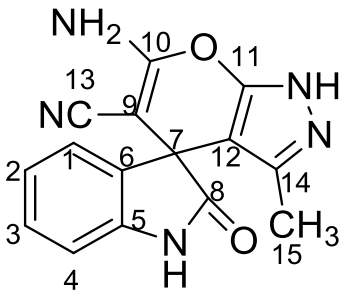

Figure 27: Structure of DBJA-2

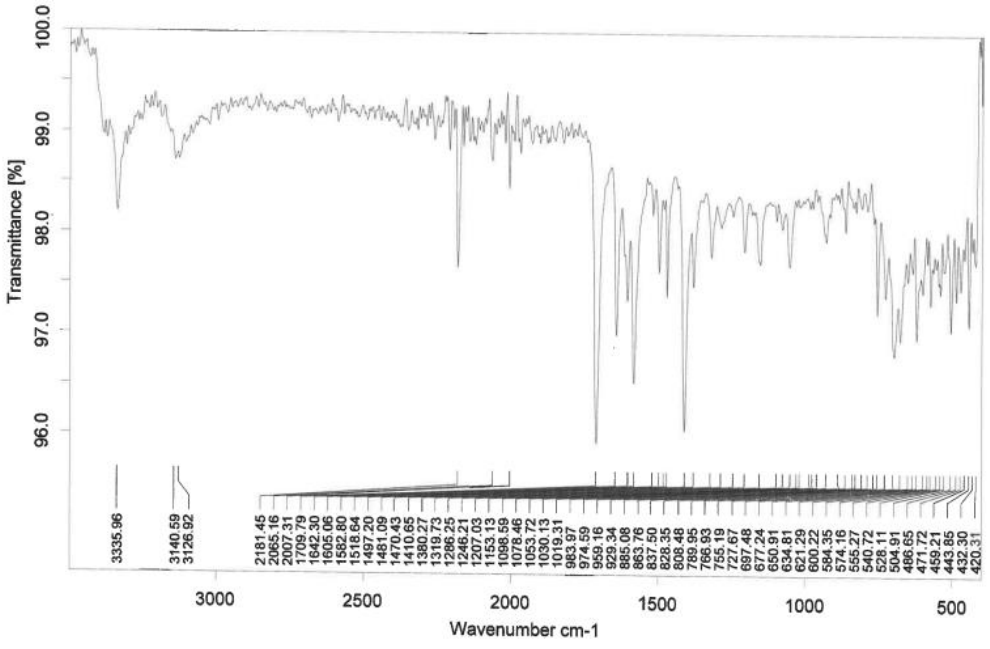

Figure 28: FT-IR spectrum of DBJA-2

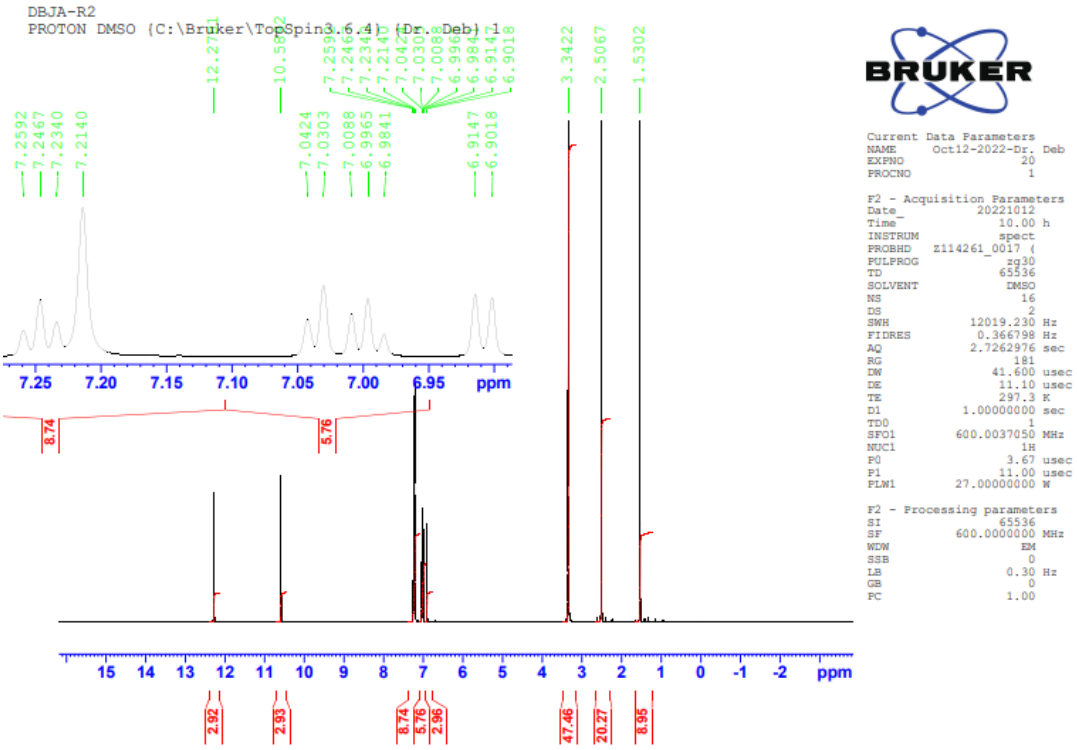

Figure 29: ^{1}H NMR spectrum of DBJA-2

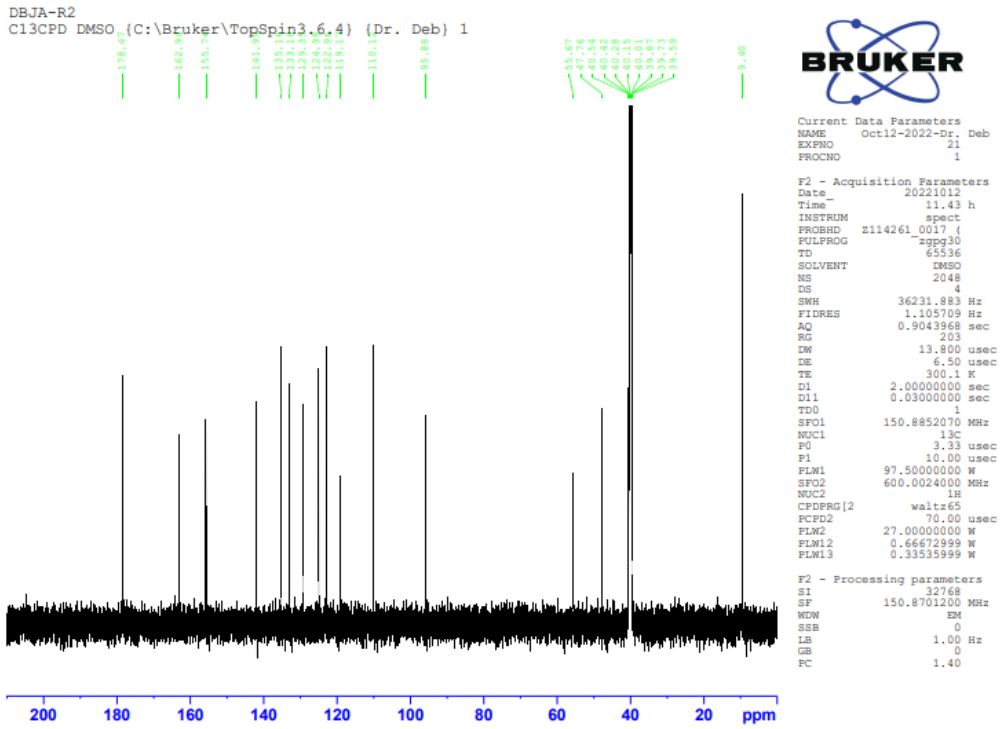

Figure 30: C^{13} NMR spectrum of DBJA-2

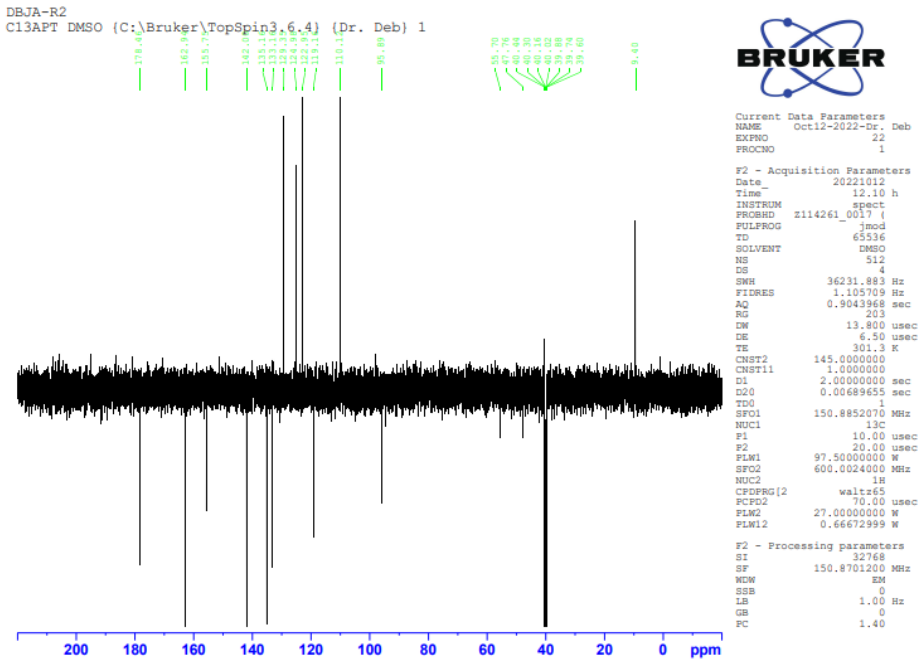

Figure 31: C^{13}APT NMR spectrum of DBJA-2

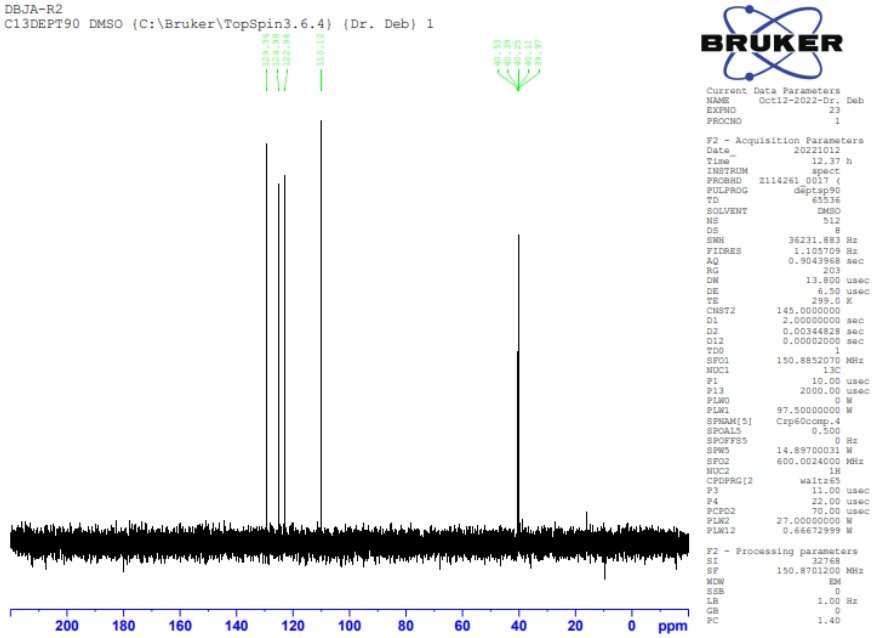

Figure 32: C^{13}DEPT90° NMR spectrum of DBJA-2

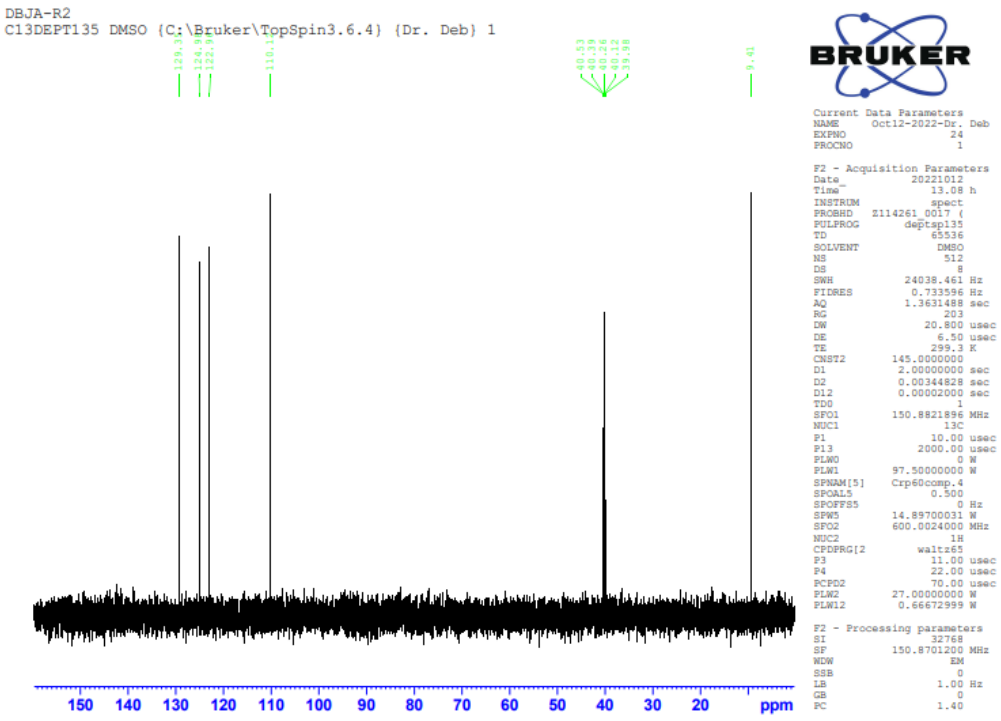

Figure 33: C^{13}DEPT135° NMR spectrum of DBJA-2

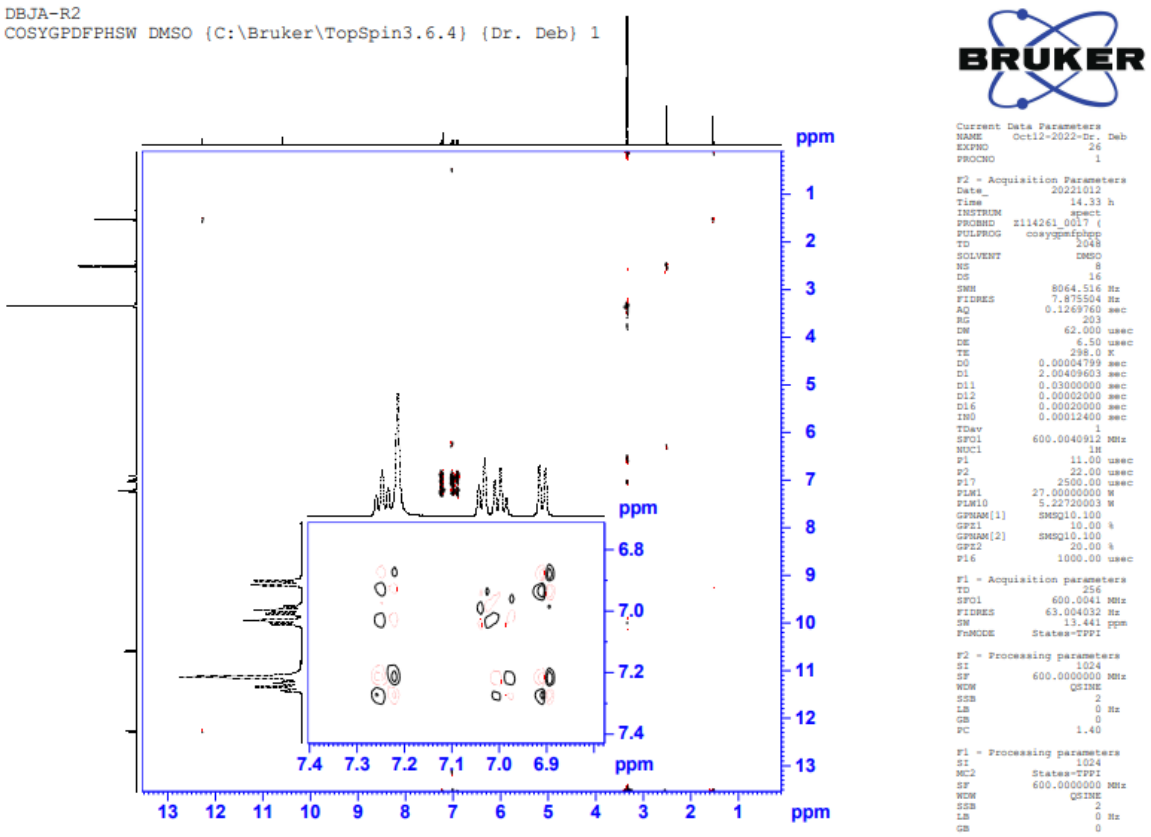

Figure 34: COSY spectrum of DBJA-2

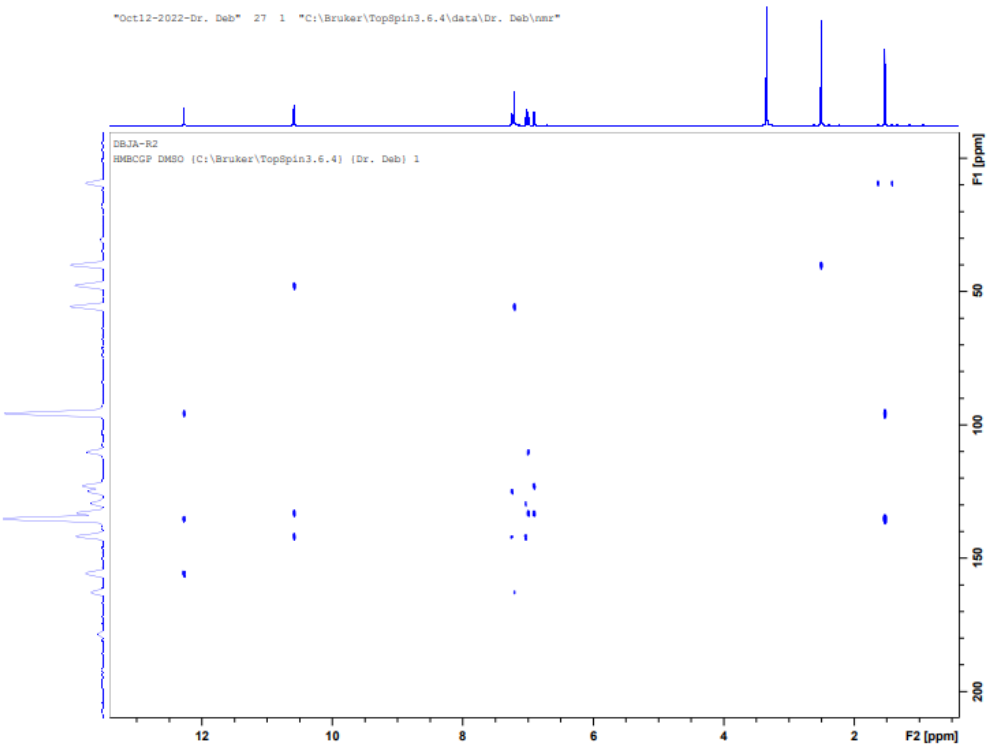

Figure 35: HMBCGP spectrum of DBJA-2

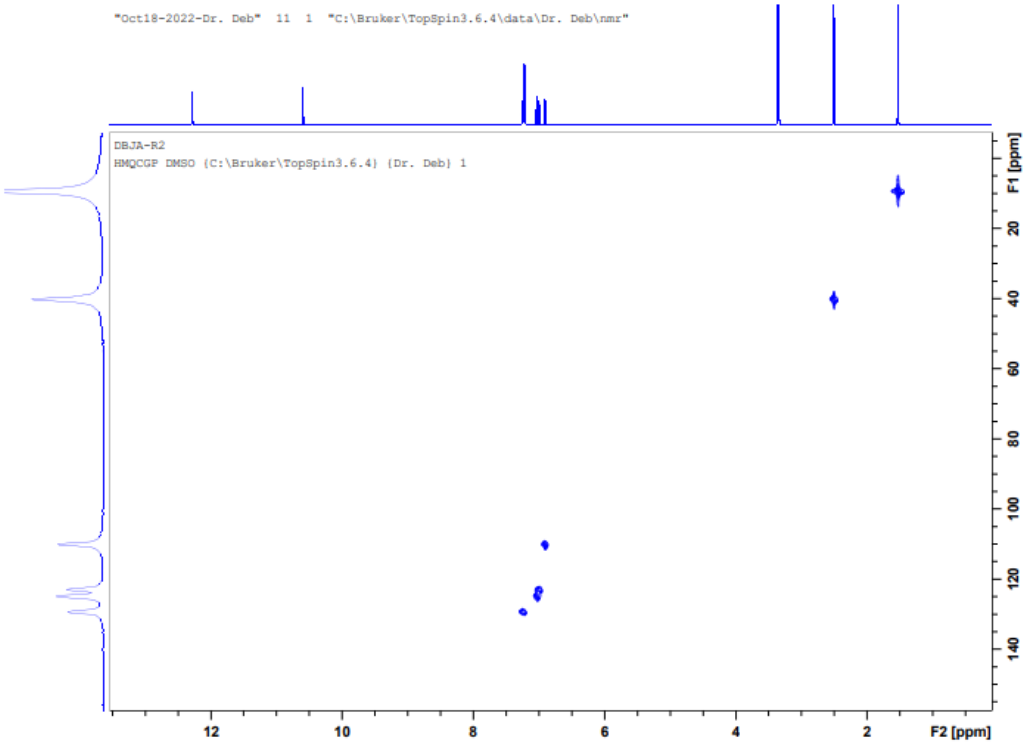

Figure 36: HMQCGP spectrum of DBJA-2

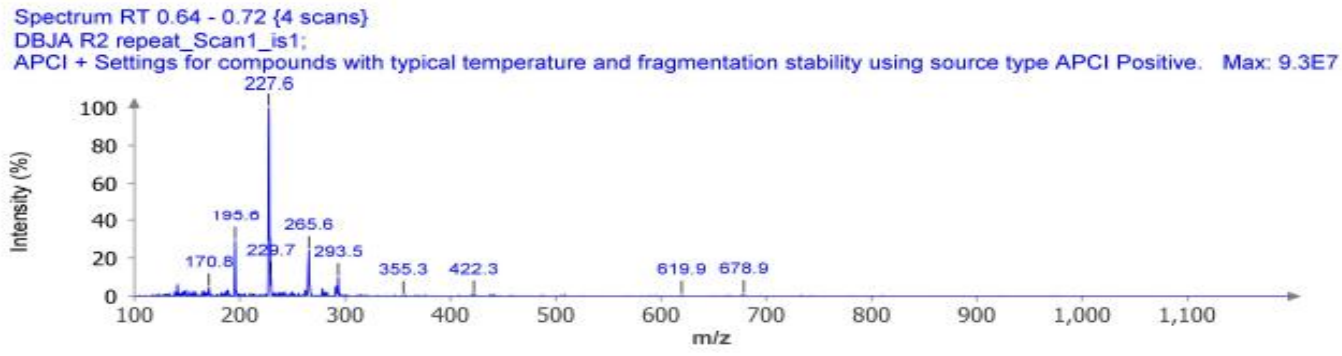

Figure 37: Mass spectroscopy spectrum of DBJA-2

Table 12: Different carbon positions in DBJA-2 and their chemical shifts

Position	**Type**	**Chemical shift, δ (ppm) ^{13}C NMR**
1	CH(=)	124.98
2	CH(=)	122.95
3	CH(=)	129.35
4	CH(=)	110.11
5	C(=)	141.99
6	C(=)	133.15
7	C	47.75
8	C=O	162.93
9	C(CN)	55.67
10	$C(NH_2)$	178.46
11	C(N)	155.73
12	C(=)	95.87

Table 12, cont.

13	CN	119.17
14	$C(CH_3)$	135.16
15	CH_3	9.41

Like DBJA-1, DBJA-2 also showed significant peaks at 3334cm^{-1} and 3294cm^{-1} in the FT-IR spectra representing the amine and amide stretch present on pyridine ring and oxindole ring in product structure. An aromatic C=C stretching vibration was also identified at 3126cm^{-1}. A significant peak at 2179 cm^{-1} representing a nitrile stretch on the pyridine ring was also observed. A strong narrow peak at 1706 cm^{-1} represents the carbonyl stretch present in amide. Also, characterization with ^{1}H NMR showed chemical shifts representing proton of an aromatic ring (δ H = 6.90 – 7.25 ppm), amide (δ H = 10.58 ppm) and methyl group (δ H = 1.53 ppm). Chemical shift at 2.50ppm and 3.34ppm represent solvent DMSO and residual water in reaction respectively. With the help of ^{13}C CPD APT and DEPT 1D NMR spectroscopy, the presence of one methyl group (δ 9.40ppm), four methine aromatic carbons (δ 110.11, 122.95, 124.98, and 129.35ppm), and eight quaternary carbons (CO at δ 178.46 ppm and CN at δ 119.17ppm) were confirmed as consistent with structure. 2D NMR spectra (COSYGPDFPHSM and HMBCGP and HMQCGP) was also used to confirm the structure of the isolated compound by showing the proton-proton correlations and proton-carbon correlations. Further characterization with mass spectroscopy showed a molecular ion peak of 293 m/z confirming the molecular mass of 293 m/z

of compound. All the spectroscopic data of DBJA-2 were similar to that of DBJA-1 hence the structures of these two compounds are similar.

Characterization of DBJA-3

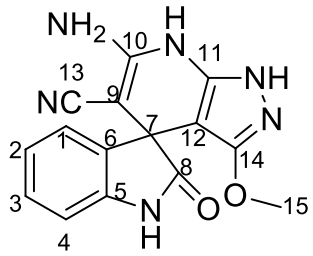

Figure 38: Structure of DBJA-3

DBJA-3: MP 229 – 230°C; FT-IR (cm^{-1}): 3449 (CONH), 3294 (NH_2), 3053 (Aromatic C=C), 2171 (CN), 1684 (CO); ^{1}H NMR (600 MHz, DMSO) δ 4.83 (s, 2H), 5.89 (s, 2H), 6.63(d, J = 1.34 Hz, 1H), 6.76 (t, J = 1.47 Hz, 1H), 6.88 – 6.98 (m, 4H), 7.05 – 7.31 (m, 6H), 8.34 (s, 1H), 9.76 (s, 1H), 13.86 (s, 1H); ^{13}C NMR (150 MHz, DMSO) δ 50.94, 55.64, 80.33, 108.48, 110.72, 116.72, 117.92, 121.08, 121.64, 121.83, 122.21, 122.67, 123.00, 126.56, 127.52, 130.59, 139.88, 142.10, 142.23, 154.65, 163.85, 165.19, 167.03, 182.01. MS: mass expected (M) = 322, mass observed (M + 28) = 350.

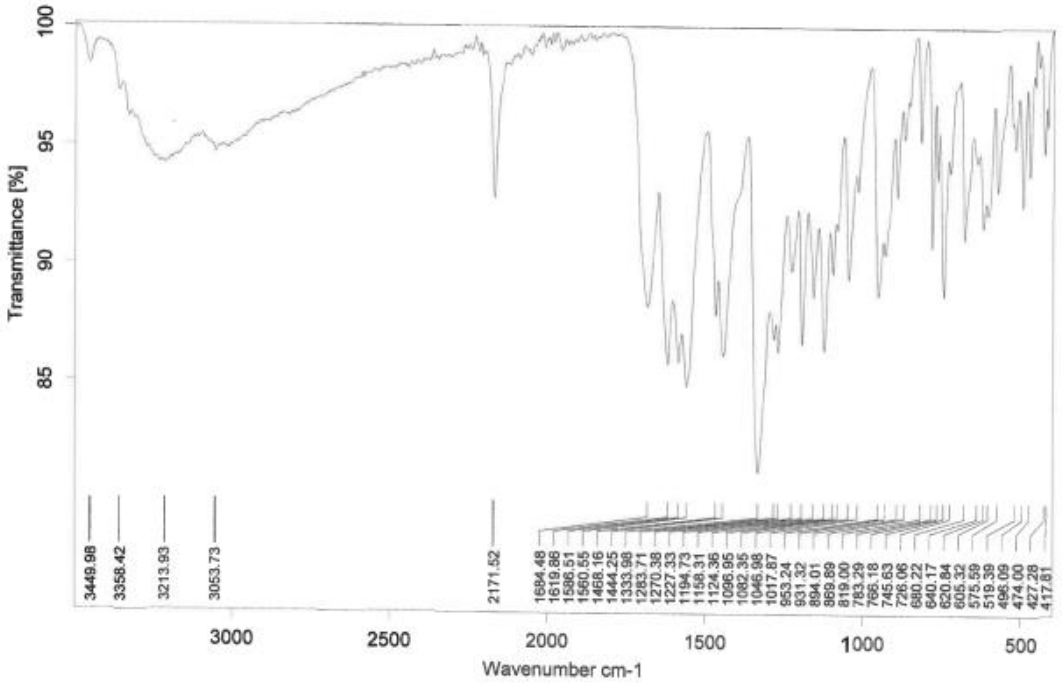

Figure 39: FT-IR spectrum of DBJA-3

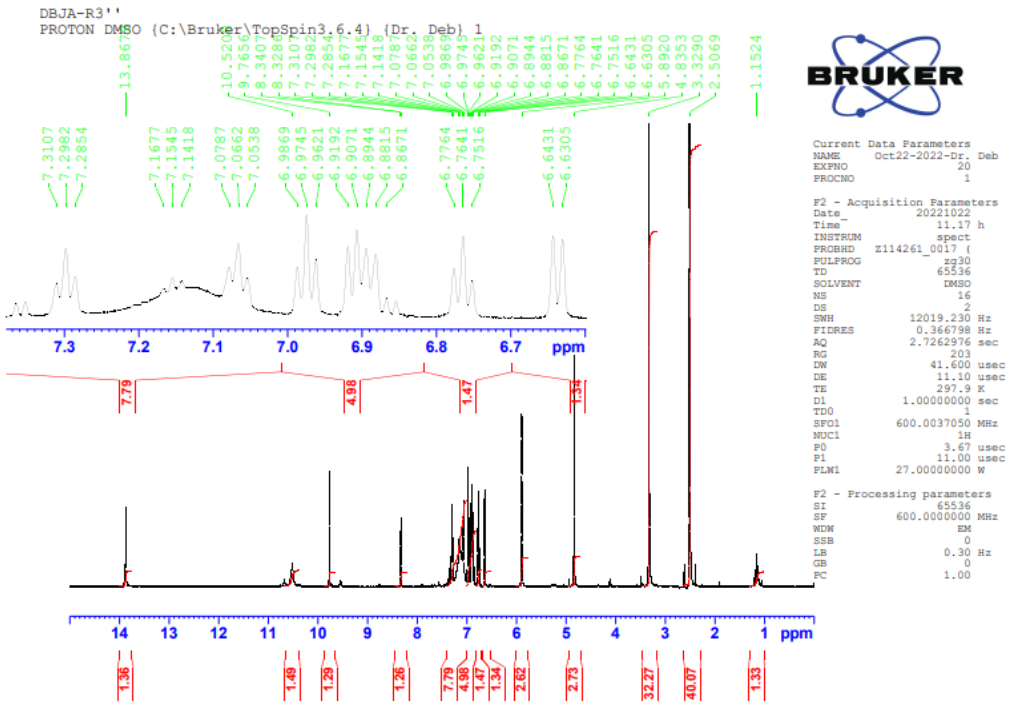

Figure 40: ^{1}H NMR spectrum of DBJA-3

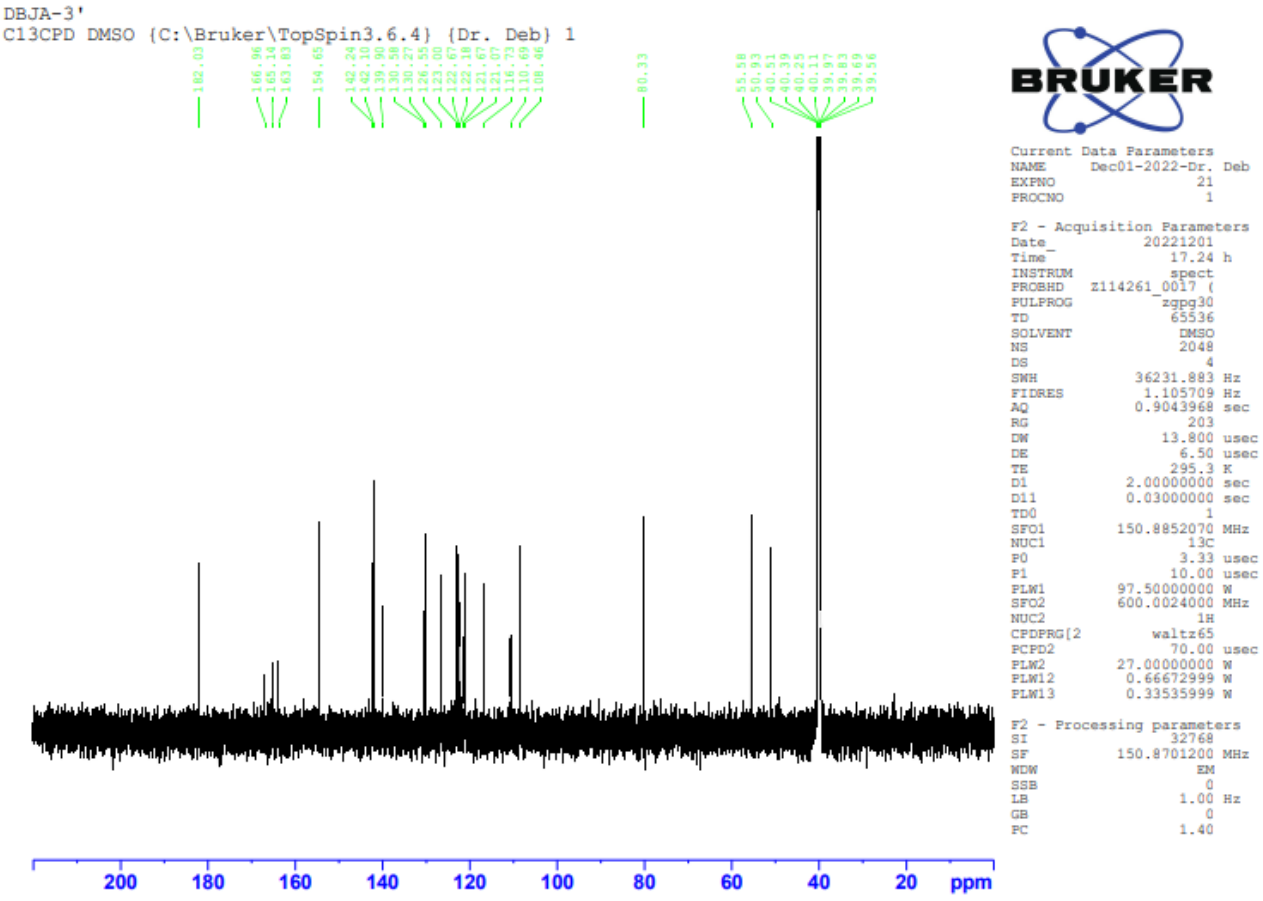

Figure 41: C^{13} NMR spectrum of DBJA-3

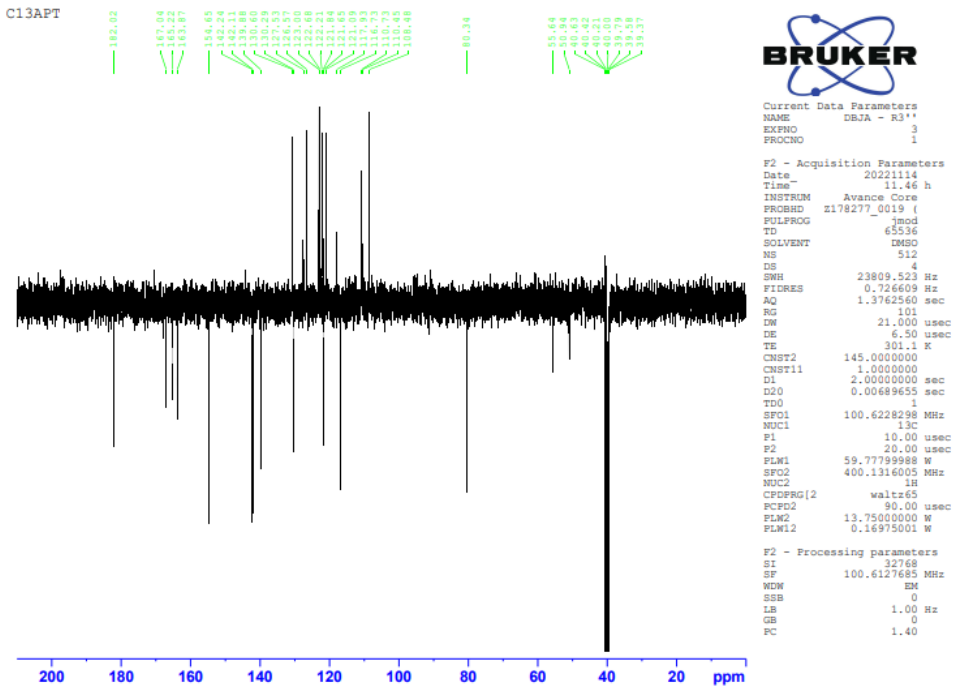

Figure 42: C^{13}APT NMR spectrum of DBJA-3

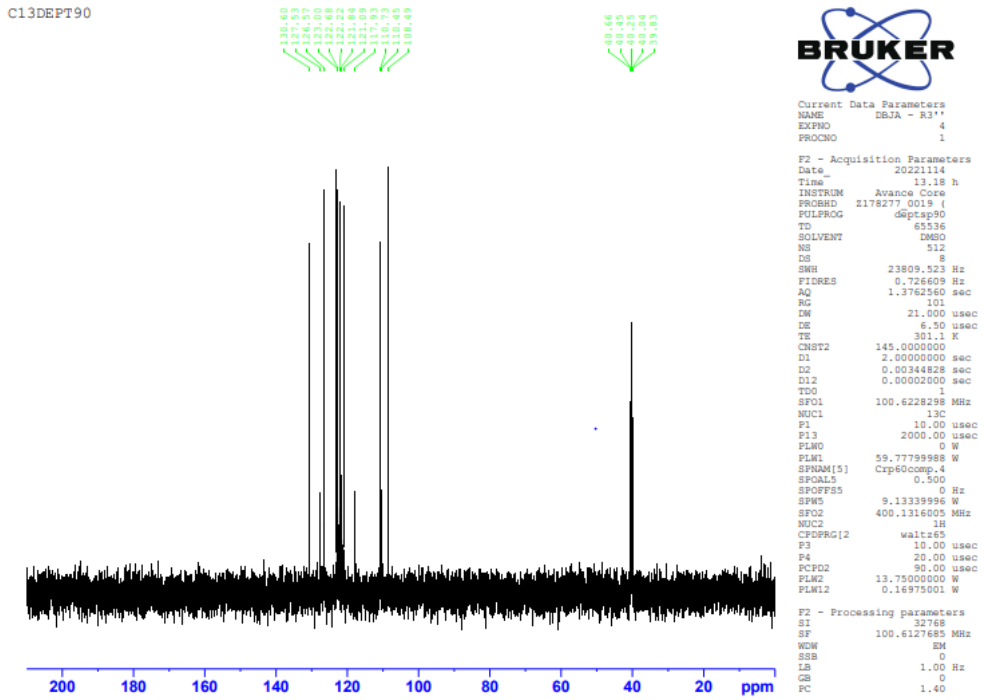

Figure 43: C^{13}DEPT90° NMR spectrum of DBJA-3

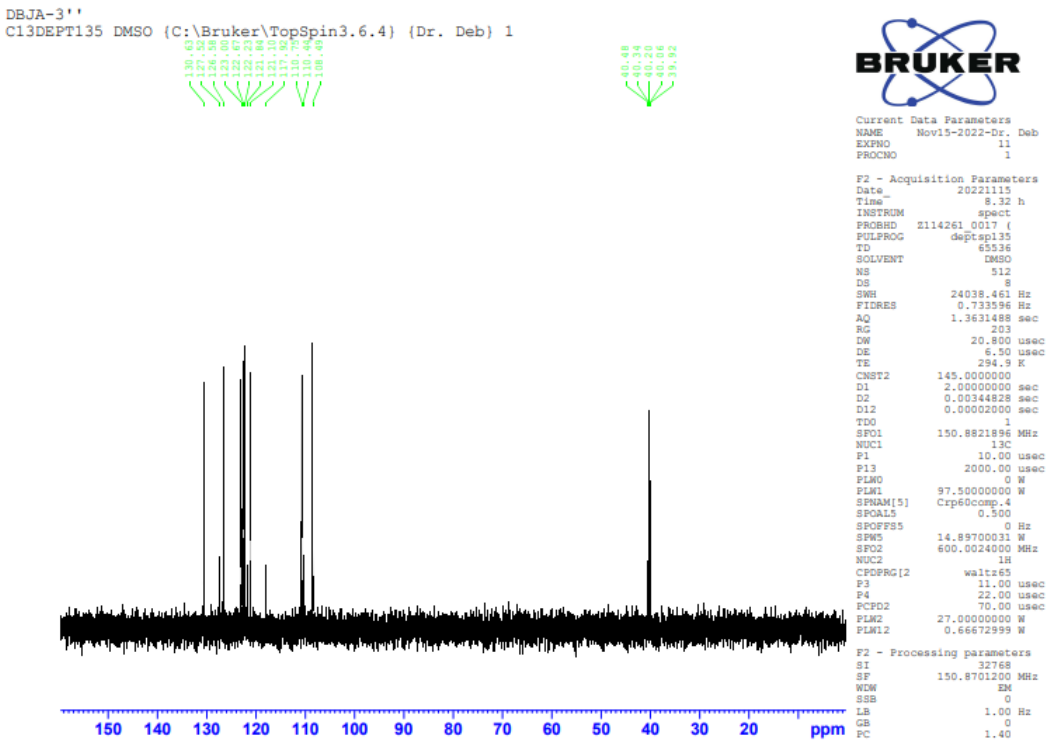

Figure 44: C^{13}DEPT135° NMR spectrum of DBJA-3

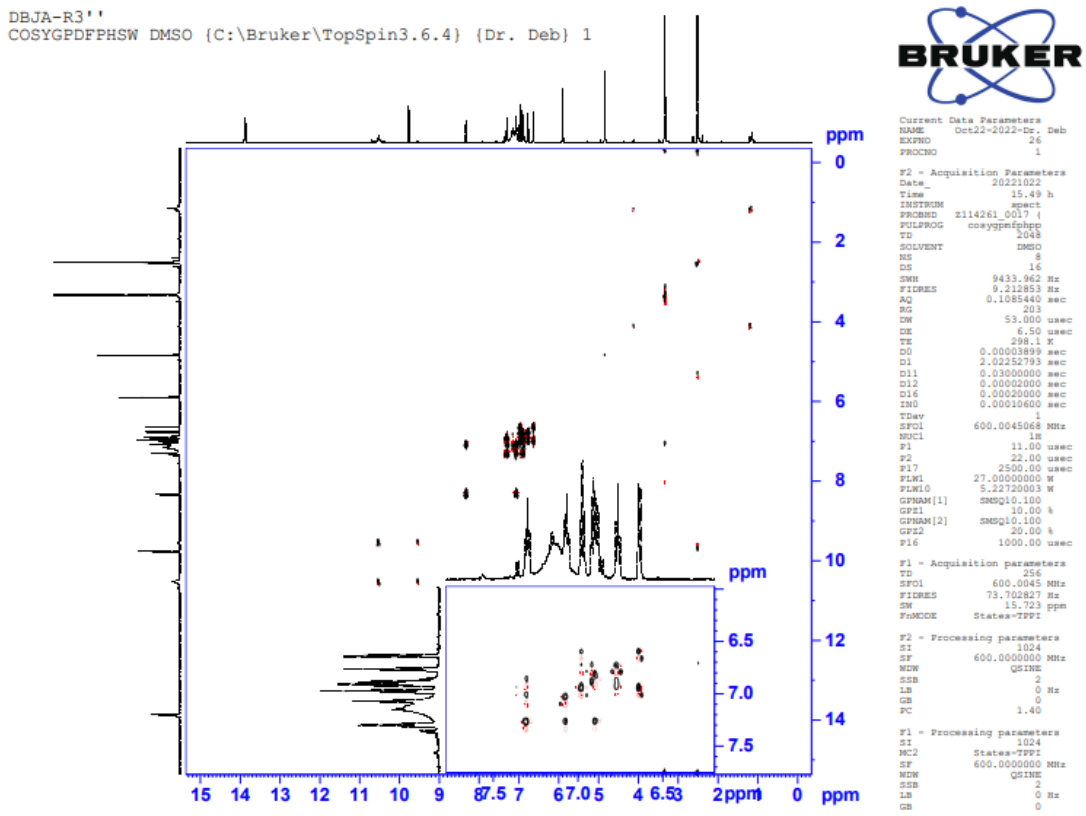

Figure 45: COSY spectrum of DBJA-3

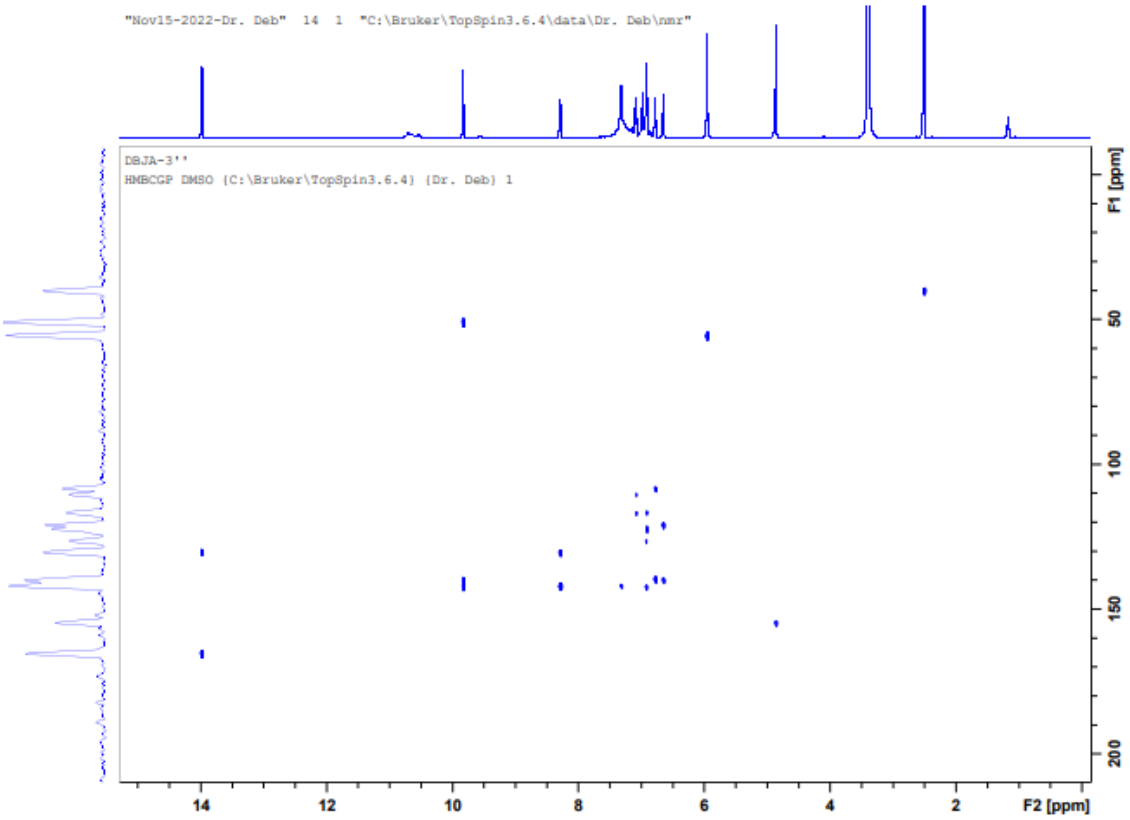

Figure 46: HMBCGP spectrum of DBJA-3

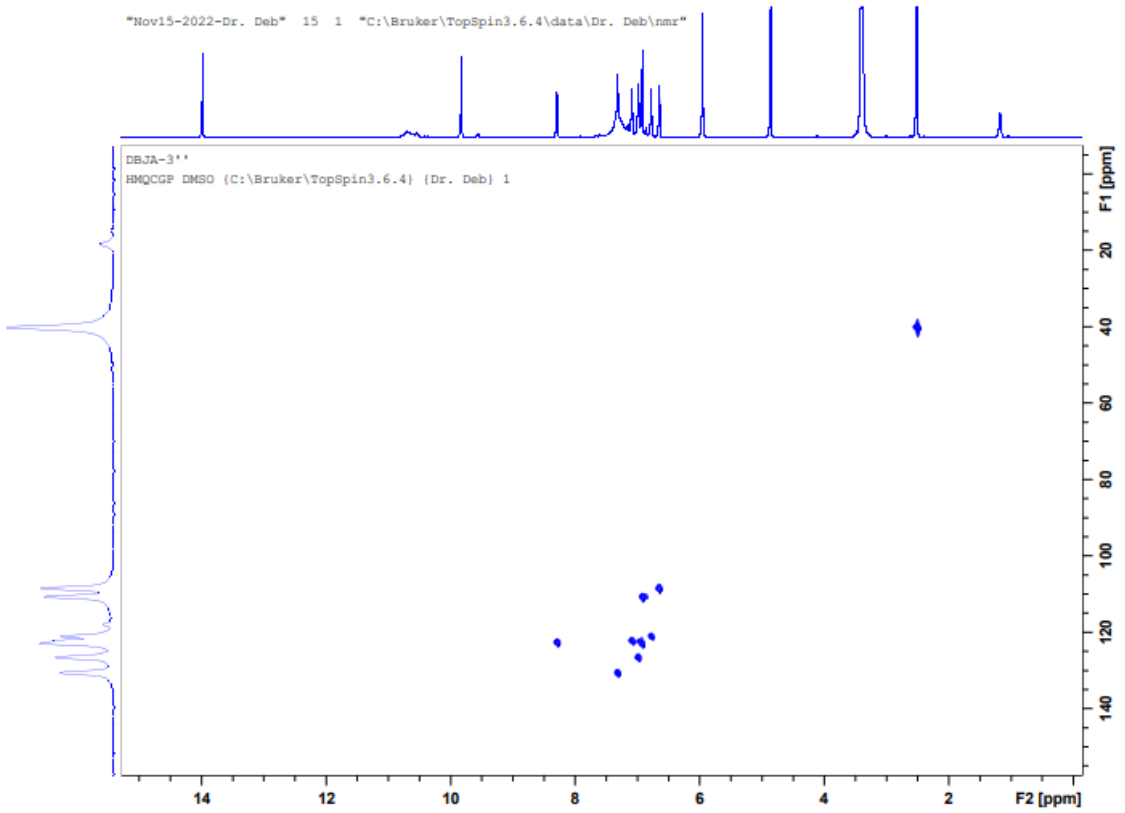

Figure 47: HMQCGP spectrum of DBJA-3

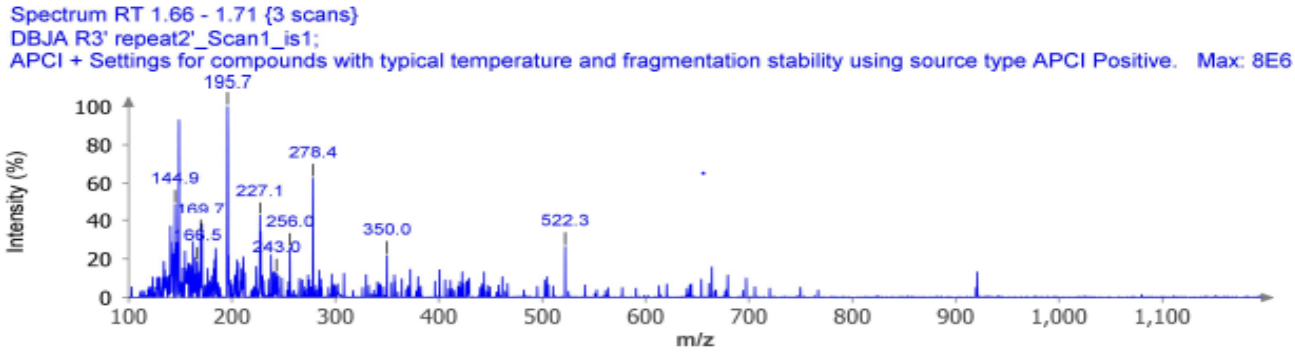

Figure 48: Mass spectroscopy spectrum of DBJA-3

Table 13: Different carbon positions in DBJA-3 and their chemical shifts

Position	**Type**	**Chemical shift, δ (ppm)** ^{13}**C NMR**
1	CH(=)	122.18
2	CH(=)	121.07
3	CH(=)	122.67
4	CH(=)	110.69
5	C(=)	142.24
6	C(=)	139.90
7	C	50.93
8	C=O	166.96
9	C(CN)	55.58
10	$C(NH_2)$	182.03
11	C(N)	163.83
12	C(=)	110.69

Table 13, cont.

13	CN	116.73
14	CO	165.14
15	CH_2	80.33
16	CH_3	-

The FT-IR spectra of DBJA-3 showed significant peaks at 3449cm^{-1} and 3358cm^{-1} representing the amine and amide stretch present on pyridine ring and oxindole ring in product structure. An aromatic C=C stretching vibration was also identified at 3213cm^{-1}. A significant peak at 2171 cm^{-1} representing a nitrile stretch on the pyridine ring was also observed. A strong narrow peak at 1684 cm^{-1} represents the carbonyl stretch present in amide. From the ^{1}H NMR, the structure of the synthesized spirocyclic compound was confirmed with the presence of chemical shift caused by the presence of NH (4.83, 5.89, 8.33, and 9.76 ppm). The aromatic ring of the oxindole fused ring showed chemical shift at 7.05 – 7.31 ppm. ^{13}C NMR along with APT, and DEPT (90° and 135°) showed the presence of quaternary (C) and methine (CH) carbons but no methylene (CH_2) or methyl (CH_3) carbons. The presence of impurities causes the appearance of peaks at 108.46, 123.00, 126.55, 130.27, 130.58, 142.10, and 154.65ppm. 2D NMR spectra (COSYGPDFPHSM and HMBCGP and HMQCGP) was also used to confirm the structure of the isolated compound by showing the proton-proton correlations and proton-carbon correlations. The expected mass of 322 was not observed in the mass spectrum but rather the peak for M + 28

(350 m/z) was observed. The Atmospheric Solids Analysis Probe (ASAP) mass spectrometry was used and hot nitrogen desolvation gas is utilized to vaporize sample hence the increase in mass of 28 observed in mass spectrum due to the addition of N_2 gas. The peak at 278 m/z (M-45) is due to the loss of C_2H_5O (mass = 45).

Characterization of DBJA-4

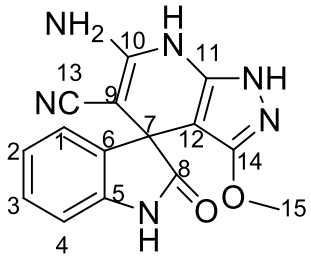

Figure 49: Structure of DBJA-4

DBJA-4: MP 216-220°C, IR (cm^{-1}): 3329 (CONH), 3169 (COOH), 3016 (Ar), 2169 (CN), 1707(CO), 1333 (OCH_3); ^{1}H NMR (6OO MHz, DMSO) δ 4.83 (s, 2H), 5.90 (s, 1H). 6.90 (q, *J*=2.69Hz, 3H), 7.06 (m, 6H), 9.78 (s, 1H), 13.88 (s, 1H); ^{13}C NMR (150 MHz, DMSO) δ 55.58, 80.34, 108.45, 110.63, 116.79, 121.04, 121.69, 122.11, 122.68, 122.98, 126.51, 130.24, 130.48, 139.96, 142.08, 142.26, 154.66, 163.77, 182.07.92; MS: expected mass = 308 (M), mass found = 293 (M - 15)

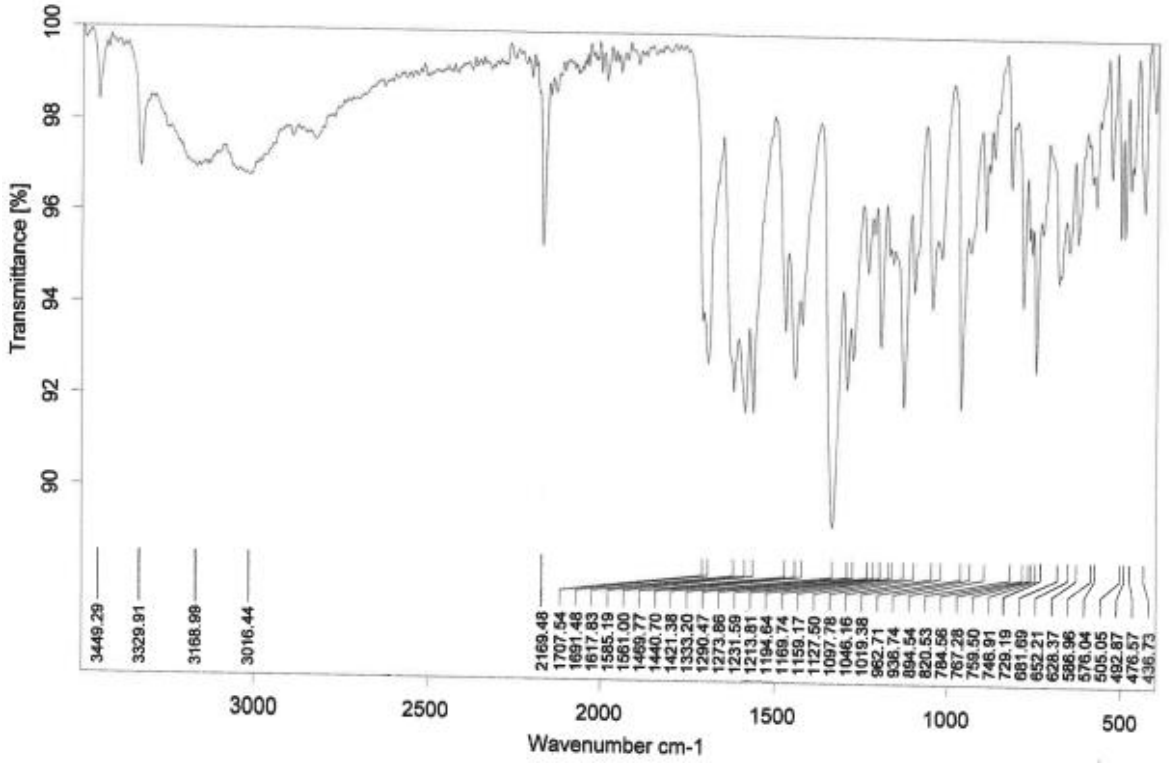

Figure 50: FT-IR spectrum of DBJA-4

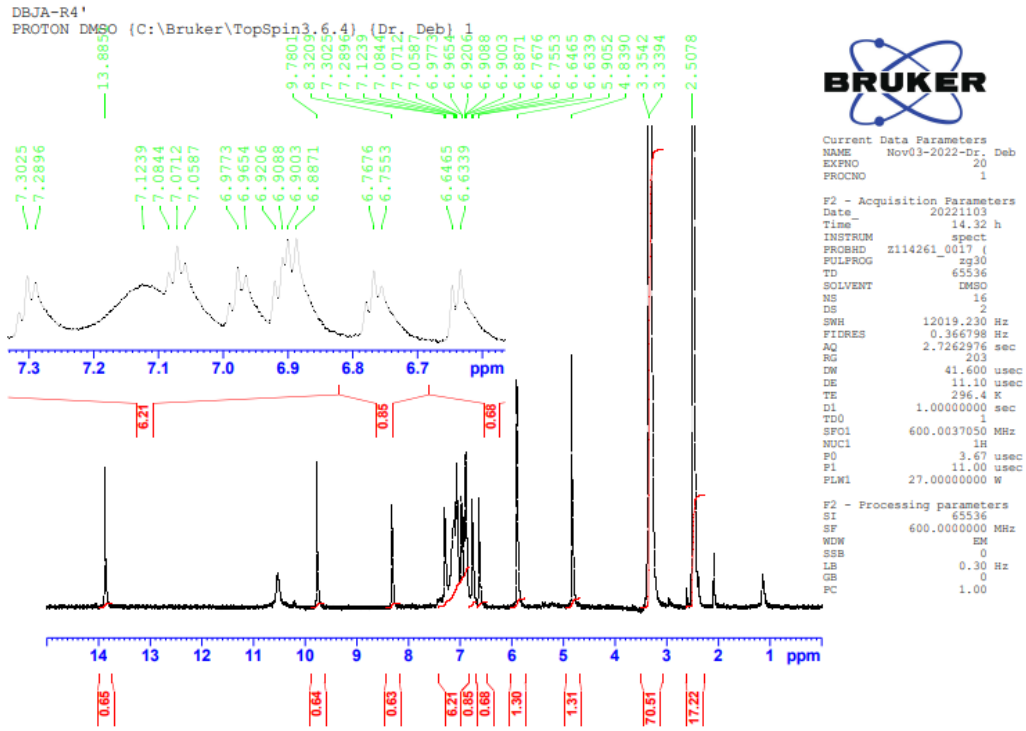

Figure 51: ^{1}H NMR spectrum of DBJA-4

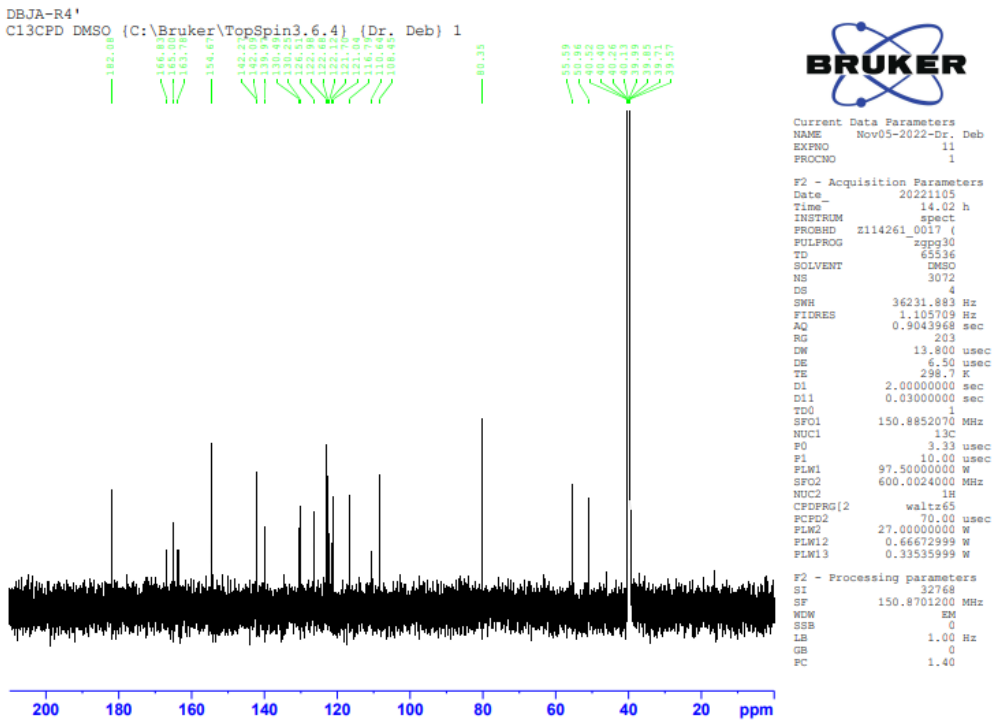

Figure 52: C^{13} NMR spectrum of DBJA-4

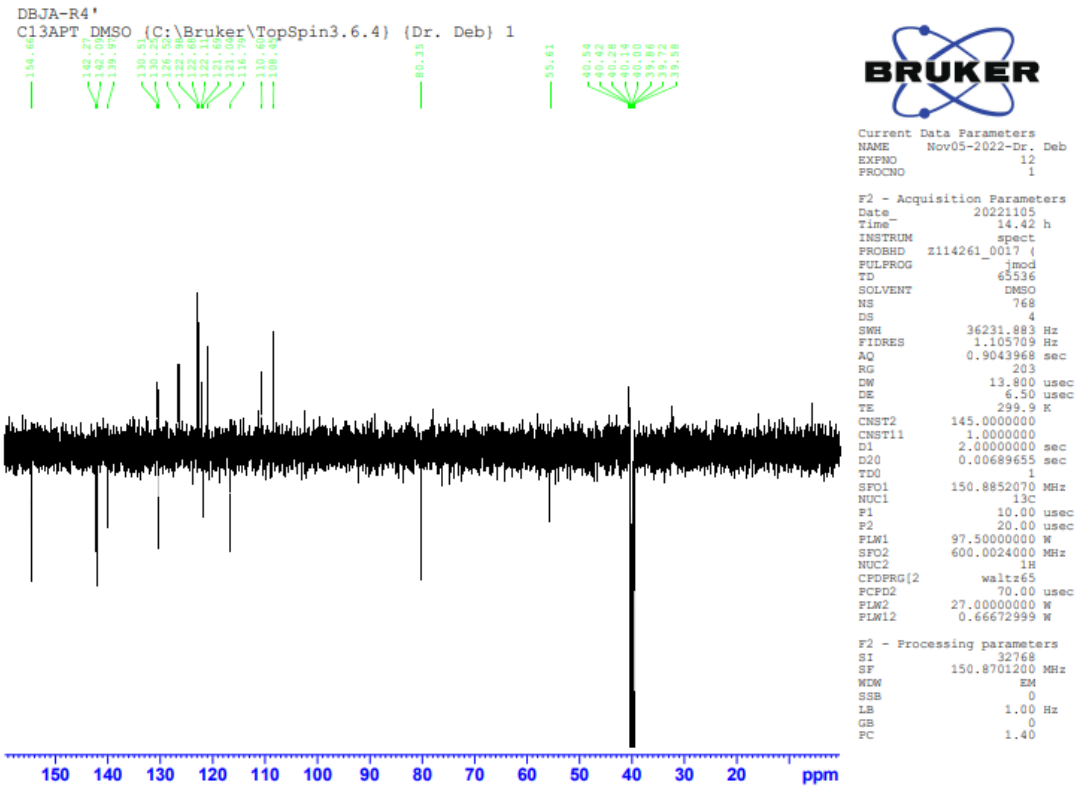

Figure 53: C^{13}APT NMR spectrum of DBJA-4

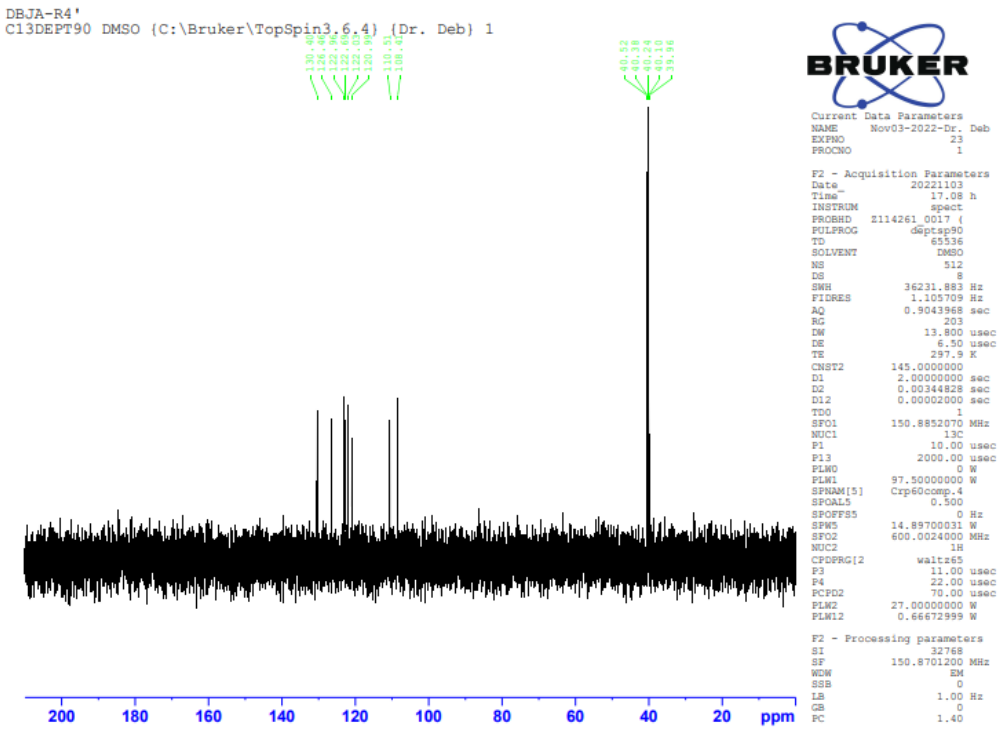

Figure 54: C^{13}DEPT90° NMR spectrum of DBJA-4

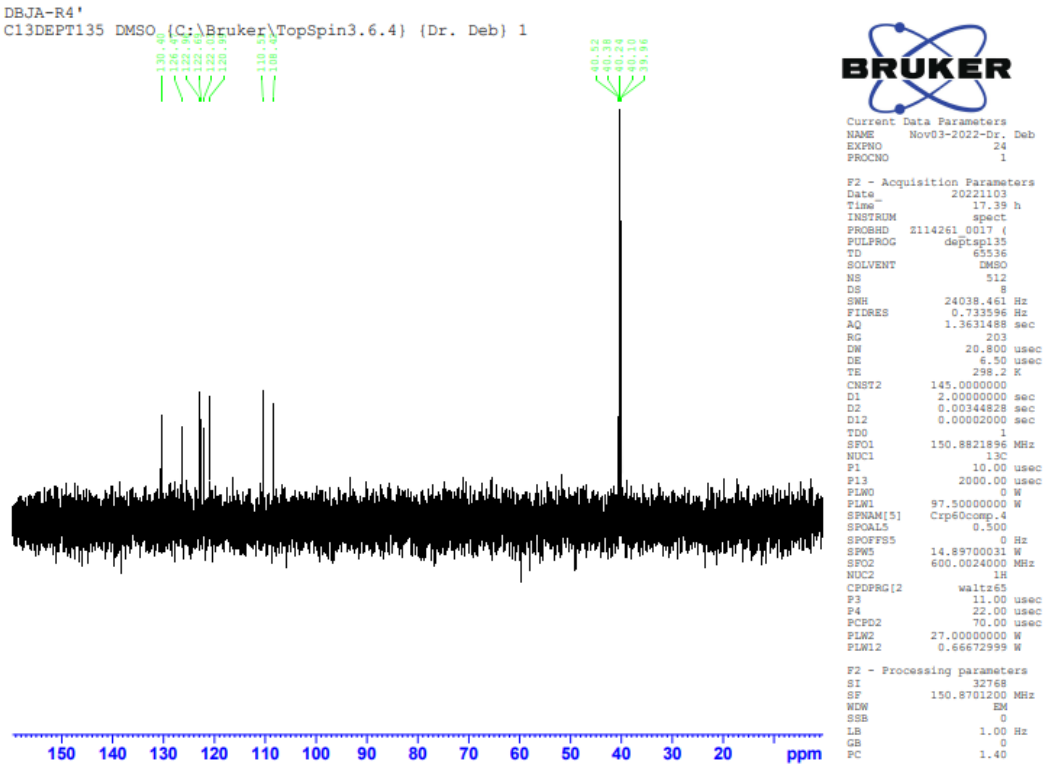

Figure 55: C^{13}DEPT135° NMR spectrum of DBJA-4

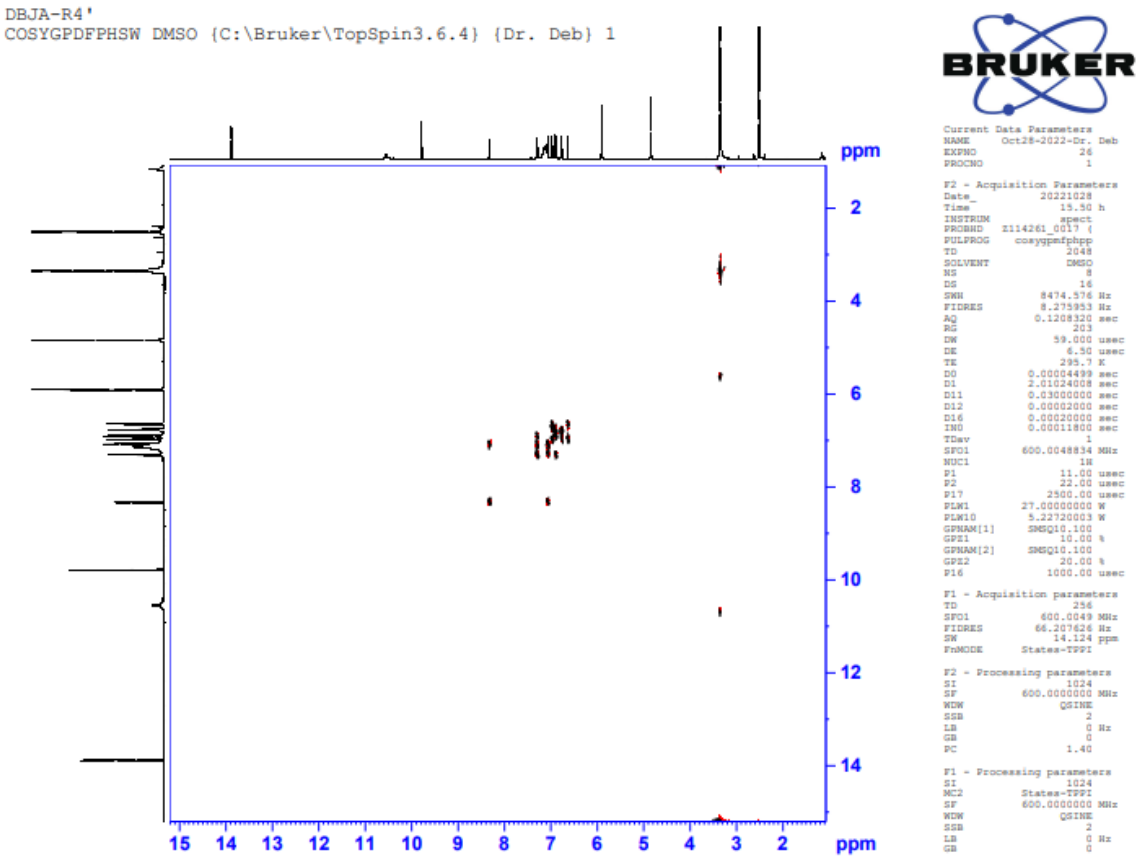

Figure 56: COSY spectrum of DBJA-4

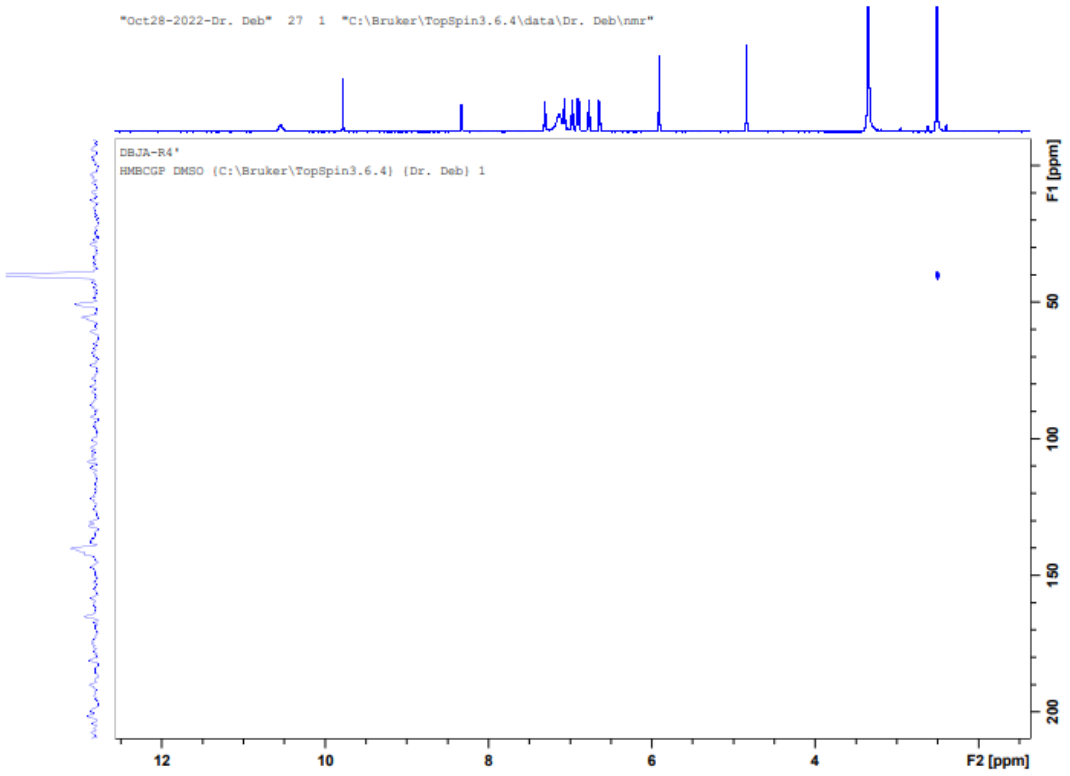

Figure 57: HMBCPG spectrum of DBJA-4

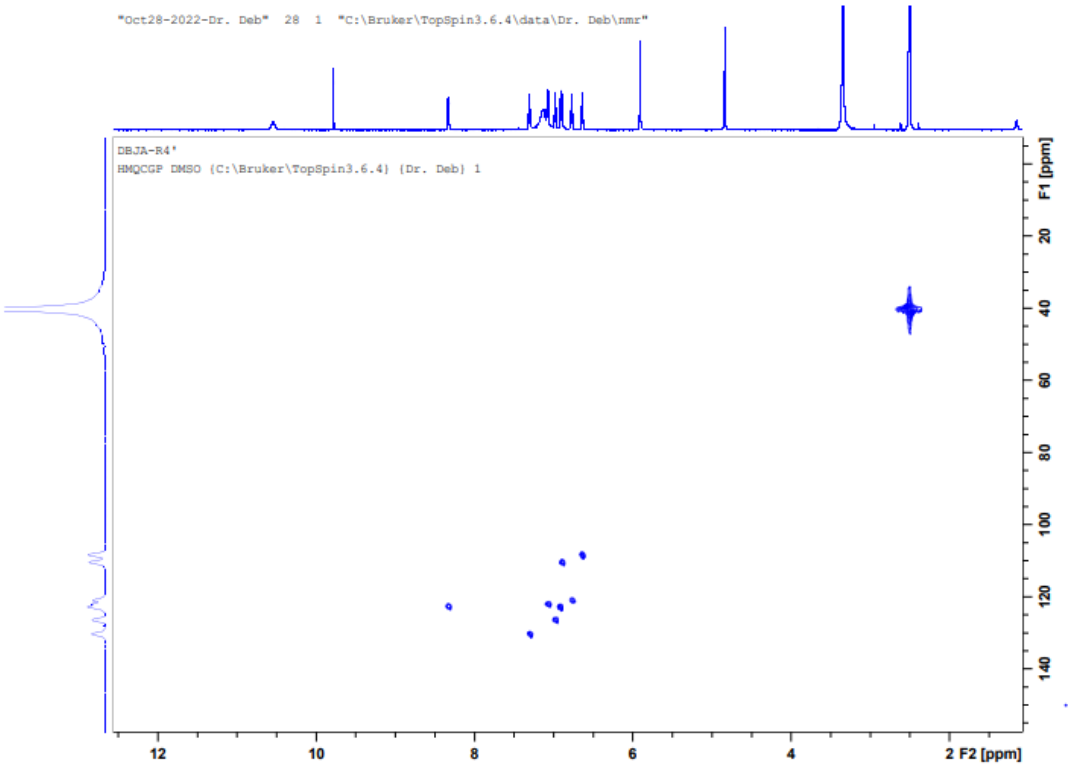

Figure 58: HMQCPG spectrum of DBJA-4

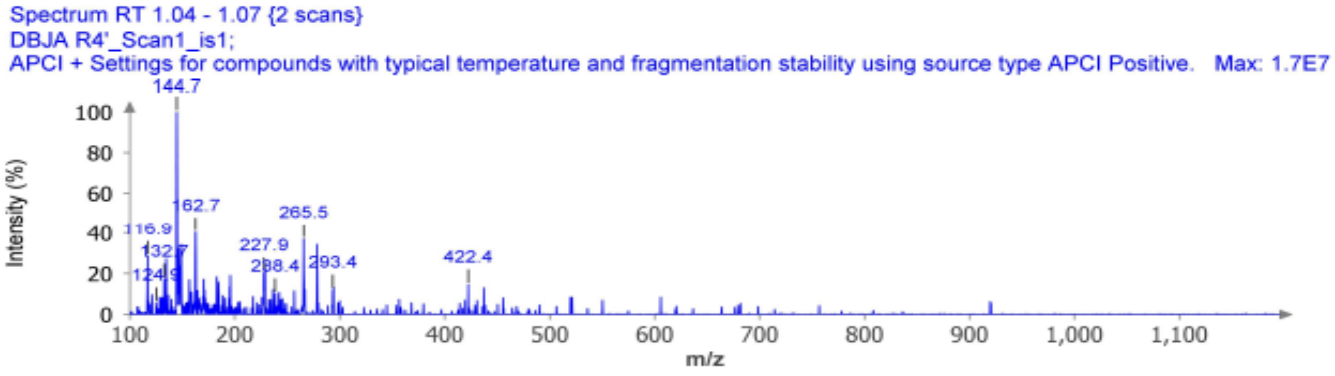

Figure 59: Mass spectroscopy spectrum of DBJA-4

Table 14: Different carbon positions in DBJA-4 and their chemical shifts

Position	**Type**	**Chemical shift, δ (ppm)** ^{13}**C NMR**
1	CH(=)	126.51
2	CH(=)	122.98
3	CH(=)	130.48
4	CH(=)	110.63
5	C(=)	142.26
6	C(=)	130.24
7	C	50.95
8	C=O	165.00
9	C(CN)	55.58
10	$C(NH_2)$	166.82
11	C(N)	154.66
12	C(=)	80.34

Table 14, cont.

13	CN	116.78
14	CO	163.77
15	CH_3	-

The FT-IR of DBJA-4 showed significant peaks at 3334cm^{-1} and 3294cm^{-1} in the FT-IR spectra representing the amine and amide stretch present on pyridine ring and oxindole ring in product structure. An aromatic C=C stretching vibration was also identified at 3126cm^{-1}. A significant peak at 2179 cm^{-1} representing a nitrile stretch on the pyridine ring was also observed. A strong narrow peak at 1706 cm^{-1} represents the carbonyl stretch present in amide on the oxindole ring. A strong peak seen at 1333.21 cm^{-1} could be the presence of an ether stretch stipulated to be present in structure of product due to the replacement of ethyl acetoacetate with dimethyl malonate. Further analysis with ^{1}H NMR showed a multiplex at 7.06 ppm, a region for chemical shifts observed in aromatic rings in this case the aromatic ring of oxindole. Singlet peaks seen at 5.9, 9.78 and 13.88 ppm chemical shifts produced by the hydrogen in the amine and amide groups found in the oxindole, pyrazole, and pyridine rings. Combining APT, DEPT (90° and 135°) 1D ^{13}C NMR showed the presence of four CH carbons from the aromatic ring of the oxindole in the ^{13}C NMR. The presence of impurities is responsible for chemical shift at 108.44, 121.04, 121.69, 122.11, 122.68, 130.48, 139.96, 142.26, 182.07 ppm. 2D NMR spectra (COSYGPDFPHSM and HMBCGP and HMQCGP) was also used to confirm the structure of the isolated compound by showing the proton-proton correlations and proton-carbon correlations.

The mass expected was 308 but the mass observed in the mass spectrum was 293 which is due to the loss of the fragment CH_3 (15).

Characterization of DBJA-9

DBJA-9 : MP 202-206°C, IR (cm^{-1}): 3319 (CONH), 3200 (NH_2), 1723 (CO); ^1H NMR (6OO MHz, DMSO) δ 1.21 (t, *J*=1.61 Hz 1H), 1.36 (t, *J*=3.19 Hz, 3H), 1.88 (t, *J*=1.92 Hz 2H), 2.09 (s, 5H), 7.24 (m, 2H), 5.33 (d, *J*=1.56 Hz 2H), 6.88 (m, 5H), 7.24 (m, J6H), 7.70 (s, 1H), 7.97 (s, 1H), 10.41 (s, 1H), 10.54 (s, 1H); ^{13}C NMR (150 MHz, DMSO) δ 11.18, 49.26, 50.21, 97.79, 109.77, 117.22, 121.64, 121.82, 123.94, 128.59, 132.34, 142.28, 164.35, 176.77; MS: expected mass = 310 (M), observed mass = 294 (M - 16)

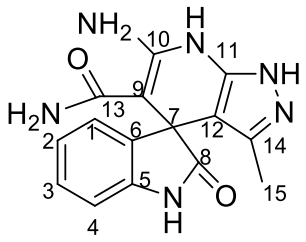

Figure 60: Structure of DBJA-9

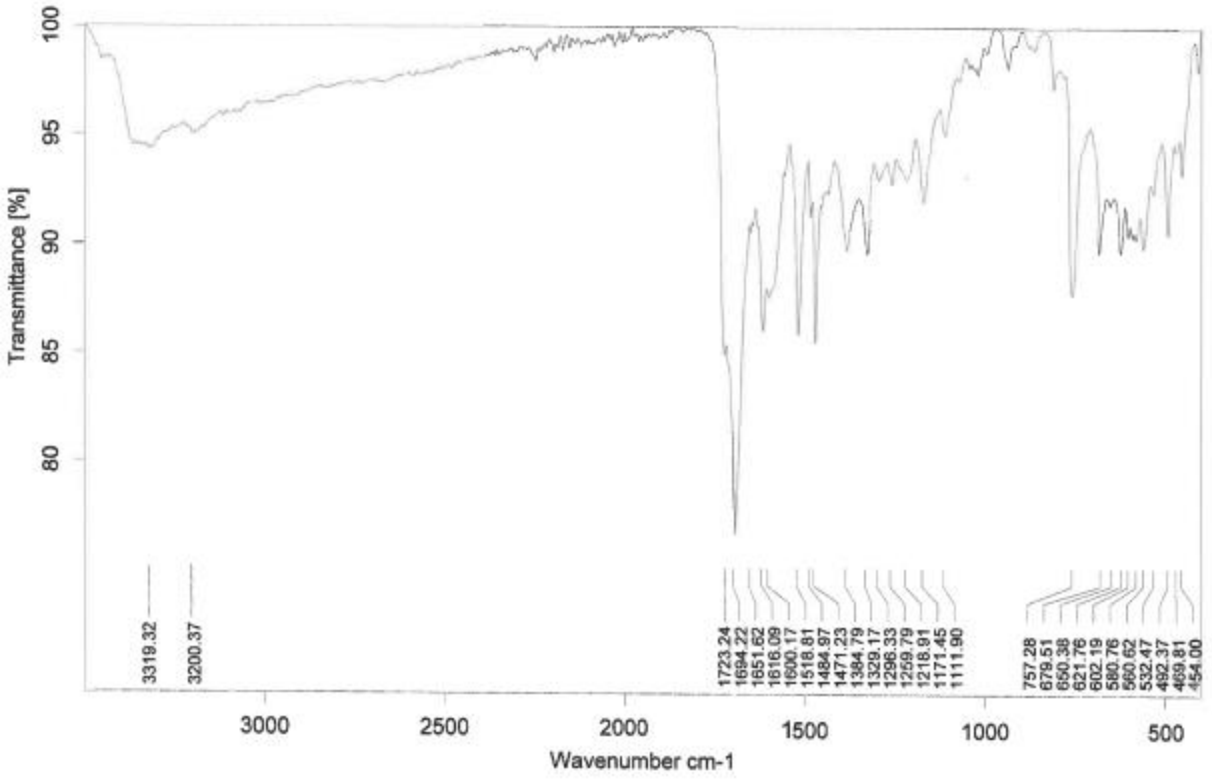

Figure 61: FT-IR spectrum of DBJA-9

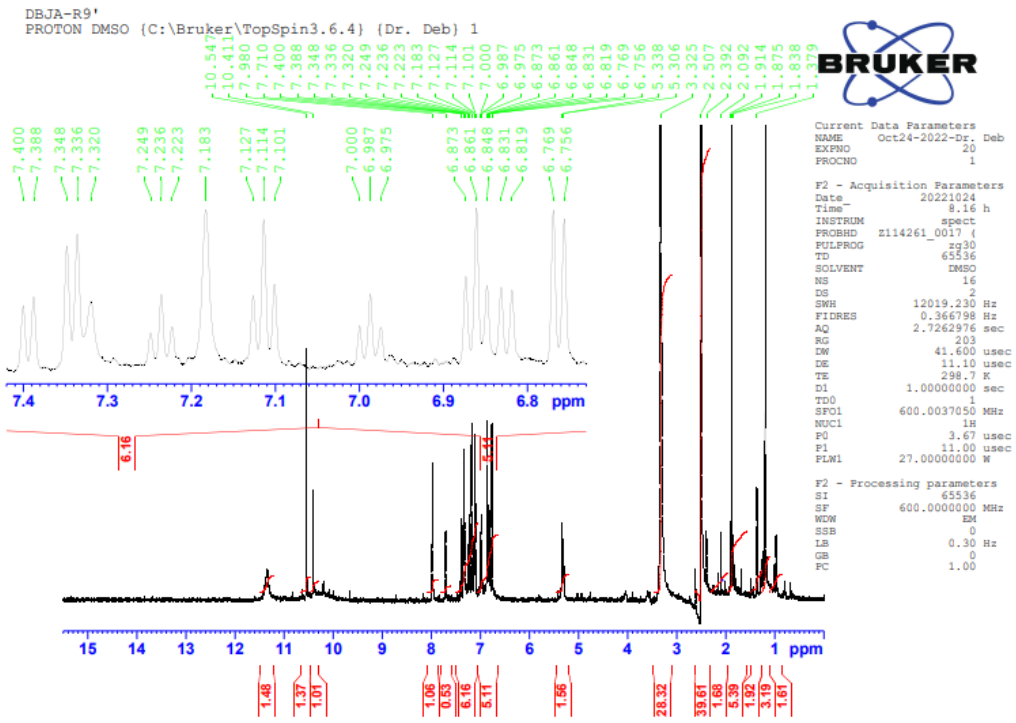

Figure 62: ^{1}H NMR spectrum of DBJA-9

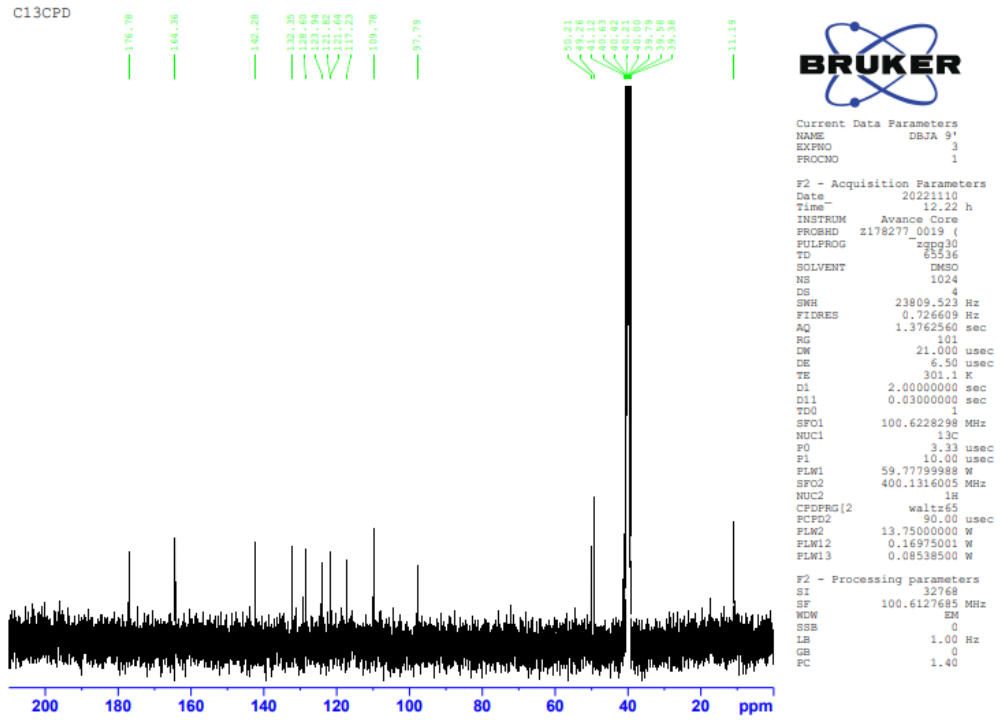

Figure 63: C^{13} NMR spectrum of DBJA-9

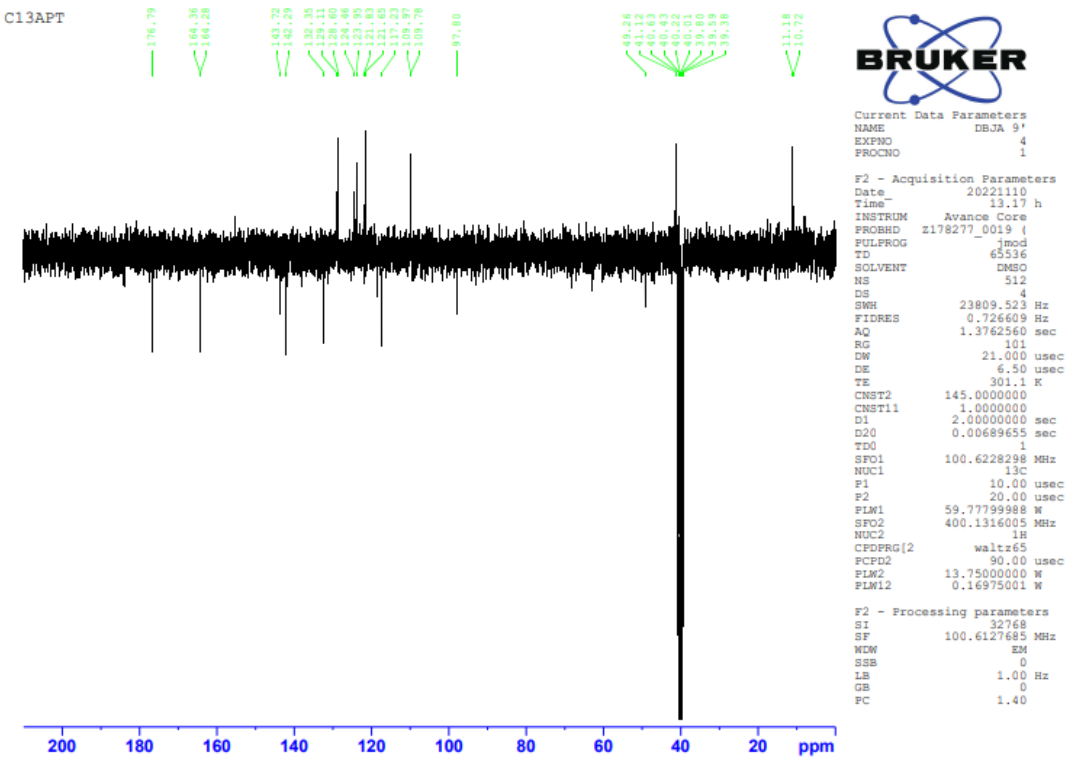

Figure 64: C^{13}APT NMR spectrum of DBJA-9

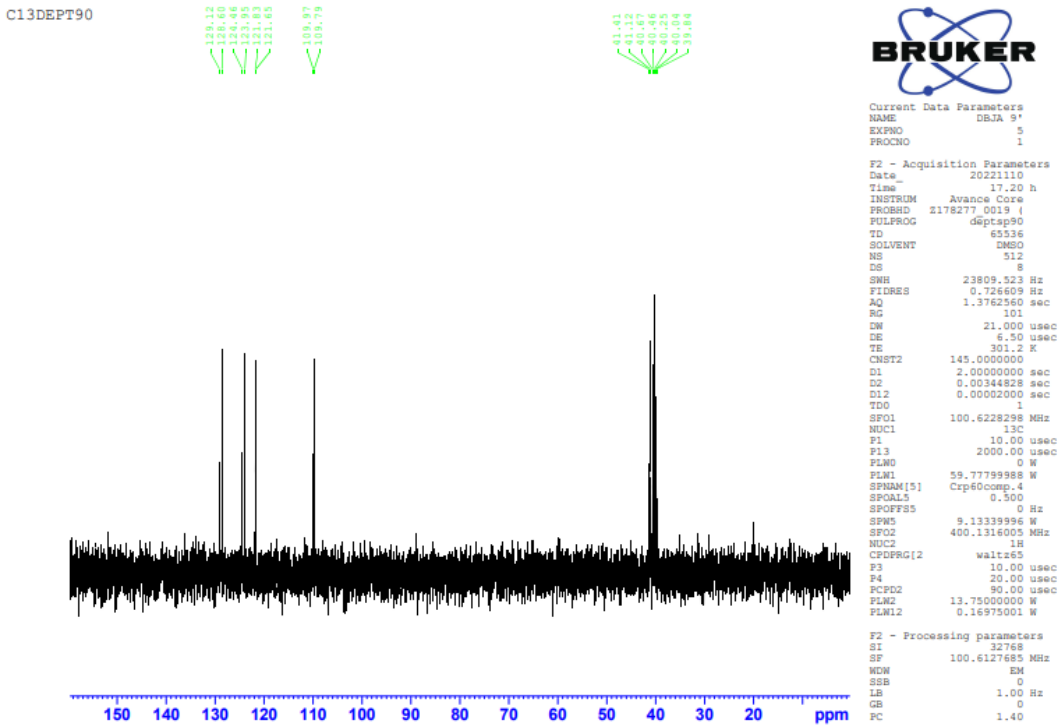

Figure 65: C^{13}DEPT90° NMR spectrum of DBJA-9

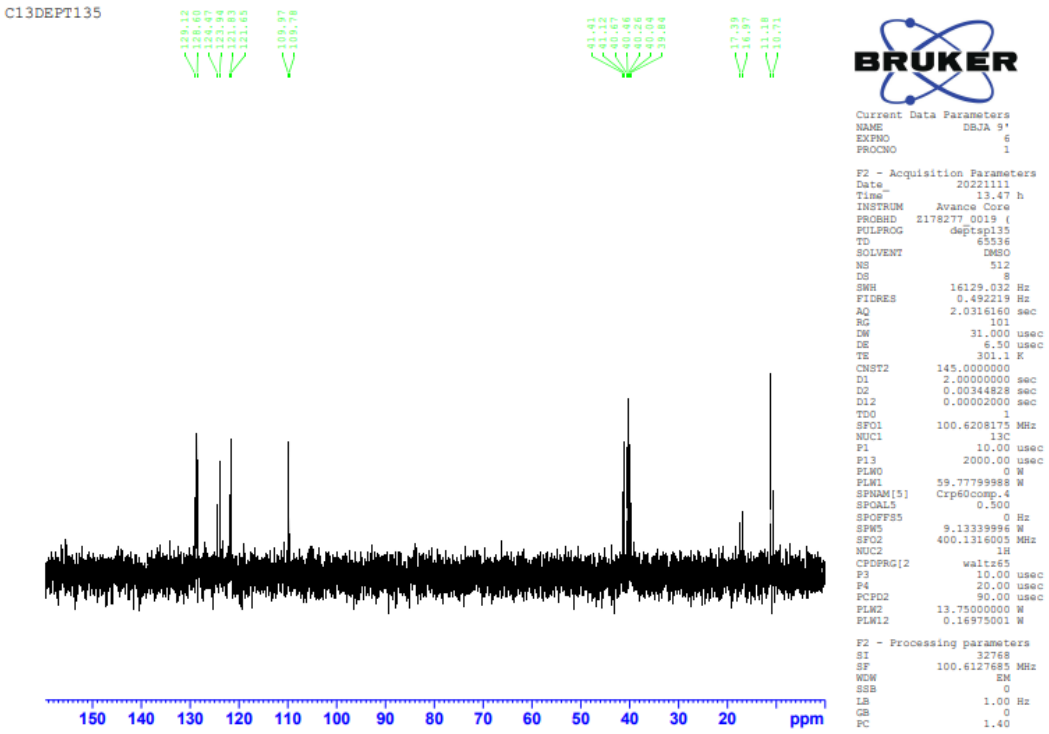

Figure 66: C13DEPT135° NMR spectrum of DBJA-9

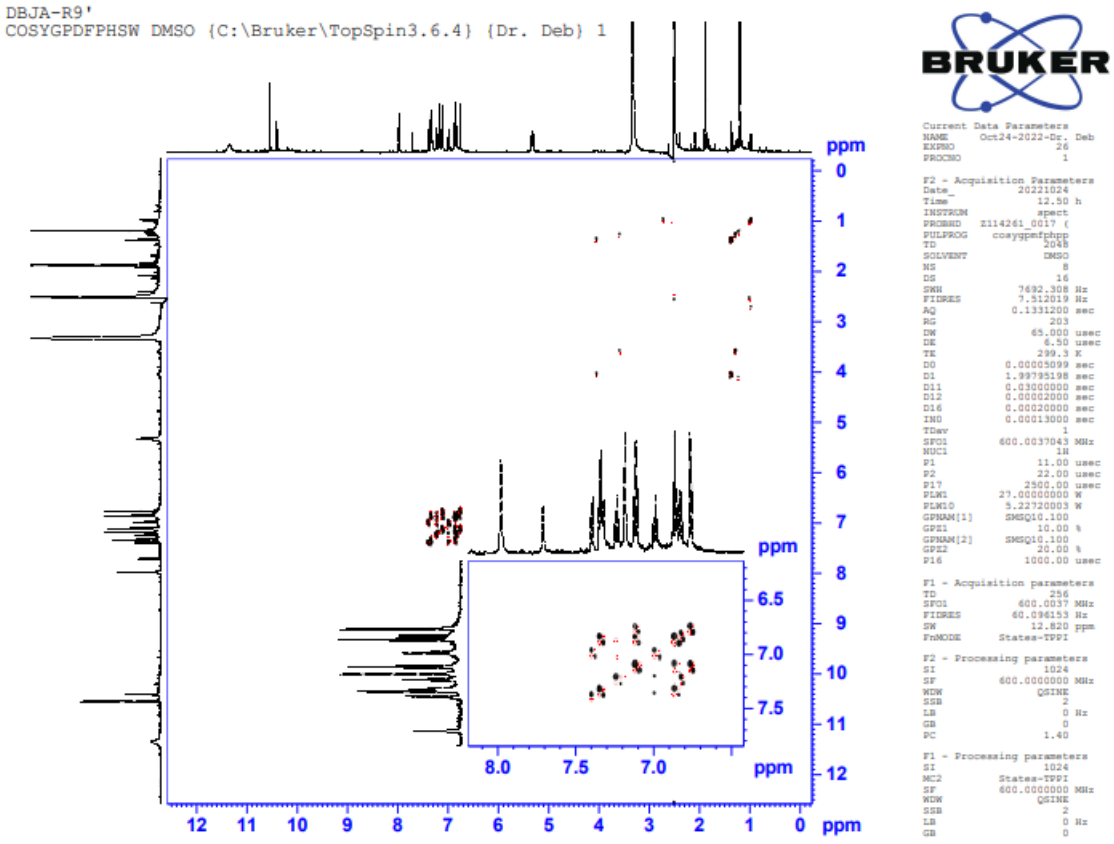

Figure 67: COSY spectrum of DBJA-9

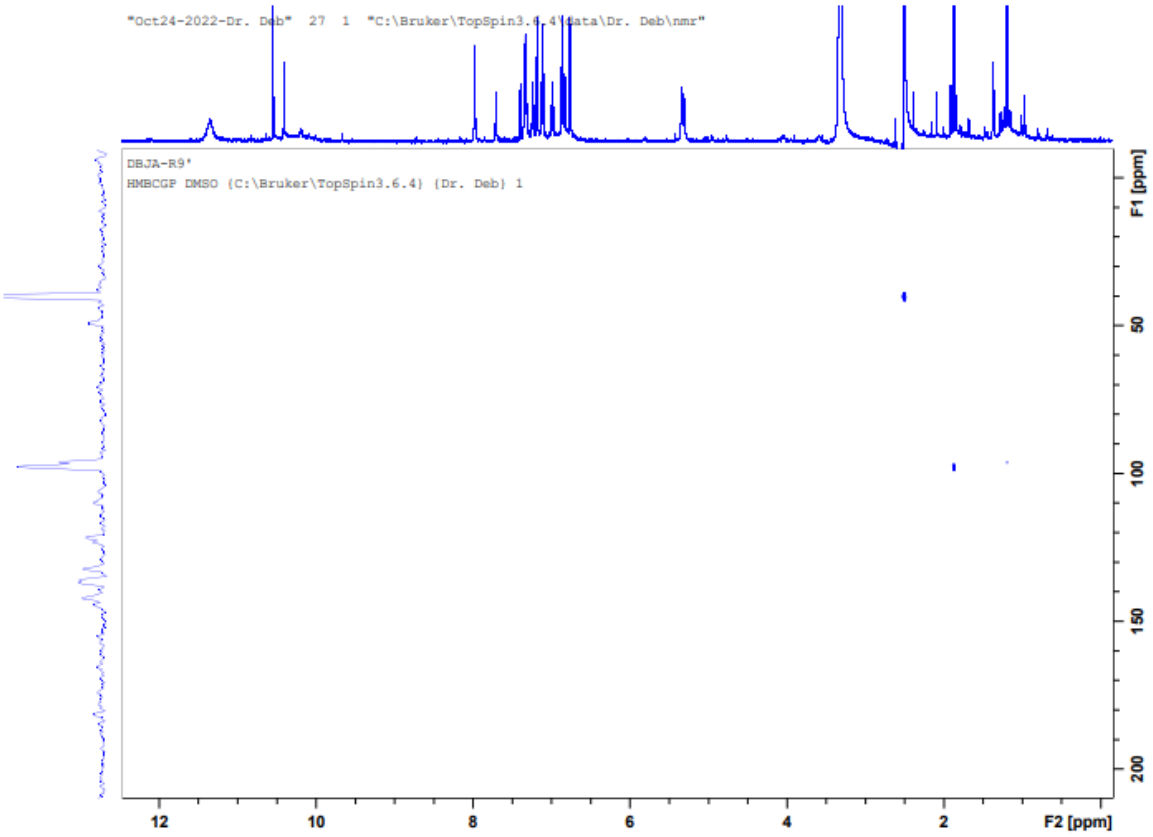

Figure 69: HMBCGP spectrum of DBJA-9

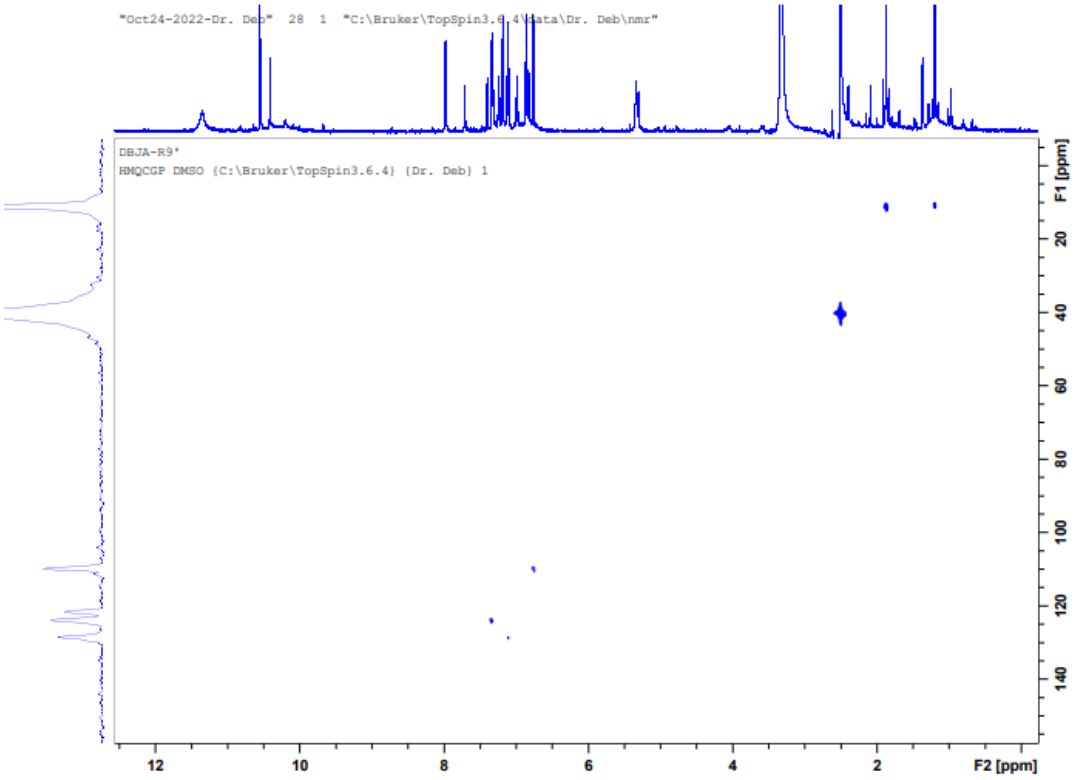

Figure 70: HMQCGP spectrum of DBJA-9

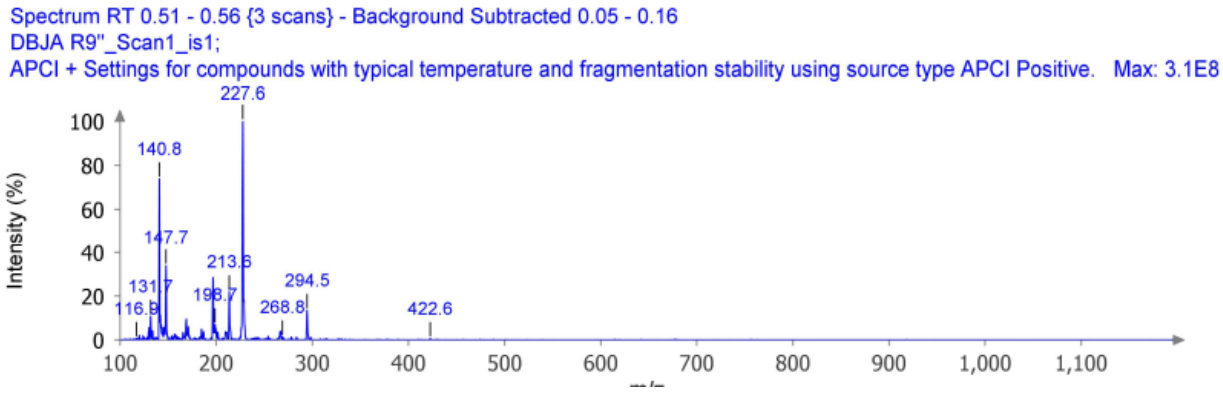

Figure 71: Mass spectroscopy spectrum of DBJA-9

Table 15: Different carbon positions in DBJA-9 and their chemical shifts

Position	**Type**	**Chemical shift, δ (ppm)** ^{13}**C NMR**
1	CH(=)	121.82
2	CH(=)	121.64
3	CH(=)	123.94
4	CH(=)	117.22
5	C(=)	142.28
6	C(=)	128.59
7	C	49.26
8	C=O	164.36
9	C(CN)	97.79
10	$C(NH_2)$	164.28
11	C(N)	142.28
12	C(=)	109.77

Table 15, cont.

13	C=O(NH_2)	176.78
14	CO	132.34
15	CH_3	11.18

The FT-IR showed the presence of amide and amine stretch at 3319 cm^{-1} and 3200 cm^{-1} respectively. The use of cyanoacetamide in place of malononitrile in reaction 9 eliminate the nitrile group and replaces it with an amide on the pyridine ring hence the absence of a peak around 2169 – 2180 cm^{-1} region. The presence of a carbonyl (C=O) stretch at 1723 cm^{-1} can also be seen as consistent with the structure of DBJA 9. ^{1}H NMR showed the presence of chemical shift of methyl (CH_3) carbon attached to the pyrazole ring. The chemical shift of NH in the different rings of the synthesized compound could be seen at 10.54 and 10.41 ppm. Chemical shift from 7.10 – 7.40 ppm were observed for the hydrogens on the aromatic ring in oxindole. ^{13}C NMR spectra in combination with APT, DEPT (90° and 135°) 1D ^{13}C NMR confirmed the presence of methyl (CH_3) carbon in structure. Four methine (CH) carbons confirmed the four CH carbons of the aromatic ring of the oxindole ring. 2D NMR spectra (COSYGPDFPHSM and HMBCGP and HMQCGP) was also used to confirm the structure of the isolated compound by showing the proton-proton correlations and proton-carbon correlations. The expected mass was 310 (M) but the observed mass in the mass spectrum was 295 (M – 16) signifying the breaking off of oxygen hence the decrease of 16 from the molecular ion (M).

Characterization of DBJA 11

DBJA 11: MP 254-256°C, IR (cm^{-1}): 3455 (CONH), 3362 (NH_2), 3109 (C=C), 2195 (CN), 1703 (CO), 1337 (NO_3); ^{1}H NMR (6OO MHz, DMSO) δ 1.17 (t, *J*=2.62 Hz 2H), 1.58 (s, , 3H), 1.99 (s, 2H), 4.03 (d, *J*=1.58 Hz 1H), 7.15 (d, *J*=1.50 Hz, 1H), 7.42 (s, 2H), 8.24 (d, *J*=1.39Hz 1H), 11.37 (s, 1H), 12.41 (s, 1H); ^{13}C NMR (150 MHz, DMSO) δ 9.56, 14.56, 21.23, 47.93, 54.31, 60.23, 67.84, 94.48, 110.65, 118.90, 120.64, 126.77, 134.22, 135.42, 143.48, 148.28, 155.68, 163.16, 178.92; MS : Expected mass = 337 (M), observed mass = 338 m/z (M+1).

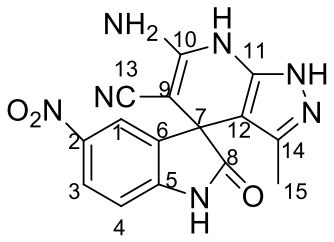

Figure 71: Structure of DBJA-11

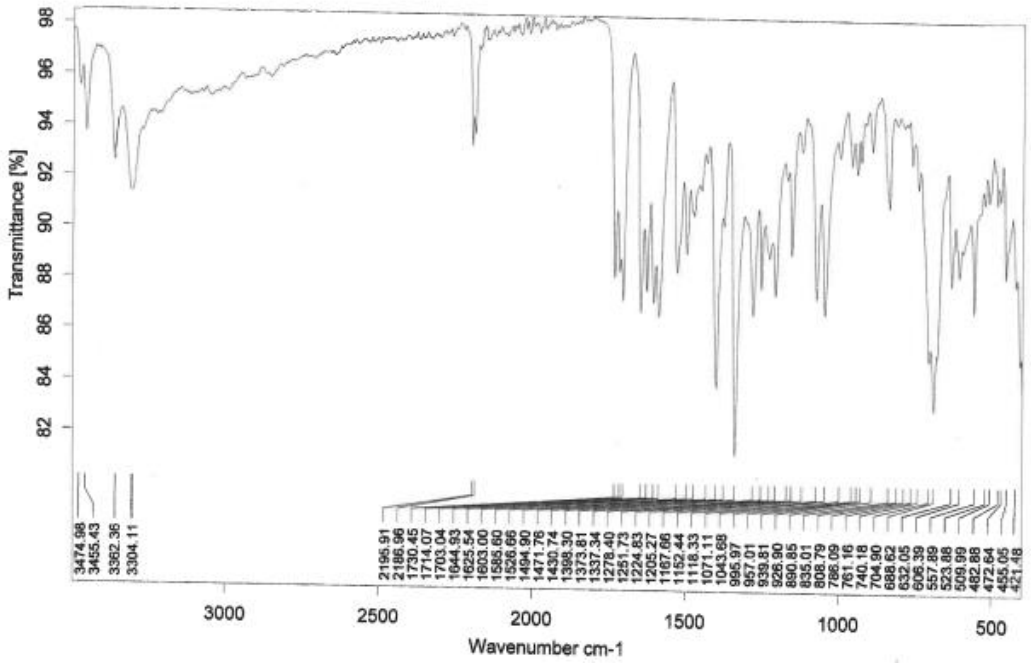

Figure 72: FT-IR spectrum of DBJA-11

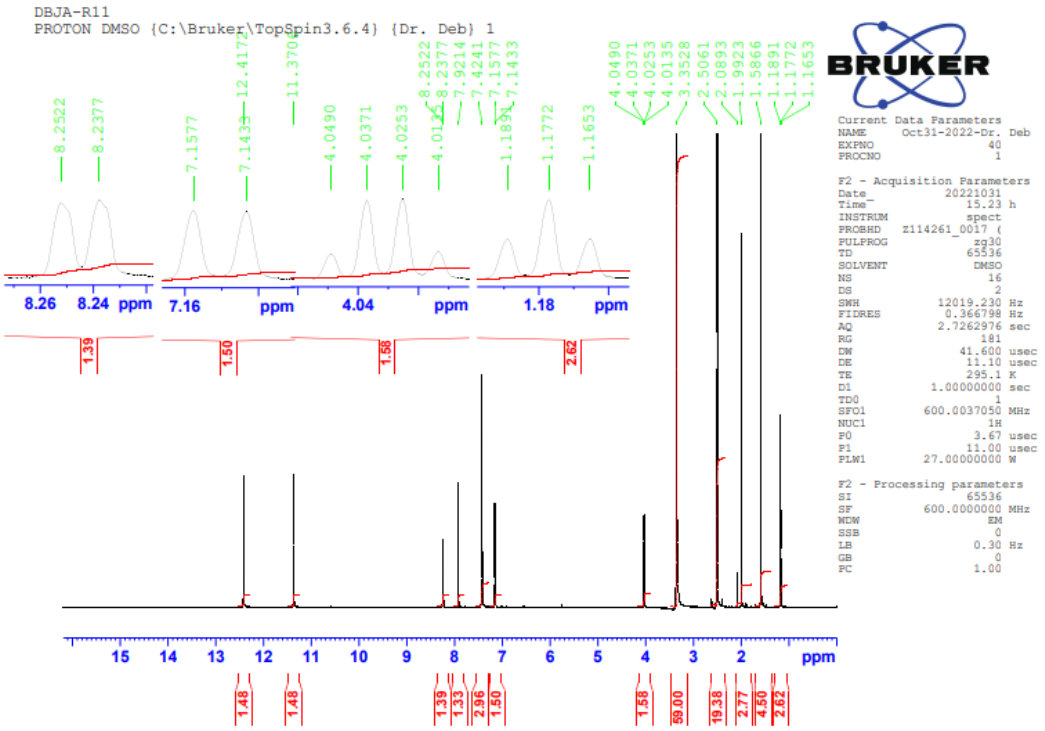

Figure 73: ^{1}H NMR spectrum of DBJA-11

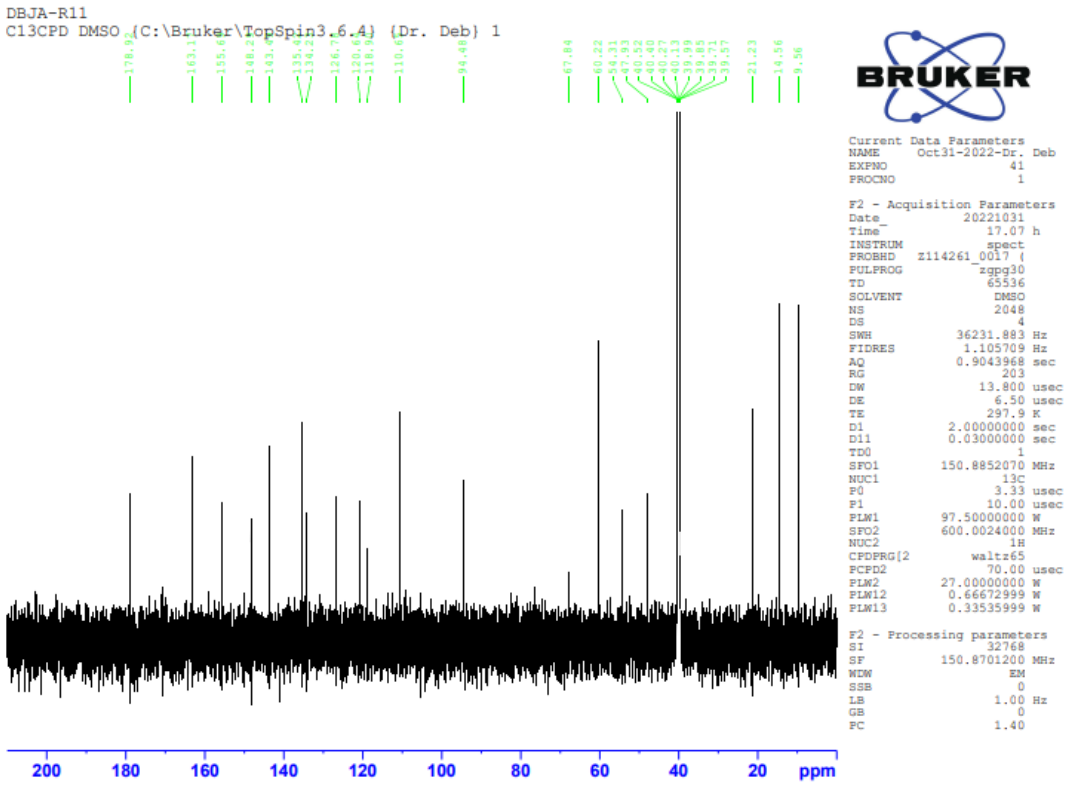

Figure 74: C^{13} NMR spectrum of DBJA-11

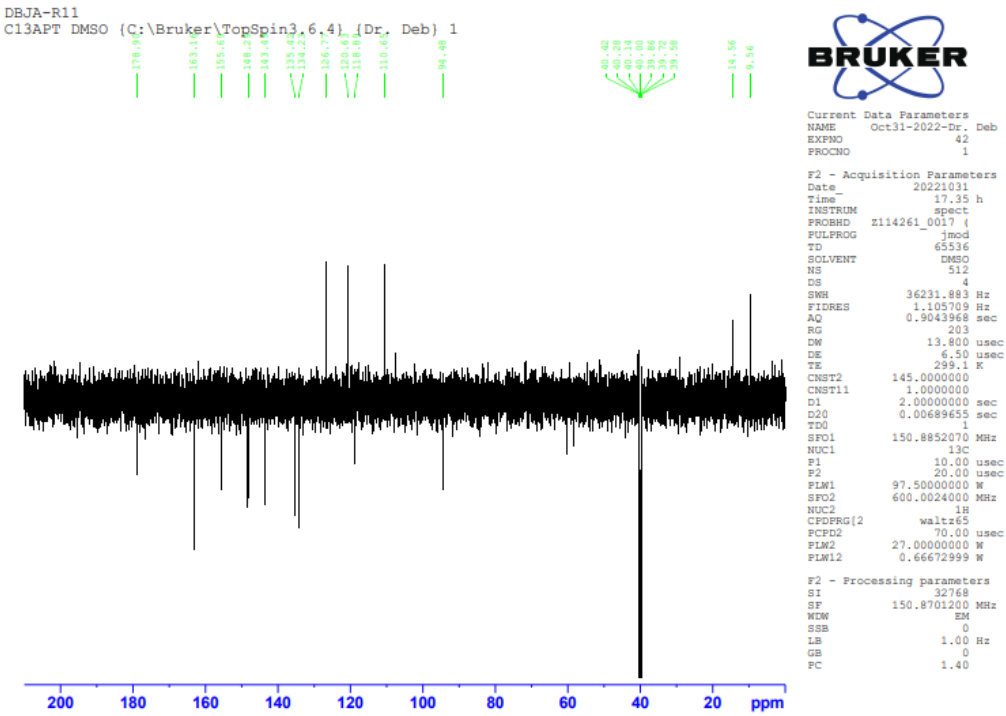

Figure 75: C^{13}APT NMR spectrum of DBJA-11

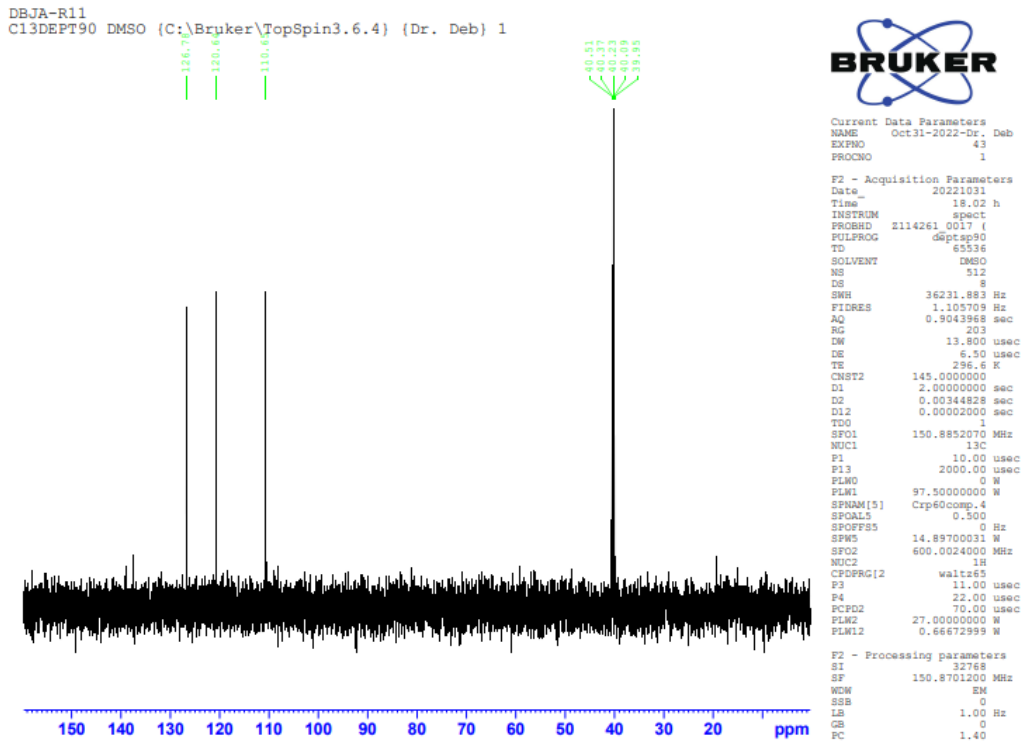

Figure 76: C^{13}DEPT90° NMR spectrum of DBJA-11

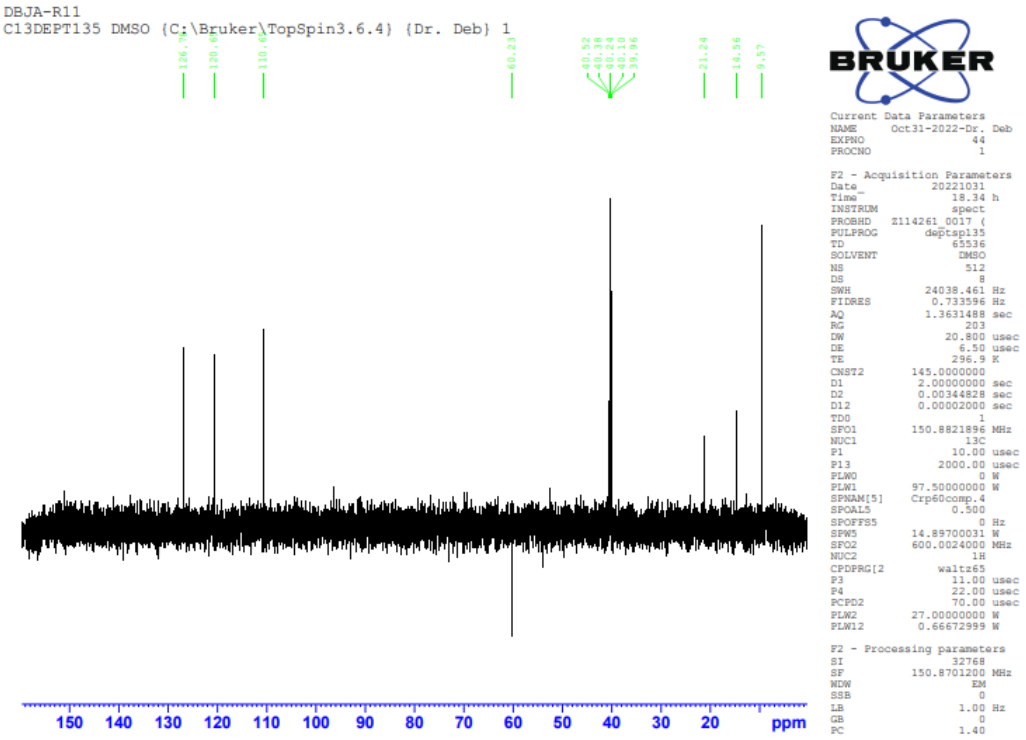

Figure 77: C13DEPT135° NMR spectrum of DBJA-11

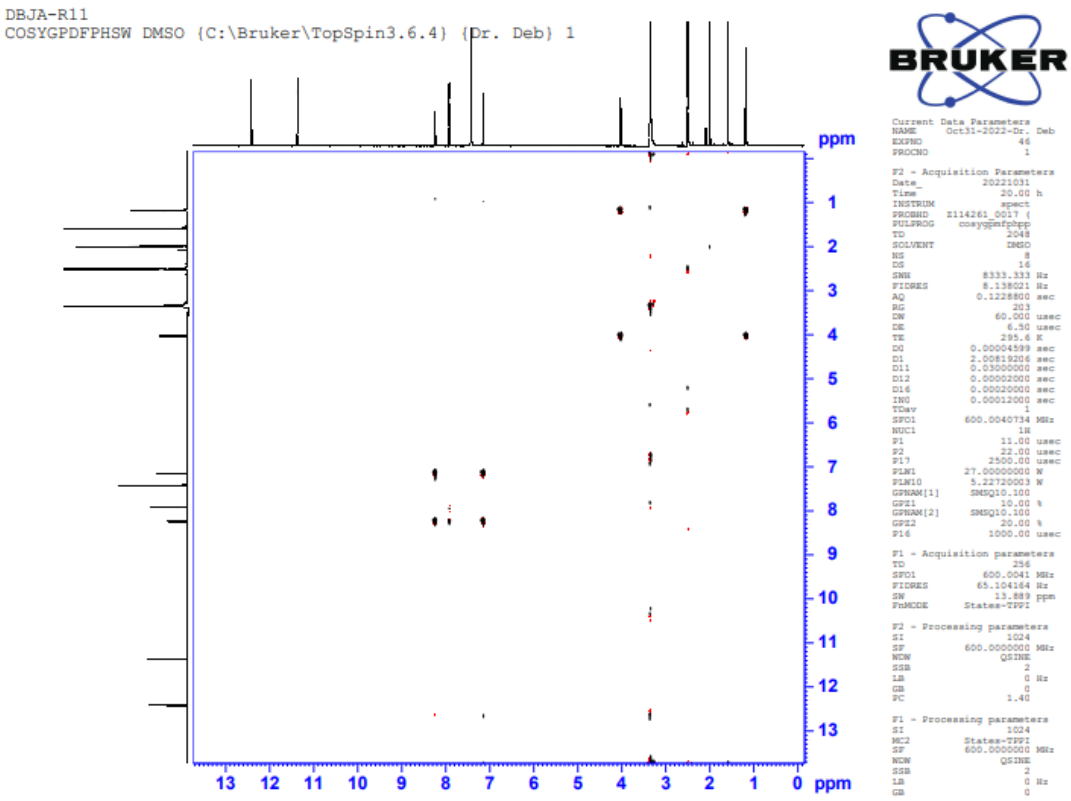

Figure 78: COSY spectrum of DBJA-11

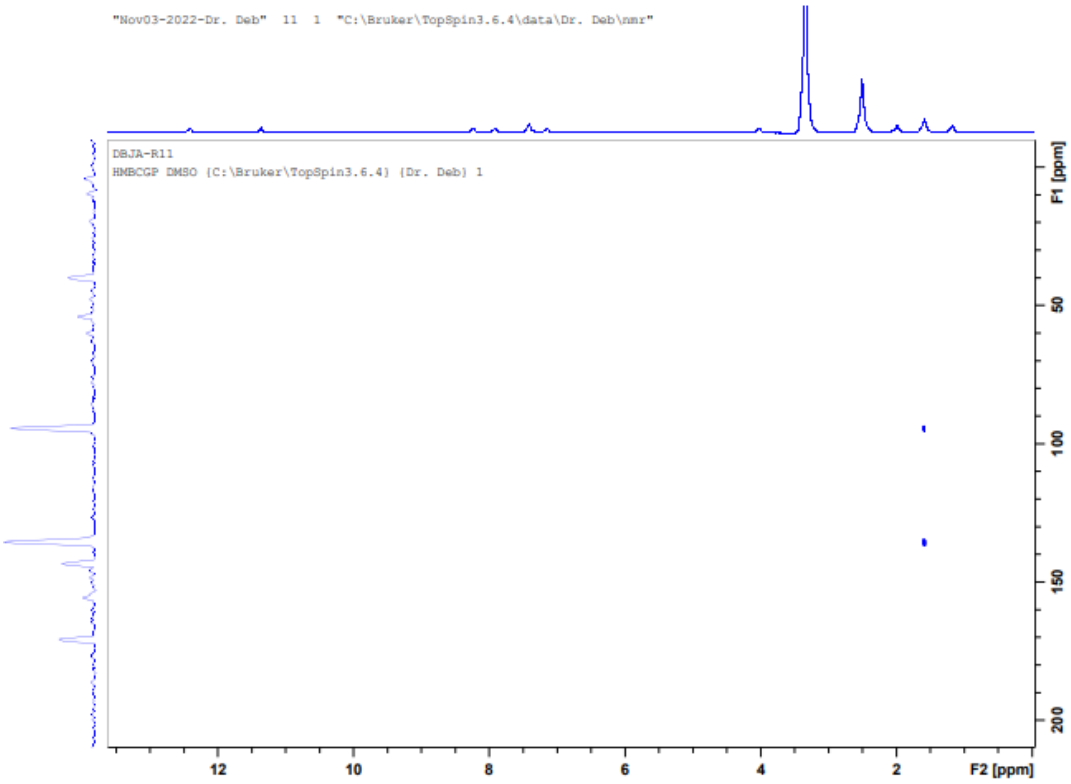

Figure 79: HMBCGP spectrum of DBJA-11

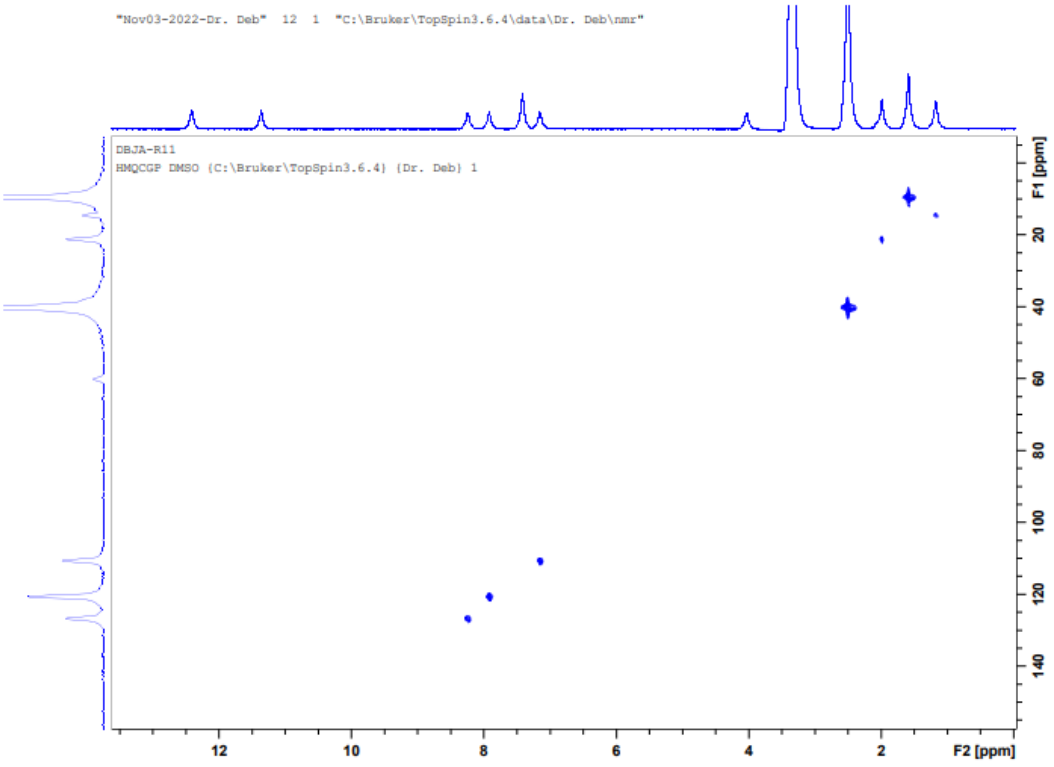

Figure 80: HMQCGP spectrum of DBJA-11

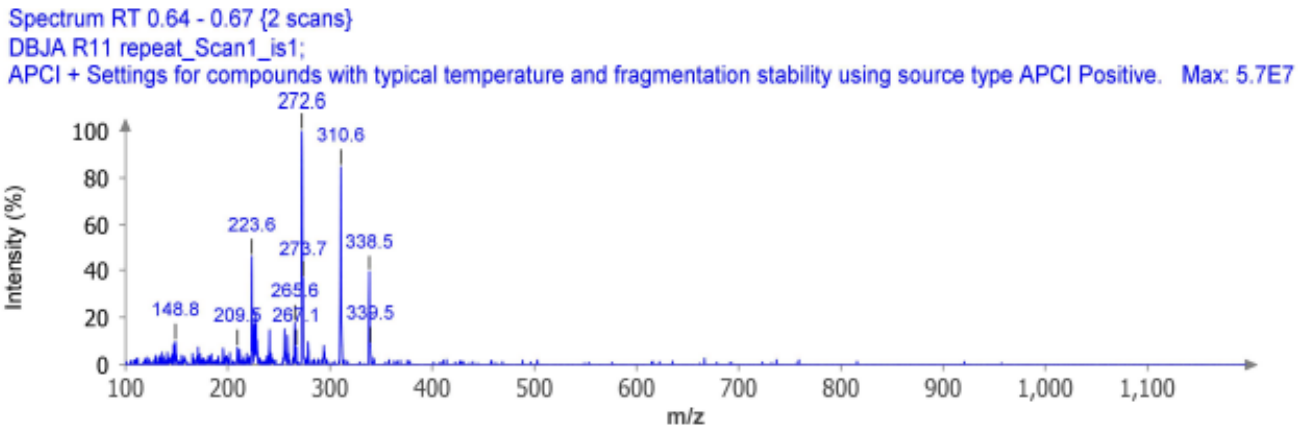

Figure 81: Mass spectroscopy spectrum of DBJA-11

Table 15: Different carbon positions in DBJA-11 and their chemical shifts

Position	**Type**	**Chemical shift, δ (ppm)** ^{13}**C NMR**
1	CH(=)	126.77
2	$C(NO_2)(=)$	143.48
3	CH(=)	120.64
4	CH(=)	110.65
5	C(=)	148.28
6	C(=)	120.64
7	C	47.93
8	C=O	163.16
9	C(CN)	67.84
10	$C(NH_2)$	178.91
11	C(N)	155.68
12	C(=)	94.47

Table 15, cont.

13	C=O(NH_2)	118.90
14	CO	135.42
15	CH_3	14.55

The FT-IR showed the presence of amide and amine stretch at 3455 cm^{-1} and 3362 cm^{-1} respectively. The replacement of oxindole with 5-nitroisatin resulted in the presence of nitro group on the oxindole fused ring. The presence of the nitro group was confirmed by a strong peak at 1337 cm^{-1} signifying NO_2 asymmetric stretch. Nitrile stretch at 2195 cm^{-1} confirmed the nitrile compound on the pyridine ring. The presence of a carbonyl (C=O) stretch at 1723 cm^{-1} can also be seen as consistent with the structure of DBJA 11. In the ^{1}H NMR, chemical shift at 1.58 ppm confirmed the presence of methyl (CH_3) on the pyrazole ring. Chemical shift at 12.41 and 11.37 ppm shows the presence of NH in structure. Chemical shifts from 7.14 – 8.25 ppm are from hydrogen on the aromatic ring of oxindole fused ring. ^{13}C NMR spectra in combination with APT, DEPT (90° and 135°) 1D ^{13}C NMR confirmed the presence of methyl (CH_3) carbon in structure. Three methine (CH) carbons instead of four confirmed that on the hydrogen atom of one of the CH carbons of the oxindole aromatic ring has been replaced by a nitro group (NO_2). The presence of impurities resulted in chemical shifts at 9.56, 21.23, 54.31, and 60.22 ppm. 2D NMR spectra (COSYGPDFPHSM and HMBCGP and HMQCGP) was also used to confirm the structure of the isolated compound by showing the proton-proton correlations and proton-carbon

correlations. From the mass spectroscopy spectrum, an M+1 peak of 338 m/z was observed confirming the expected mass of DBJA-11 (337).

CHAPTER V

CONCLUSION

Mother nature is a huge reservoir of many bioactive compounds that can be useful in curing or managing the many diseases and illnesses that plague both plants and animals in the globe. Camu-camu fruit has become popular for its high vitamin C content and the fruit along with the plant's different parts (seed, peels, leaves, root) have shown a wide range of biological activities. It is important therefore for isolate and identify the bioactive compounds responsible for the observed activities. The steroid compound isolated from the diethyl ether leaf extract of camu-camu was found to be β-sitosterol. This steroid has been previously isolated from the root bark of *M. parviflora* by Ododo et al. and was found to inhibit the bacteria growth of *S. aureus* and *E. coli* (Messina and Barnes, 1991).

Also, six different spiro pyridine derivatives were successfully synthesized in this study using environmentally benign solvent, water, and catalyst, DIPEA to give good yields of products. The compounds were successfully characterized using FT-IR, MS, and NMR.

REFERENCES

Adriane L.; Jochen R. Photophysical properties of popular fluorescent adenosine nucleotide analogs used in enzyme mechanism probing, Archives of Biochemistry and Biophysics, 2008, Volume 473, Issue 1, Pages 16-24, ISSN 0003-9861.

Aguiar, J.P.L. and Souza, F.C.A. Antioxidants, Chemical Composition and Minerals in Freeze-Dried Camu-Camu (Myrciaria dubia (H.B.K.) Mc Vaugh) Pulp. Food and Nutrition Sciences, 2015, 6, 869-874. http://dx.doi.org/10.4236/fns.2015.610091

Ahreum Ju, Kyung Bin Song, Development of teff starch films containing camu-camu (Myrciaria dubia Mc. Vaugh) extract as an antioxidant packaging material, Industrial Crops and Products. 2019, Volume 141, 111737, ISSN 0926-6690, https://doi.org/10.1016/j.indcrop.2019.111737.

Aldeghi, M.; Malhotra, S.; Selwood, D. L.; Chan, A. W. E. Chem. Biol. Drug Des. 2014, 83, 450

Anastas PT, Eghbali N Green chemistry: principles and practice. Chem Soc Rev. 2010, 39:301–312. https://doi.org/10.1039/ B918763B

Anastas P. T.; Warner JC. Green Chemistry: theory and practice. Oxford University Press, Oxford. Antioxidant compounds and antioxidant capacity of Peruvian camu camu (Myrciaria dubia (H.B.K.) McVaugh) fruit at different maturity stages, Food Chemistry, 2010, Volume 120, Issue 4, Pages 1019- 1024, ISSN 0308-8146,https://doi.org/10.1016/j.foodchem.2009.11.041.

Aparna D.; Bimal K. B., Dipole moment in medicinal research: Green and sustainable approach, Editor(s): Bimal Krishna Banik, In Advances in Green and Sustainable Chemistry, Green Approaches in Medicinal Chemistry for Sustainable Drug Design, Elsevier, 2020, Pages 921-964, ISBN 9780128175927, https://doi.org/10.1016/B978-0-12-817592-7.00021-6.

Arpi M.; Ragini G.; Anshu J. Microwave-assisted synthesis of nitrogen-containing heterocycles, Green Chemistry Letters and Reviews, 2013, 6:2, 151-182, DOI: 10.1080/17518253.2012.733032

Atif B. A.; Karen C. C.; Arthur C. D.; Carol S. F. Peanuts as a Source of β-Sitosterol, a Sterol With Anticancer Properties, Nutrition and Cancer, 2000, 36:2, 238-241, DOI: 10.1207/S15327914NC3602_14

Cella, J. A.; Brown, E. A.; Burtner, R. R. Steroidal Aldosterone Blockers. I. J. Org. Chem. 1959, 24 (6), 743−748.

Cella, J. A.; Tweit, R. C. Steroidal Aldosterone Blockers. II1. J. Org. Chem. 1959, 24 (8), 1109−1110

Debasish B., Bimal K. B., Chapter 3 - Microwave-assisted synthesis of medicinally privileged heterocycles, Editor(s): Goutam Brahmachari, Green Synthetic Approaches for Biologically Relevant Heterocycles (Second Edition), Elsevier, 2021, Pages 49-110, ISBN 9780128205860, https://doi.org/10.1016/B978-0-12-820586-0.00009-1.

Demain, A. L. Microbial production of primary metabolites. Naturwissenschaften, 1980, 582-587,Vol 67,12,1432-1904 doi: 10.1021/jf051357v

Dress, B. E.; Chakravarty, L.; Prestwich, G. D.; Dorman, G.; Kavecz, M.; Lukacs, A.; Urge, L.; Darvas, F.; Rzepecki, P. W.; Ferguson, C. Compounds having Inhibitive Activity of Phosphatidylinositol 3-Kinase and Methods of Use Thereof. G.W.O. Patent 016, 245, 2005 (Chem. Abstr. 2005, 142, 261534).

Ekor, M. The Growing Use of Herbal Medicines: Issues Relating to Adverse Reactions and Challenges in Monitoring Safety. Front. Pharmacol. 2014, 4, 177.

Elger, W.; Beier, S.; Pollow, K.; Garfield, R.; Shi, S. Q.; Hillisch, A. Conception and Pharmacodynamic Profile of Drospirenone. Steroids 2003, 68 (10−13), 891−905.

Fidelis M.,; Santos J. S.; Escher G. B.; Vieira do Carmo M.; Azevedo L.; Cristina da Silva M., Putnik P.; Granato D. In vitro antioxidant and antihypertensive compounds from camu-camu (Myrciaria dubia McVaugh, Myrtaceae) seed coat: A multivariate structure-activity study. Food Chem Toxicol. 2018 Oct;120:479-490. doi: 10.1016/j.fct.2018.07.043. Epub 2018 Jul 25. PMID: 30055315.

Flores, J. L. (2020). Chemical investigaion of camu camu (0RW1S34RfeSDcfkexd09rT2myrciaria dubia1RW1S34RfeSDcfkexd09rT2) leaves and roots (Order No. 28261014). Available from

ProQuest Dissertations & Theses Global. (2595486352). Retrieved from https://go.openathens.net/redirector/utrgv.edu?url=https://www.proquest.com/dissertations-theses/chemical-investigaion-camu-em-myrciaria-dubia/docview/2595486352/se-2

Fujita, A.; Dipayan S. B.; Shibiao W. C.; Edward K. C.; Kalidas S. B.; Maria I. G. Evaluation of phenolic-linked bioactives of camu-camu (Myrciaria dubia Mc. Vaugh) for antihyperglycemia, antihypertension, antimicrobial properties and cellular rejuvenation. Food Research International (2015), http://dx.doi.org/10.1016/j.foodres.2015.07.009

Garthwaite, S. M.; McMahon, E. G. The Evolution of Aldosterone Antagonists. Mol. Cell. Endocrinol. 2004, 217 (1−2), 27−31.

Ghasemzadeh, M.A.; Mirhosseini-Eshkevari, B.; Abdollahi-Basir, M.H. Green synthesis of spiro[indoline-3,4′-pyrano[2,3-c]pyrazoles] using Fe_3O_4@L-arginine as a robust and reusable catalyst. *BMC Chemistry*, 2019, 13, 119. https://doi.org/10.1186/s13065-019-0636-1

Gould, C.; Jones, R.; LeRoy, G, Wissler; R.; Taylor, C. Absorb-ability ofb-sitosterol in humans.Metabolism. 1969, 18, 652–662, 2.

Han Y. N.; Choo Y.; Lee Y. C.; Moon Y. I.; Kim S. D.; Choi J. W. Arch. Pharm. Res.,2001, 24, 51–54.

Hany S. I.; Wagdy M. E.; Anna L. F.; Esam R. A.; Hazem A. G.; Mahmoud M. E.; Maurizio B.; Sahar M. A.; Hatem A. A.. One-pot synthesis of spiro(indoline-3,4 - pyrazolo[3,4-b]pyridine)-5 -carbonitriles as p53-MDM2 interaction inhibitors, Future medicinal chemistry. 2018, VOL. 10, NO. 24. https://doi.org/10.4155/fmc-2018-0288

Hiesinger, K.; Dar'in, D.; Proschak, E.; Krasavin, M. Spirocyclic Scaffolds in Medicinal Chemistry, Journal of Medicinal Chemistry, American Chemical Society, 2021, SN - 0022-2623, VL - 64, doi: 10.1021/acs.jmedchem.0c01473.

Inoue T.; Komoda H.; Uchida T.; Node K. Tropical fruit camu-camu (Myrciaria dubia) has anti-oxidative and anti-inflammatory properties. J Cardiol. 2008 Oct;52(2):127-32. doi: 10.1016/j.jjcc.2008.06.004. Epub 2008 Jul 29. PMID: 18922386.

Jampilek, J. "Heterocycles in Medicinal Chemistry" *Molecules*. 2019, 24, no. 21: 3839. https://doi.org/10.3390/molecules24213839

Jefferson Y-A.; Dayanne C. F.; Silas F. E.; Gustavo S. C.; Paulo F. M.; Fausto A. M.-N.; João B.K. F.; Flávio R. de M., Julieta R. E. de M. Dietary camu camu, Myrciaria dubia, enhances immunological response in Nile tilapia, Fish & Shellfish Immunology. 2016, Volume 58, Pages 284-291, ISSN 1050-4648, https://doi.org/10.1016/j.fsi.2016.08.030.

Jessyca R. W.; Graziela B. E.; Tai K.; Marianna M. F.; Anderson S. Sant'Ana; Mariana A. V. do C. ;Luciana A. ;Daniel G. Response surface optimization of phenolic compounds extraction from camu-camu (Myrciaria dubia) seed coat based on chemical properties and bioactivity. j.foodchem. 2020 https://doi.org/10.1111/1750-3841.15327

Juliana C. S. de A.; Alice F.; Edson L. de O.; Maria I. G.; Roberta T. P. C. Dried camu-camu (Myrciaria dubia H.B.K. McVaugh) industrial residue: A bioactive-rich Amazonian powder with functional attributes, Food Research International, 2014, Volume 62, Pages 934-940, ISSN 0963-9969.

Kazunaga Y.; Katsumi S.; Atsushi H.; Miyuki S.; Tomoyuki K. Anti-Inflammatory Effects of Seeds of the Tropical Fruit Camu-Camu (*Myrciaria dubia*), Journal of Nutritional Science and Vitaminology, 2011, Volume 57, Issue 1, Pages 104-107, Released on J-STAGE April 22, 2011, Online ISSN 1881-7742, Print ISSN 0301-4800, https://doi.org/10.3177/jnsv.57.104

Kung, D. W. S.; Wager, T. T. Pyrazolo[3,4-b]pyridin-6-ones as GSK-3 Inhibitors. WO Patent 2005000304 A1, 2005.

Lovering, F. Med. Chem. Commun. 2013, 4, 515.

Lovering, F.; Bikker, J.; Humblet, C. J. Med. Chem. 2009, 52, 6752

Lubineau, André; Augé, Jacques. Water as Solvent in Organic Synthesis. Springer-Verlag Berlin Heidelberg. 10.1007/3-540-48664-X_1

Maria L. G.; Edvan A. C.; Bala R.; Pollyana C. C.; Antonia R. V. da S., Sara T. M. S.; Railin R. de O. "Qualitative evaluation and biocompounds present in different parts of camu-camu (Myrciaria dubia) fruit." African Journal of Food Science. 2017, 11, no. 5: 124-129. https://doi.org/10.5897/AJFS2016.1574

Mariana A. V. D. C.; Marina F.; Carolina G. P.; Marcos J. M.; Angel M. C.-G., Takao M., Daniel G., Luciana A. Hydroalcoholic Myrciaria dubia (camu-camu) seed extracts prevent chromosome damage and act as antioxidant and cytotoxic agents, Food Research International, 2019,Volume 125, 108551, ISSN 0963-9969, https://doi.org/10.1016/j.foodres.2019.108551.

Marina F.; Mariana A. V. do C.; Thiago M. da C.; Luciana A.; Takao M.; Marianna M. F.; Mariza B. M.; Anderson S. Sant'Ana, Maria I. G.; Won Y. O.; Mingchun W.; Fereidoon S.; Liang Z.; Marcelo F.; Severino M. de A.; Pedro L. R.; Daniel G. Camu-camu seed (*Myrciaria dubia*) – From side stream to an antioxidant, antihyperglycemic, antiproliferative, antimicrobial, antihemolytic, anti-inflammatory, and antihypertensive ingredient, Food Chemistry, 2020, Volume 310, 125909, ISSN 0308-8146, https://doi.org/10.1016/j.foodchem.2019.125909.

Mathur, S., Hoskins, C."Drug development: Lessons from nature (Review)". Biomedical, 2017, Reports 6, no. 6: 612-614. https://doi.org/10.3892/br.2017.909

Messina, M.; Barnes, S. The role of soy products in reducing the risk of cancer. JNCI83,541–546, 1991.4.

Myoda, T.; Fujimura, S.; Park, B.; Nagashima, T.; Nakagawa, J.; Nishizawa, M. Antioxidative and antimicrobial potential of residues of camu-camu juice production. Journal of Food, Agriculture and Environment. 2010, 8.

Naglaa, F. H. M.; Rizk, S. A.; Galal, A. E. *et al.* Expeditious microwavable one-pot synthesis and biological exploration of spiro[indoline-3,4′-pyrazolo[3,4-b] pyridine derivatives. *J IRAN CHEM SOC,* 2022, 19, 3711–3719. https://doi.org/10.1007/s13738-022-02568-x

Nasser, A.; Ibrahim, S. A. El-K., Sameh A. R.; Ali K. A. Regioselective Synthesis, Spectroscopic Characterization, and Computational Chemical Study of Spiro[Indoline-3,4’-Pyrazolo[3,4-b] Pyridine Derivatives as Agrochemical Agents, Polycyclic Aromatic Compounds, 2022, 42:8, 5567-5584, DOI: 10.1080/10406638.2021.1942083

Nishanth R. R.; Jena, S.; Mukherjee, M. *et al.* Green synthesis of biologically active heterocycles of medicinal importance: a review. *Environ Chem Lett*, 2021, 19, 3315–3358. https://doi.org/10.1007/s10311-021-01232-9

Ododo, M. M.; Choudhury, M. K.; Dekebo, A. H. Structure elucidation of β-sitosterol with antibacterial activity from the root bark of Malva parviflora . SpringerPlus, 2016, 5, 1210. https://doi.org/10.1186/s40064-016-2894-x

Pisha, E.; Chai H.; Lee I. S.; Chagwedera, T. E.; Farnsworth, N. R.; Cordell, G. A.; Beecher, C. W.; Fong H. H.; Kinghorn, A. D.; Brown, D. M.; Wani, M. C.; Wall, M. E.; Hieken, T. J.; Das, G. T. K.; Pezzuto, J. M. Discovery of betulinic acid as a selective inhibitor of human melanoma that functions by induction of apoptosis. Nat Med, 1995, 1: 1046-1051.

Pradhan, R.; Manabendra, P.; Ajaya, K. B.; Bijay K. M.; Rajani K. B. "A Synthon Approach to Spiro Compounds." *ChemInform*, 2006, 37: n. pag

Quintavalla, A. Spirolactones: Recent Advances in Natural Products, Bioactive Compounds and Synthetic Strategies. Curr. Med. Chem. 2018, 25 (8), 917−962.

Gedye, R.; Smith, F.; Westaway, K.; Ali H.; Baldisera, L.; Laberge, L.; et al., The use of microwave ovens for rapid organic synthesis, Tetrahedron Lett. 1986, 27, 279-282.

Rao, A. V.; Janezic, S. A. The role of dietary phytosterols in coloncarcinogenesis.Nutr Cancer, 1992, 18,43–52, 3.

Richie, T. J.; Macdonald, S. J.; Young, R. J.; Pickett, S. D. Drug Discovery Today 2009, 14, 1011

Rose, D. P.; Boyar, A. P.; Wynder, E. L. International comparisons of mortality rates for cancer of the breast, ovary, prostate and colon, and per capita food consumption. Cancer, 1986, 58,2363–2371.

Rosella, C.-C.; Gabriela, U.-U.; Dyanne, M.-F.; Stefany, C.-G.; Frank, M.-T.; Juana, del V.-M. Antibacterial activity of *Myrciaria dubia* (Camu camu) against Streptococcus mutans and Streptococcus sanguinis, Asian Pacific Journal of Tropical Biomedicine, 2016, Volume 6, Issue 9, Pages 740-744, ISSN 2221-1691, https://doi.org/10.1016/j.apjtb.2016.07.008.

Roumy, V.; Ruiz, M. J. C.; Bonneau, N.; Samaillie, J.; Azaroual, N.; Encinas, L. A.; Rivière, C.; Hennebelle, T.; Sahpaz, S.; Antherieu, S.; Pinçon, C.; Neut, C.; Siah, A.; Gutierrez-Choquevilca A. L.; Ruiz L. Plant therapy in the Peruvian Amazon (Loreto) in case of

infectious diseases and its antimicrobial evaluation. J Ethnopharmacol. 2020, Mar 1;249:112411. doi: 10.1016/j.jep.2019.112411. Epub 2019 Nov 18. PMID: 31751651.

Saeidnia, S.; Manayi, A. R.; Gohari, A.; Abdollahi, M. The Story of Beta-sitosterol- A Review. European Journal of Medicinal Plants, 2014, 4(5), 590-609. https://doi.org/10.9734/EJMP/2014/7764

Santhosh G.; Sumaiya T. Sulphuric acid supported silica gel (H2SO4-SiO2) as an efficient catalyst for one-pot multicomponent synthesis of pyrano[2,3-c]pyrazol-amines under ultrasonication, Materials Today: Proceedings, 2021, Volume 45, Part 3, Pages 3762-3768, ISSN 2214-7853, https://doi.org/10.1016/j.matpr.2021.01.273.

Suga, A.; Takaishi, Y.; Nakagawa, H.; Iwasa, T.; Sato, M.; Okamoto, M. Nat. Med. (Tokyo), 59, 70–75 (2005).

Swetha, Y.; Adinarayana, M. A.; Rajiv, T.; Balaji, R.; Reddy, S. P.; Sridhar, B. Spirooxindole-fused pyrazolo pyridine derivatives: NiO–SiO2 catalyzed one-pot synthesis and antimicrobial activities, Synthetic Communications, 2018, 48:3, 255-266, DOI: 10.1080/00397911.2017.1393687

Tai, K.; Takao, M.; Kazuki, T.; Takane, F.; Makoto, N. Antimicrobial constituents of peel and seeds of camu-camu (*Myrciaria dubia*), *Bioscience, Biotechnology, and Biochemistry*, 2017, Volume 81, Issue 8, , Pages 1461–1465, https://doi.org/10.1080/09168451.2017.1320517

Tai, K.; Takao, M.; Mayuko, N.; Takane, F.; Kazuki, T.; Makoto, N. Antioxidant activity of C-Glycosidic ellagitannins from the seeds and peel of camu-camu (Myrciaria dubia), LWT - Food Science and Technology, 2016, Volume 69, Pages 76-81, ISSN 0023-6438, https://doi.org/10.1016/j.lwt.2016.01.024

Tai, K.; Takao, M.; Kazuki, T.; Takane, F.; Makoto, N. Antioxidative Constituents in Camu-camu Fruit Juice Residue, Food Science and Technology Research, 2013, Volume 19, Issue 2, Pages 223-228, Released on J-STAGE April 13, 2013, Online ISSN 1881-3984, Print ISSN 1344-6606, https://doi.org/10.3136/fstr.19.223

Takada, Y.; Aggarwal, B. B. 2003. Betulinic acid suppresses carcinogen-induced NF-κB activation through inhibition of IκBα kinase and p65 phosphorylation: abrogation of cyclooxygenase-2 and matrix metalloprotease-9. J Immunol 171: 3278-3286.

Toshiyuki, A.; Yasuyuki, S.; Takumi, K.; Hirokazu, K.; Tatsuya, M.; Kimio, S. 1-Methylmalate from Camu-Camu (*Myrciaria dubia*) Suppressed D-Galactosamine-Induced Liver Injury in Rats, *Bioscience, Biotechnology, and Biochemistry*, March 2010, Volume 74, Issue 3, 23, Pages 573–578, https://doi.org/10.1271/bbb.90775

Ueda, H.; Kuroiwa, E.; Tachibana, Y.; Kawanishi, K.; Ayala, F.; Moriyasu, M. Aldose reductase inhibitors from the leaves of Myrciaria dubia (H. B. & K.) McVaugh. Phytomedicine. 2004 Nov;11(7-8):652-6. doi: 10.1016/j.phymed.2003.12.002. PMID: 15636180

Verotta, L. Are acylphloroglucinols lead structures for the treatment of degenerative diseases?. Phytochemistry Reviews, 2002, 1, 389–407. https://doi.org/10.1023/A:1026069624278

Welsch, M. E.; Snyder, S. A.; Stockwell, B. R. Privileged scaffolds for library design and drug discovery. Curr. Opin. Chem. Biol. 2010, 14(3), 347–361.

Wu, G.; Yin, W.;Shen, H. C.; Huang, Y. One-pot synthesis of useful heterocycles in medicinal chemistry using a cascade strategy,Green Chem., 2012,vol-14, issue-3, pg 580-585,The Royal Society of Chemistry",10.1039/C2GC16457D.

Wu, X.; Beecher, G. R.; Holden, J. M.; Haytowitz, D. B.; Gebhardt, S. E.; Prior, R. L. Lipophilic and hydrophilic antioxidant capacities of common foods in the United States. Journal of Agricultural and Food Chemistry, 2004, 52, 4026–4037.

Yogesh, M. K.; Mithula, S.; Sankaranarayanan, M.; Kondapalli, V. G. C. S. Oxindole and its derivatives: A review on recent progress in biological activities. Biomedicine & Pharmacotherapy, Elsevier, 2021, 111842.

Yuyama, K.; Aguiar, J. P. L.; Yuyama, L. K. O. Camu-Camu: Um fruto fantástico como fonte de vitamina C. Acta Amaz., Manaus, 2002, 32, 169-174.

Zanatta, C. F.; Cuevas, E.; Bobbio, F. O.; Winterhalter, P.; Mercadante, A. Z. Determination of Anthocyanins from Camu-camu (Myrciaria dubia) by HPLC-PDA, HPLC-MS, and NMR. J. Agric. Food Chem. 2005, Vol 53, Is 24, 0021-8561.

Zhao, H.; Akritopoulou-Zanze, I. When analoging is not enough: scaffold discovery in medicinal chemistry. Expert Opin. Drug Discovery, 2010, 5(2), 123–134.

Zheng, Y.; Tice, C. M.; Singh, S. B. The use of spirocyclic scaffolds in drug discovery. Bioorg Med Chem Lett. 2014 Aug 15;24(16):3673-82. doi: 10.1016/j.bmcl.2014.06.081. Epub 2014 Jul 5. PMID: 25052427.

Zheng, Y.; Tice, C. M.; Singh, S. B. The use of spirocyclic scaffolds in drug discovery. Bioorg. Med. Chem. Lett. 2014, 24(16), 3673–3682.

Zheng, W.; Wang, S. Oxygen radical absorbing capacity of phenolics in blueberries, cranberries, chokeberries, and lingonberries. Journal of Agricultural and Food Chemistry, 2003, 51, 502–509.

BIOGRAPHICAL SKETCH

Judith Anane attained her Bachelor of Science degree in Chemistry from the Kwame Nkrumah University of Science and Technology (KNUST), Ghana in 2018. She pursued a Master of Science in chemistry at the University of Texas Rio Grande Valley (UTRGV), Edinburg Texas from January 2021 and was conferred the degree in December 2022. Her research was on the green synthesis of spiro indoline pyrazolo-pyridine compounds and the phytochemical investigation of diethyl ether fraction of camu-camu (*Myrciaria dubia*) leaves and was conducted under the supervision of Dr. Debasish Bandyopadhyay. During her studies, she was awarded the Graduate Sustainability Fellowship for the 2021-2022 academic term since her research was in line with some of the UN sustainable goals. She can be reached via email at: judithanane3000@gmail.com